博士論文

Structural and Environmental Dependence of Superlubricity in Ion Vapor Deposited Hydrogenated Amorphous Carbon Films

（イオン化蒸着法により作製した水素化アモルファス炭素膜の超潤滑特性とその構造および環境依存性）

陳　新春

Structural and Environmental Dependence of Superlubricity in Ion Vapor Deposited Hydrogenated Amorphous Carbon Films

（イオン化蒸着法により作製した水素化アモルファス炭素膜の超潤滑特性とその構造および環境依存性）

陳　新春

(Chen Xinchun)

A dissertation presented in
partial fulfillment of the requirements for the
DEGREE OF DOCTOR OF MECHANICAL ENGINEERING

Supervisor: Prof. Dr. Takahisa Kato

Department of Mechanical Engineering
The University of Tokyo

August 2014

© 2014 - Xinchun Chen

All rights reserved.

To my family, from whom I owe everything,

To my wife, for always standing by my side,

and to my friends, for your companionship.

Acknowledgements

The work presented in this thesis was supported by and completed in Surface Science & Tribology Laboratory (SSTL) in Department of Mechanical Engineering at The University of Tokyo.

I sincerely acknowledge my supervisor, Professor Takahisa Kato, for his important guidance. I thank all the opportunities, the support, the communications and the encouragement. I will be grateful forever for all I have gained.

I acknowledge Dr. Masahiro Kawaguchi for his assistance in doing experiments in Tokyo Metropolitan Industrial Technology Research Institute (TIRI).

I acknowledge associate Professor Junho Choi and Professor Masataka Nosaka for their support in some experiments and valuable discussions.

I acknowledge Dr. Naohiro Matsumoto for his help in AFM and Mass Spectroscopy measurements, and for the precious friendship.

I acknowledge Tokyo Metropolitan Industrial Technology Research Institute (TIRI), Elionix Inc., Taiho Kogyo Co. Ltd. and Maruyama Laboratory for the access to some experimental facilities.

I acknowledge Toshio Itoh for his assistance in HRTEM measurement.

I acknowledge Jiao Xu, Shu Sawai, Satoko Horikohi, Takayuki Hibi, Yuushi Yamagami and all of the other fellow members in SSTL for their friendship and companionship in the past three years.

I acknowledge my good friends who have supported me all the time. Best thanks to Sudong Wu, Kehang Cui, Yingzong Liang, Qiong Ma, Qianyan Fu, Jun Dai, and Rui Chen.

Abstract

Superlubricity, a near-frictionless lubrication state, is of high significance for its potential industrial applications since friction and wear is one of the major causes for energy loss and equipment failure during industrial actives. As a solid lubricant, amorphous carbon (a-C) or diamond-like carbon (DLC) film has attracted special attention owing to their superior anti-friction properties. Hydrogenated amorphous carbon (a-C:H) is particularly promising for achieving this superlubric state, for instance, superlow friction in dry inert gas. However, the lubrication mechanism underlying this exceptional phenomenon is not well understood. Moreover, it is still a great challenge to achieve superlubricity in ambient air due to the complex tribo-interactions in the presence of oxygen, water and other gaseous molecules.

The aim of this thesis is to develop a new superlubric-material system based on C-Si-H ternary phase, namely a-C:H and Si-incorporated a-C:H (a-C:H:Si) films. To realize this purpose, the ion vapor deposition (IVD) system was chosen as the synthesis method due to its accurate control of incident ion energy. First, the growth mechanism for achieving ultrasmooth surface under energetic ions was investigated to serve as the basic knowledge for synthesizing the required films. Special attention was paid to the ion-energy-dependence of structural evolution of a-C:H:Si films. Second, the key factors controlling the superlubric behaviors of hydrogen-rich a-C:H film was systematically studied. Following this, the possibility for suppressing moisture sensitivity by Si-incorporation and the requirements for achieving superlow friction in humid air were investigated. Afterwards, the lubrication effect of hydrogen in a-C:H:Si was highlighted for the purpose to obtain superlow friction in dry N_2 and reactive H_2.

Finally, a polymer-like a-C:H:Si film was proposed for its particularly superior anti-friction behaviors in multi-environments. The underlying tribo-chemical lubrication mechanisms were presented. The major achievements in this thesis were summarized as follows:

The IVD system is effective in growing ultrasmooth film surface. The roughness of the as-grown a-C:H:Si films is extremely low (~0.1 nm), and the derived roughness exponent and growth exponent by dynamic scaling theory are α~0.51 and β~0, respectively. The extremely small growth exponent during ion dominated deposition requires the presence of energetic ion-impact induced subsurface "polishing" process. Depending on the incident ion energy, the bonding structure of a-C:H:Si films evolves from hydrogen-rich chain-developed polymer-like, to hard cross-linked diamond-like, and finally to hydrogen-deficient sp^2-bonded a-C.

The hydrogen-rich (39.3 at.% H) a-C:H film shows high friction and severe wear in humid air when sliding against bare SUJ2 ball, while superlow friction could be achieved in dry N_2. The film structure, counterpart material (self-mated or bare steel ball), atmospheric environment, contact pressure (non-Amontonian behavior) and sliding velocity are playing paramount roles in determining the friction behavior of a-C:H film. An extremely low friction coefficient of ~0.001 can be obtained at normal load of 10 N. Such a near-frictionless rubbing hardly results in any wear and loss of material.

Ultralow and even superlow friction is feasible for a-C:H:Si films in humid air. The surface density of silicon hydroxyl group (Si-OH), humidity level and contact pressure determine the frictional performance of a-C:H:Si films. The dissociative formation of OH-terminated surface and the orientation of molecular structure of adsorbed water is the origin of ultralow friction in humid air. At an appropriate RH level, the formation of a low shear-strength layer-like H_2O film provides effective boundary lubrication.

The hydrogen-induced structural diversity of a-C:H:Si films such as polymer-like, diamond-like or sp^2-bonded a-C significantly affects the frictional behaviors. A proper range of hydrogen content in the film is required to achieve stable superlow friction in a distinct gaseous atmosphere, i.e., dry N_2, reactive H_2 or humid air. The polymer-like a-C:H:Si (31.9 at.% H) film can exhibit superlow friction (μ~0.001-0.01) in various environments including humid air, dry inert gas (N_2 and Ar) and reactive gas (H_2) and it

can even maintain ultralow friction (μ~0.084) in a corrosive gas (O_2). The occurrence of superlubricity in a-C:H:Si films is attributed to a synergistic effect of phase transformation, surface passivation and shear localization, for example, the acquisition of an extremely low friction coefficient of ~0.001 in dry N_2. The present realization of superlubricity by one material such as the polymer-like a-C:H:Si film in multi-environments may open up a new pathway for designing more efficient lubricating materials in the near future.

TABLE OF CONTENTS

Chapter 1

Introduction

In this chapter, a brief introduction focuses on the definition and history of tribology. The state of the art of superlubricity is highlighted for its major significance from the viewpoint of industrial application. Special attention is given to amorphous carbon, which is the most promising solid lubricant to provide diverse structures, superior mechanical properties and anti-friction performances in various service environments and tribological fields.

1.1 History of Tribology

The word *tribology* is a derivative from the combination of the Greek roots "tribos" and "ology", in which *tribos* means "rubbing" and *ology* stands for "knowledge of". Therefore, the direct meaning of tribology is "the knowledge of rubbing" [1.1, 2]. It was originally created by the British physicists Tabor and Bowden [1.3], and also formally proposed by Peter Jost in his famous "The Jost report" in 1964 [1.4]. Equivalently, lubrication science or friction and wear is also frequently used. From a scientific point of view, tribology is generally defined as the science and engineering of surfaces in contact and in relative motion. It is highly correlated with every facet of our daily life, from blood transportation to walking on foot to engine and airspace lubrication. Tribology is a complex interdiscipline subject since the rubbing process between two surfaces involves materials engineering, physics, chemistry, liquid and solid mechanics, shear rheology, thermodynamics and so on [1.2].

The study of tribology is far more long-standing than we think. According to the historical records, ancient Egyptians circa 2400 BC used friction-reduction devices to

transport large stone blocks by a sledge. Some lubricants, most likely water, were poured in front of the wooden track to facilitate the transportation. Other primitive anti-friction constructions such as wheel bearings were also found to improve the transportation efficiency [1.1, 2]. In the 15th century, talented Leonardo da Vinci was deemed as the first person to scientifically study the friction phenomenon concerning the sliding motion of a rectangular block on a flat surface. He firstly introduced the concept of friction coefficient to describe the relationship between the normal load and friction force. However, his discovery was not published for a long time. Until 17th (1699) century, Amontons re-discovered the friction law as follows: first, the friction force resisting the sliding motion is proportional to the normal load, and second, the friction force is independent of the apparent contact area [1.5]. Soon afterwards, the French physicist Coulomb discovered the third rule governing the friction behavior between two contact surfaces: the dynamic friction is independent of sliding velocity and the critical static friction is larger than the dynamic friction [1.6]. All these three friction-related rules are in general called Classical Friction Laws. Even in modern society, these empirical rules are still playing important roles in machine design and industrial activities [1.1, 2].

With the development of science and technology, more and more sub-branches emerge as new research topics in tribology. For instance, the hydrodynamic lubrication started to draw extensive attention from the first experimental study by Tower [1.7] and theoretical research by Reynolds at the end of 19th century [1.8]. Numerous efforts are still devoted in investigating this prevalent lubrication phenomenon. In the 20th century, the inventions of atomic force microscopy (AFM) and surface force apparatus (SFA) significantly promote the study of tribology at nano-scale, namely nanotribology. It provides possibility for understanding the energy dissipation and surface modification process of tribology from the perspective of inter-atom interactions [1.2]. Biotribology is another attractive research topic in tribology due to its vast potential application in biomedical field for human body such as artificial joint. More recently, *superlubricity*,

has become one of the hottest researches in tribology since a nearly friction-free state is of high significance in industry especially in the present condition that energy conservation has aroused extensive concerning around the world due to the shortage of natural resources as the modern society rapidly advances.

1.2 The State of The Art of Superlubricity

The term *superlubricity*, originally proposed by Hirano and Shinjo in 1990 [1.9], describes a theoretical sliding state where friction or resistance to sliding nearly vanishes. Based on the Frenkel-Kontorova model, it was emphasized that superlubricity would appear when the two contact surfaces are of high dimensionality architectures (i.e., incommensurability). Under this condition, superlubricity is a general phenomenon, appearing either for strong metallic bonds or for weak van der Waals interactions [1.10]. This special lubrication state was first confirmed experimentally by measuring the friction of clean mica surfaces with respect to the lattice misfit. Anisotropic frictional behaviors depending on the misfit angle can be observed for the contact mica surfaces in a dry atmosphere, and the friction force significantly decreased when the misfit angle approached θ=30° [1.11]. It should be mentioned that Hirano's research pointed out the crucial role of incommensurability for achieving superlubricity in crystal materials. However, subsequent work by other researchers has confirmed that superlubricity is also achievable in non-crystalline materials such as amorphous carbon or diamond-like carbon. As a measure for superlubricity, a sliding state with friction coefficient μ below 0.01 can be deemed as a superlubric stage. Note that superlow friction is generally detected in the range of $0.001<\mu<0.01$ since friction coefficient measurements below 0.001 are beyond the measurement accuracy for most of the available tribotesting systems [1.12].

The predictive existence of such a near-frictionless state stimulates numerous theoretical and experimental studies on superlubricity. Statistic reports estimate that as much as ~30-50% of the annual energy consumption in the world is lost due to friction

and wear. Moreover, wear of sliding contact surfaces leads to equipment failure, resulting in massive economic and environmental costs [1.4, 13]. Therefore, the realization of a friction-free state is therefore of high significance both from the basic scientific perspective of tribology and in view of the potential industrial applications it carries. In the past several decades, remarkable advances have been realized in lubricant technologies, which undoubtedly decrease the frictional energy loss by introducing newly developed lubricant materials into contact surfaces. In 2007, Erdemir and Martin edited and published a book summarizing the relevant advancements in superlubricity, which was definitely a sign of huge progress in this field [1.12]. From the viewpoint of material science, the well-known lubricants for achieving superlubricity can be divided into two categories, namely solid superlubric materials and liquid superlubric materials, as shortly summarized below. A recent review paper can be found to discuss this topic in detail [1.14].

1.2.1 Solid Superlubric Materials

1.2.1.1 Graphite

Graphite is the most well-known solid lubricant mainly for its low friction in humid environment. The underlying lubrication mechanism of graphite was mainly attributed to the lamellar structure since Bragg first confirmed it using X-ray diffraction in 1928 [1.15]. However, the slipperiness of graphite is not only an intrinsic property, but also significantly influenced by the gaseous atmosphere. Abnormally high friction and wear rate was discovered for graphite in the late 1930s when it was used in the aircraft brushes. This catastrophic high-friction behavior, also known as “dusting”, was thought to originate from the low humidity [1.16]. In 1987, Mate et al. first observed superlubricity with an extremely low friction coefficient of ~0.005 in atomic-scale friction of a tungsten tip on a graphite surface [1.17]. After that, numerous studies focused on the superlubricity of graphite. For example, Dienwiebel et al. discovered a near-frictionless state for graphite by rotating the contact angle and contributed this

anisotropic friction phenomenon to the immensurability between rotated graphite layers [1.18]. The following other works also confirmed the incommensurate contact theory as the basic origin of superlubricity in graphite [1.19, 20].

1.2.1.2 Molybdenum Disulfide (MoS_2)

Molybdenum disulfide is another famous lamellar solid lubricant. Martin's group first observed superlow friction behaviors for pure MoS_2 coatings in ultrahigh vacuum (UHV) and dry N_2 in 1992 [1.21]. It was emphasized that superlubricity of MoS_2 was mainly attributed to the friction-induced basal plane orientation during sliding. However, the presence of oxygen or H_2O molecules in the surroundings such as humid air would destroy the superlubric state of MoS_2 [1.22]. To maintain the superlubric properties of MoS_2 in ambient gas, Chhowalla and Amaratunga synthesized fullerene-like MoS_2 nanoparticles to reduce the moisture sensitivity. The results indicated that such a new MoS_2 film could exhibit a superlow friction of ~0.003 in a humid atmosphere of 45% RH [1.23].

1.2.1.3 Carbon Nitride (CN_x)

Carbon nitride has been once predicted as the most promising mechanical material for its possible ultra-high hardness if possessing an ideal atomic structure of β-C_3N_4 [1.24]. However, most fabricated carbon nitride films have amorphous structures rather than crystal textures, thus defined as CN_x [1.25]. Even so, these CN_x films still have some excellent properties such as anti-friction performance. Kato and his co-workers systematically investigated the frictional behaviors of CN_x in various atmospheres. Superlow friction is more feasible for CN_x in dry N_2 [1.26]. Recent study by Wang has demonstrated that the formation of a naked-eye-invisible amorphous carbon tribolayer with thickness of ~10 nm on the contact surfaces is the crucial point to achieve ultralow or superlow friction in N_2 [1.27].

1.2.1.4 Diamond-Like Carbon (DLC)

Diamond-like carbon (DLC) or amorphous carbon (a-C) has attracted extensive research attention due to their outstanding properties such as high hardness, chemical inertness, low friction, wear resistance and optical transparency [1.28]. As a solid lubricant, the breakthrough work in superlubricity for DLC was accomplished by Erdemir et al. and Donnet et al. in the early 21^{th} century [1.29, 30]. A highly-hydrogenated amorphous carbon (a-C:H) film grown from a mixture plasma of 25% CH_4 + 75% H_2 by PECVD can exhibit extremely low friction coefficients of 0.001-0.003 and wear rates of 10^{-9}-10^{-10} mm^3/Nm in dry N_2 [1.29]. The up-to-now achievements in this special carbon material concerning the bonding structure, superior anti-frictional behaviors as well as the existing problems will be discussed in detail in the following Section 1.3.

1.2.2 Liquid Superlubric Materials

1.2.2.1 Polymer Brushes

Polymer-based hydration lubrication has been investigated for a long time due to their widespread applications, especially in the biomedical field. Klein et al. has devoted many years to studying the superior anti-friction behaviors and the corresponing lubrication mechanim underlying this kind of soft material such as polyelectrolytes in water [1.31, 32]. In general, the friction-reduction effect of polymer brushes is ascribed mainly to the produced repulsiion forces between polymer-brush-grafted surfaces such as mica, and partically to the formed hydratiion water layers [1.33]. For instance, the friction coefficient between surfaces bearing poly[2-(methacryloyloxy)ethyl phosphorylcholine] brushes decresed to 0.0004 in pure water at a pressure as high as ~8 MPa [1.34]. However, it is a urgent mission to improve the load capacity of polymer brushes if more wide applications are required.

1.2.2.2 Glycerol

Glycerol is a hydrophilic chemical substance due to the existence of three hydroxyl groups in its molecules. In 2008, Matta observed a superlow friction behavior of ta-C under the lubrication of pure glycerol at 80° [1.35]. It was speculated that the low friction phenomenon mainly originated from the rubbing-induced OH-terminated surfaces and the dissociative formation of a nanometer-thick layer of organic acids and water. More interestingly, superlubricity can be realized for steel surfaces at room temperature by a solution of *myo*-inositol in glycerol at high contact pressure [1.35]. Similarly, Ma et al. discovered that superlow friction could be achieved for the sliding pair between glass plate and Si_3N_4 ball under a mixture lubrication of glycerol and boric acid [1.36].

1.2.2.3 Phosphoric Acid Solution

Phosphoric acid solution is a recently discovered lubrication medium which can provide possibility for achieving superlow friction. Li et al. found that a friction coefficient of ~0.004 was achieved for Si_3N_4/glass and sapphire/sapphire counterparts under the lubrication of a phosphoric acid aqueous solution (pH 1.5) at high contact pressure of ~1.65 GPa [1.37]. The friction-reduction mechanism is largely described to the formation of a low-shear strength hydrogen-bonded water layer, and the produced Coulomb repulsion force from the interfacial dipole-dipole [1.37].

1.3 Amorphous Carbon (a-C) Films

1.3.1 Categories of Bonding Structures

Amorphous carbon (a-C) or diamond-like carbon (DLC) is a metastable form of carbon with a significant fraction of sp^3-C bonds. As we all know, carbon has three hybridization forms including linear sp^1, trigonal sp^2 and tetrahedral sp^3. In the sp^3 configuration, the carbon atoms' four valence electrons are distributed in a tetrahedral orbital, forming strong σ bonds. In sp^2 configuration, it forms σ bonds in a plane and simultaneously a weak π bond with another π orbital. According to the ratio of sp^2/sp^3

and hydrogen incorporation, DLC can have various bonding structures, as shown in Figure 1.1 [1.28]. For example, when sp^3 content in the film reaches a critical high value, i.e, 70%, this kind of DLC film is also defined as tetrahedral amorphous carbon (ta-C). For the hydrogenated amorphous carbon (a-C:H), Casiraghi et al. classified them into three groups based on the hydrogen content in the films: PLCH (40-60 at.% H), DLCH (20-40 at.% H) and GLCH (less than 20 at.% H) [1.38]. In addition to these basic structural forms, many novel DLC variants such as non-metal/metal-doped nanocomposite [1.39-41], multilayered [1.42], fullerene-like a-C:H [1.43, 44] and graphene-embedded carbon [1.45], have been developed to exploit new properties.

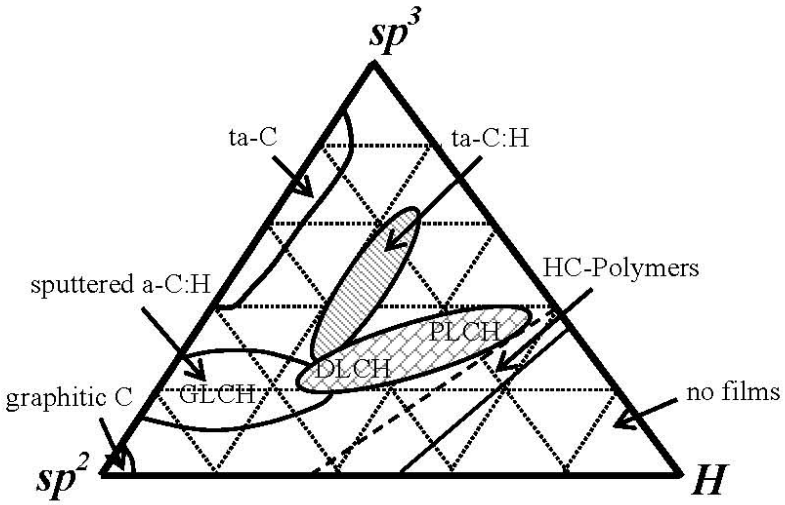

Figure 1.1 Ternary phase diagram showing different bonding structures in amorphous carbon-hydrogen alloy. (Reproduced from Ref. [1.28])

1.3.2 Superior Anti-Friction Properties of a-Cs

In the past several decades, great achievements have been obtained in the research of amorphous carbon materials, especially the tribological properties. Excellent reviews are available for details about this subject [1.46, 47]. To gain an ultralow friction or even a near-frictionless state, modified a-C structures such as incorporation of non-metal elements (i.e., N, Si) [1.26, 39], metal-doped nanocomposite (i.e., Ti, W, Cr, Ag) [1.40, 41, 48], nano-scale multilayer [1.42], functionally graded [1.49],

fullerene-like [1.43, 44], highly-hydrogenated [1.29, 30] and graphene-embedded a-C films [1.45] have been put forward for this possibility. For the convenience of comparison, Table 1.1 summarizes the basic features of different a-C variants, which possess superior anti-friction properties.

Table 1.1 Comparison of a-C variants showing superior anti-friction properties.

No.	Film type	Sliding pair	Environment	Load (N)	μ	Ref.
1	Highly-hydrogenated a-C:H (PECVD)	Self-mate	Dry N_2	10	0.001	1.29
2	a-C:H (PECVD)	Steel	UHV H_2 (10 hPa)	1	0.003	1.30
3	CN_x (Reactive MS)	Self-mate	Dry N_2	0.1	0.009	1.26
4	Fullerene-like a-C:H (RF-PECVD)	Self-mate	Dry N_2 20% RH	10/20 N	~0.01	1.43
5	Fullerene-like a-C:H:(Si,Al) (RF-MS)	Self-mate	HV (10^{-4} Pa)	2	~0.001	1.44
6	a-C:H:(5 at.% S) (MS)	Self-mate	50% RH	0.5	0.003	1.50
7	a-C:H:(Si,Ti) (Reactive MS)	steel	40% RH	2	<0.01	1.51
8	a-C:H/TiC (Reactive MS)	100Cr6	50% RH	5	~0.02	1.40
9	ta-C (Arc-ion plating)	Self-mate	Glycerol	0.27 MPa	<0.01	1.35, 52
10	a-C:H:Si (PECVD+MS)	Si_3N_4	69% RH Water	5	~0.02 <0.01	1.53
11	a-C:H:(Si,O) (PECVD)	Si_3N_4	Dry N_2	~0.05-1	~0.02	1.54

From Table 1.1, we can see that a quite large number of a-C based materials can exhibit ultralow or even superlow friction after structure modification. Superlow friction is more feasible for a-Cs in dry N_2 or H-bearing atmosphere such as H_2. In contrast, it is still a great challenge to achieve a durable superlubric effect with a lowest possible

friction coefficient in water-present environment such as ambient air.

1.4 Research Purpose of This Thesis

As described above, superlubricity is of high significance due to its possibly extensive applications in energy savings and industrial equipment protections. Amorphous carbons have been proved as one of the most promising materials for achieving superlubricity. The previous studies in tribological community has emphasized that one type of a-C material can only exhibit superlow friction in one distinct atmosphere. It is especially difficult to realize superlubricity in ambient environment due to the presence of various gaseous molecules. Moreover, the occurrence of superlubricity for most a-C materials has a close relationship with hydrogen. However, the exact lubrication mechanism underlying a-Cs, especially the role of tribolayer involved in the friction-reduction, is still obscure due to the complexity of the rubbing process. Therefore, in this thesis, we are trying to show some experimental results, in which some key requirements for achieving superlow friction in a-Cs are presented. Special efforts are devoted to developing a new type of a-C material, namely polymer-like a-C:H:Si film, with the aim to realize superlubricity in multi-environments including ambient air. The possible lubrication mechanisms are systematically investigated from both the structural and environmental aspects.

References

[1.1] D. Dowson. *History of Tribology*. Professional Engineering Publishing, London, 2nd Edition, 1998.

[1.2] B. Bhushan. Introduction – Measurement Techniques and Applications. In *Nanotribology and Nanomechanics Vol. 1*, Springer-Verlag, Heidelberg, 3nd Edition, 2011, Chapter 1, pp 1-4.

[1.3] F. P. Bowden, D. Tabor. *The Friction and Lubrication of Solids*, Clarendon Press, Oxford, 1964.

[1.4] P. Jost. *Lubrication (Tribology) – A Report on the Present Position and Industry's Needs*. Department of Education and Science, H.M. Stationary Office, London, 1966.

[1.5] G. Amontons. De la resistance causee dans les machines. *Mem. Acad. R. A.* **1699**, 1706, 257–282.

[1.6] C. A. Coulomb. Theorie des machines simples, en ayant regard an frottement de leurs parties et a la roideur des cordages. *Mem. Math. Phys. X* **1785**, 10, 161–342.

[1.7] B. Tower. Report on friction experiments. *Proc. Inst. Mech. Eng.* **1884**, 632, 29–35.

[1.8] O. O. Reynolds. On the theory of lubrication and its applications to Mr. Beauchamp tower's experiments. *Philos. Trans. R. Soc. Lond.* **1886**, 117, 157–234.

[1.9] M. Hirano, K. Shinjo. Atomistic locking and friction. *Phys. Rev. B* **1990**, 41, 11837-11851.

[1.10] K. Shinjo, M. Hirano. Dynamics of friction: superlubric state. *Surf. Sci.* **1993**, 283, 473-478.

[1.11] M. Hirano, K. Shinjo, R. Kaneko, Y. Murata. Anisotropy of friction forces in muscovite mica. *Phys. Rev. Lett* **1991**, 67, 2642-2645.

[1.12] J.-M. Martin. In *Superlubricity*; A. Erdemir, J.-M. Martin, Eds.; Elsevier: Amsterdam, The Netherlands, 2007; pp 208.

[1.13] K. Holmberg, P. Andersson, A. Erdemir. Global energy consumption due to friction in passenger cars. *Tribol. Int.* **2012**, 47, 221-234.

[1.14] J. Li, J. Luo. Advancements in superlubricity. *Sci. China Tech. Sci.* **2013**, 56, 2877-2887.

[1.15] W. H. Bragg. In *An Introduction to Crystal Analysis*, Bell, Landon, 1928, pp 64.

[1.16] D. Ramadanoff, S. W. Glass. High-altitude brush problem. *Trans. Am. Inst. Electr. Eng.* **1944**, 63, 825-829.

[1.17] C. M. Mate, G. M. McClelland, R. Erlandsson, S. Chiang. Atomic-scale friction of a tungsten tip on a graphite surface. *Phys. Rev. Lett.* **1987**, 59, 1942-1945.

[1.18] M. Dienwiebel, G. S. Verhoeven, N. Pradeep, J. W. M. Frenken, J. A. Heimberg, H. W. Zandbergen. Superlubricity of graphite. *Phys. Rev. Lett.* **2004**, 92, 126101.

[1.19] A. S. de Wijn, C. Fusco, A. Fasolino. Stability of superlubric sliding on graphite. *Phys. Rev. E* **2010**, 81, 046105.

[1.20] Z. Liu, J. Yang, F. Grey, J. Z. Liu, Y. Liu, Y. Wang, Y. Yang, Y. Cheng, Q. Zheng. Observation of microscale superlubricity in graphite. *Phys. Rev. Lett.* **2012**, 108, 205503.

[1.21] J.-M. Martin, C. Donnet, T. Le Mogne, T. Epicier. *Phys. Rev. B* **1993**, 48, 10583-10586.

[1.22] C. Donnet, J.-M. Martin, T. Le Mogne, M. Belin. *Tribol. Int.* **1996**, 29, 123-128.

[1.23] M. Chhowalla, G. A. J. Amaratunga. Thin films of fullerene-like MoS_2 nanoparticles with ultra-low friction and wear. *Nature* **2000**, 407, 164-167.

[1.24] A. I. Liu, M. L. Cohen. Prediction of new low compressibility solid. *Science* **1989**, 245, 841-842.

[1.25] A. C. Ferrari, S. E. Rodil, J. Robertson. Interpretation of infrared and Raman spectra of amorphous carbon nitrides. *Phys. Rev. B* **2003**, 67, 155306.

[1.26] K. Kato, N. Umehara, K. Adachi. Friction, wear and N_2-lubrication of carbon nitride coatings: a review. *Wear* **2003**, 254, 1062-1069.

[1.27] P. Wang, M. Hirose, Y. Suzuki, K. Adachi. Carbon tribo-layer for super-low friction of amorphous carbon nitride coatings in inert gas environments. *Surf. Coat. Technol.* **2013**, 221, 163-172.

[1.28] J. Robertson. Diamond-like amorphous carbon. *Mater. Sci. Eng. R* **2002**, 37, 129-281.

[1.29] A. Erdemir, O. L. Eryilmaz, G. Fenske. Synthesis of diamondlike carbon films with superlow friction and wear properties. *J. Vac. Sci. Technol.* **2000**, 18, 1987-1992.

[1.30] C. Donnet, J. Fontaine, A. Grill, T. Le Mogne. The role of hydrogen on the friction mechanism of diamond-like carbon films. *Tribol. Lett.* **2000**, 9, 137-142.

[1.31] J. Klein, D. Perahia, S. Warburg. Forces between polymer-bearing surfaces undergoing shear. *Nature* **1991**, 352, 143-145.

[1.32] J. Klein, E. Kumacheva, D. Mahalu, D. Perahia, L. J. Fetters. Reduction of frictional forces between solid-surfaces bearing polymer brushes. *Nature* **1994**, 370, 634–636.

[1.33] J. Klein. Hydration lubrication. *Friction* **2013**, 1, 1–23.

[1.34] M Chen, W. H. Briscoe, S. P. Armes, J. Klein. Lubrication at physiological pressures by polyzwitterionic brushes. *Science* **2009**, 323, 1698-1701.

[1.35] C. Matta, L. Joly-Pottuz, M. I. D. Bouchet, J.-M. Martin, M. Kano, Q. Zhang, W. A. Goddard III. Superlubricity and tribochemistry of polyhydric alcohols. *Phys Rev B* **2008**, 78, 085436.

[1.36] Z. Ma, C. Zhang, J. Luo, X. Lu, S. Wen. Superlubricity of a mixed aqueous solution. *Chin. Phys. Lett.* **2011**, 28, 056201.

[1.37] J. Li, C. Zhang, J. Luo. Superlubricity behavior with phosphoric acid - water network induced by rubbing. *Langmuir* **2011**, 27, 9413-9417.

[1.38] C. Casiraghi, A. C. Ferrari, J. Robertson. Raman spectroscopy of hydrogenated amorphous carbons. *Phys Rev B* **2005**, 72, 085401.

[1.39] K. Oguri, T. Arai. Low friction coatings of diamond-like carbon with silicon prepared by plasma-assisted chemical vapor deposition. *J. Mater. Res.* **1990**, 5, 2567–2571.

[1.40] Y. T. Pei, D. Galvan, J. Th. M. De Hosson. Nanostructure and properties of TiC/a-C:H composite coatings. *Acta Mater.* **2005**, 53, 4505-4521.

[1.41] S. Zhou, L. Wang, Z. Lu, Q. Ding, S. C. Wang, R. J. K. Wood, Q. Xue. Tailoring microstructure and phase segregation for low friction carbon-based nanocomposite coatings. *J. Mater. Chem.* **2012**, 22, 15782–15792.

[1.42] Y. N. Koka, P. Eh. Hovsepian, Q. Luo, D. B. Lewis, J. G. Wen, I. Petrov. Influence of the bias voltage on the structure and the tribological performance of nanoscale multilayer C/Cr PVD coatings. *Thin Solid Films* **2005**, 475, 219-226.

[1.43] L. Ji, H. Li, F. Zhao, W. Quan, J. Chen, H. Zhou. Fullerene-like hydrogenated carbon films with super-low friction and wear, and low sensitivity to environment. *J. Phys. D Appl. Phys.* **2010**, 43, 015404.

[1.44] X. Liu, J. Yang, J. Hao, J. Zheng, Q. Gong, W. Liu. A near-frictionless and extremely elastic hydrogenated amorphous carbon film with self-assembled dual nanostructure. *Adv. Mater.* **2012**, 24, 4614-4617.

[1.45] C. Wang, D. Diao. Cross-linked graphene layer embedded carbon film prepared using electron irradiation in ECR plasma sputtering. *Surf. Coat. Technol.* **2011**, 206, 1899-1904.

[1.46] A. Erdemir, C. Donnet. Tribology of diamond-like carbon films: recent progress and future prospects. *J. Phys. D Appl. Phys.* **2006**, 39, R311-R327.

[1.47] J. Fontaine. Towards the use of diamond-like carbon solid lubricant coatings in vacuum and space environments. *P. I. Mech. Eng. J-J. Eng.* **2008**, 222, 1015-1029.

[1.48] Y. Liu, M. Gubisch, T. Haensel, L. Spiess, J. A. Schaefer. Evaluation of the friction of WC/DLC solid lubricating films in vacuum. *Tribol. Int.* **2006**, 39, 1584-1590.

[1.49] X. Chen, Z. Peng, Z. Fu, S. Wu, W. Yue, C. Wang. Microstructural, mechanical and tribological properties of tungsten-gradually doped diamond-like carbonfilms with functionally graded interlayers. *Surf. Coat. Technol.* **2011**, 205, 3631-3638.

[1.50] C. A. Freyman, Y. Chen, Y.-W. Chung. Synthesis of carbon films with ultra-low friction in dry and humid air. *Surf. Coat. Technol.* **2006**, 201, 164-167.

[1.51] J. Jiang, J. Hao, P. Wang, W. Liu. Superlow friction of titanium/silicon codoped hydrogenated amorphous carbon film in the ambient air. *J. Appl. Phys.* **2010**, 108, 033510.

[1.52] J.-M. Martin, M.-I. De Barros Bouchet, C. Matta, Q. Zhang, W. A. III Goddard, S. Okuda, T. Sagawa. Gas-Phase Lubrication of ta-C by Glycerol and Hydrogen Peroxide. Experimental and Computer Modeling. *J. Phys. Chem. C* **2010**, 114, 5003-5011.

[1.53] F. Zhao, H. X. Li, L. Ji, Y. F. Mo, W. L. Quan, H. D. Zhou, J. M. Chen. Structural, mechanical and tribological characterizations of a-C:H:Si films prepared by a hybrid PECVD and sputtering technique. *J. Phys. D Appl. Phys.* **2009**, 42, 165407.

[1.54] T. W. Scharf, J. A. Ohlhausen, D. R. Tallant, S. V. Prasad. Mechanisms of friction in diamondlike nanocomposite coatings. *J. Appl. Phys.* **2007**, 101, 063521.

Chapter 2

Energetic Growth Mechanism and Dynamic Smoothening Behavior of Ultrasmooth a-C:H and a-C:H:Si Films

In this chapter, attention focuses on introducing the ion vapor deposition (IVD) system for synthesizing hydrogenated amorphous carbon (a-C:H) and Si-containing hydrogenated amorphous carbon (a-C:H:Si) films using toluene and toluene/tetramethylsilane gas precursors, respectively. Dynamic scaling theory is utilized to investigate the ion-impact-induced subsurface smoothening mechanism of these atomically smooth carbon films. Ion energy, controlled by the substrate bias voltage, is highlighted for its paramount role in determining the structural properties, i.e., hydrogen content in a-C:H:Si films.

2.1 Background

As discussed in Chapter 1, hydrogenated amorphous carbon (a-C:H) film is one of the most promising lubricants for achieving superlubricity. Especially for the hydrogen-rich one (polymer-like), the correlation between synthesis method, growth process and film structure needs special attention. Besides a-C:H, hydrogenated Si-incorporated amorphous carbon (a-C:H:Si) is another excellent lubricant which has great technological potential for serving as functional or protective coatings due to their high hardness, reduced residual stress, wide optical band gap, high thermal stability, good adhesion to many substrates and low friction coefficients with high moisture insensitivity. Numerous efforts have concentrated on the effect of Si content on the

microstructures and mechanical properties of a-C:H:Si films [2.1-5]. In general, the Si incorporation reduces the density and size of sp^2 graphitic defects [2.1, 2], stabilizes the sp^3 bonding [2.3, 6] and promotes the development of polymer-like structure [2.6, 7] when increasing the flow rate of Si-containing gas precursors such as tetramethylsilane (TMS).

Compared to Si incorporation, very few studies [2.8, 9] have been devoted to investigating the role of hydrogen in a-C:H:Si films, which exists as an accompanying element during the gas ionization of organic silicon hydrides. As described in the carbon-hydrogen ternary phase diagram by Robertson [2.10], the hydrogen content and the sp^3 bonded carbon sites act as the two most important factors determining the structure and properties of a-C:H films. Diverse bonding hybridizations available to carbon (linear-sp^1, trigonal-sp^2 and tetrahedral-sp^3) and the ability to introduce hydrogen atoms into the amorphous network allow a-C:Hs to have their properties tailored to be more polymer-like (40-60 at.% H, PLCH), diamond-like (20-40 at.% H, DLCH), or graphite-like (less than 20 at.% H, GLCH) [2.11]. Hydrogen may either bond to carbon atoms to form C-H covalent bonds or stay unbound as molecular H_2 trapped in internal microvoids [2.12]. The unbound hydrogen along with the covalently bonded hydrogen affects the structural flexibility, mass density, void distribution, stress state, optical transparency, thermal stability and frictional property of a-C:H film [2.13-15]. Pioneering work in tribological field has pointed out the key influence of hydrogen in achieving low friction for a-C:H films [2.16, 17]. A highly hydrogenated a-C:H film can exhibit extremely low friction coefficient down to 0.001, referred as "superlubricity", under dry inert gas environment such as N_2 [2.16]. It was suggested that the chemical inertness of the contact surface grown from a hydrogen-rich plasma (i.e., H/C ratio of ~10), as well as the continuous passivation of those newly formed dangling bonds during sliding by unbound hydrogen diffused from inside the film, is one of the principle mechanism of superlow friction of a-C:H films [2.17].

The hydrogen content incorporated into a-C:H film can be controlled either by the

hydrogen-to-carbon ratio in the precursor gases [2.16] or by the bias voltage applied in the ion radicals [2.18]. For a-C:H:Si films as described above, the hydrogen incorporation was usually promoted when increasing the gas fraction of Si-containing precursors such as silane or TMS to obtain high Si content. In most reported results, this synthesizing process was preferably accomplished by a chemical vapor deposition such as PECVD at a constant and relatively high bias voltage (i.e., $V_b \geq 300$ V) [2.3, 4, 7, 19]. Thus, the a-C:H:Si films prepared under this condition possess a more diamond-like characteristic with a relatively low hydrogen content, i.e., 20-30 at.% H. It is commonly emphasized that the hydrogen inclusion into a-C:H:Si films induces a softening effect including an increase in the void density and an associated reduction in the connectivity of carbon network and the release of its residual stress [2.5, 8, 20]. In the extreme case of hydrogenated amorphous silicon (a-Si:H), a large volume of molecular H_2 clusters existed in the internal microvoids can be detected by NMR (Nuclear Magnetic Resonance) [2.21].

The ion vapor deposition (IVD) system in our laboratory is a multi-functional coater which can synthesize structured a-C:H or metal/non-metal doped a-C:H films by accurately controlling the deposition parameters such as gas precursor, flow rate and bias voltage. One interesting finding is that ultrasmooth surface with atomic-scale roughness is feasible for the as-grown a-C:H and a-C:H:Si films. In addition, by changing the bias voltage applied in the substrate, the as-grown films have totally different mechanical properties. However, the underlying growth mechanism of such a ultrasmooth interface, the specific role of ion energy in influencing the film structure such as the hydrogen incorporation and its effect on the friction-reduction performance of a-C:H:Si films remain unclear. For instance, the ion-surface interactions such as the C-H and C-Si bonds depletion, atomic hydrogen abstraction and penetration, dangling bonds formation and growing interface morphology are strongly dependent on the incident ion energy (i.e., bias voltage).

This chapter has two main aims: first, to understand the growth mechanism of

ultrasmooth surface by the dynamic scaling theory and second, to provide a systematic interpretation of compositional evolution with respect to the ion energy as the microstructure of a-C:H:Si film evolves from polymer-like to diamond-like to sp^2-bonded a-C. To realize these aims, we have prepared a set of a-C:H:Si films by ion vapor deposition (IVD) with a wide range of bias voltage from 0.25 to 3.5 kV. The carbon network evolution, nanomechanical property, viscoplastic behavior as well as the superlubric performance are investigated with respect to the hydrogen content in the a-C:H:Si films.

2.2 Experimental Methodology

2.2.1 Deposition Procedure

The a-C:H and a-C:H:Si films were prepared by ion vapor deposition system (NPS330S, Nanotec Corp., Japan) using toluene (C_7H_8) and C_7H_8/TMS mixture as gas source, respectively. This coating method, based on ion beam technique, was originally developed by Weissmantel et al. in 1979 [2.22-24], and is further modified by Nanotec Corp. The essential part of the present system is the ionization assembly which comprises a hot tungsten filament cathode, a clover-shaped anode and a negatively biased cylinder reflector. An efficient ionization of gaseous molecules is achieved by impacting electrons generated from the tungsten filament. The ionization efficiency per electron is greatly enhanced by forcing the electrons to move along oscillating orbits between the reflector walls before they have a chance to find the anode. Then, the ionized species are extracted and accelerated by a negative pulsed bias voltage (0-5 kV) connected to the substrates. When the ions are accelerated in the direction of substrate, the energy distribution of the total flux splits up into a narrow peak attributed to ions and a branch corresponding to thermal neutrals. According to Weissmantel's analysis, the as-grown a-C:H films by such a coating system are predominantly built up from the condensing energetic ions, while low contribution of thermal neutrals is likely to be

incorporated into the films only in the case of low bias voltages [2.24]. Since the intense ion flux extracted from the ionizer forms a broad beam with little scattering by gas phase collisions, this deposition technique is also named as ion beam plating (IBP) [2.23], to distinguish from the traditional ion beam deposition (IBD).

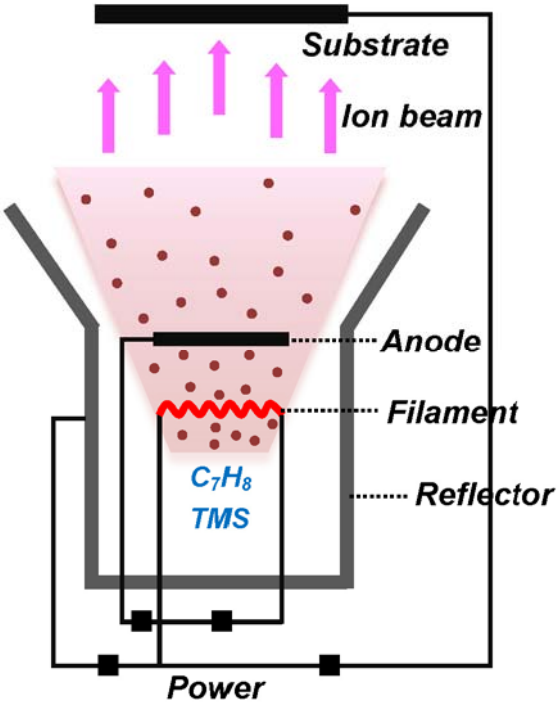

Figure 2.1 Schematic diagram of the ion vapor deposition (IVD) system (NPS330S, Nanotec Corp., Japan) showing the growth architecture for a-C:H and a-C:H:Si films.

In order to minimize the oblique incidence effect, the coating specimens in an appropriate size are placed in the central route of the incoming ions. The specific coating procedures used in this work are shortly summarized as follows: (1) Si (100) wafers (*Ra*=0.12 nm) as well as SUJ2 balls (for friction test) after ultrasonic cleaning were selected as coating substrates, (2) the chamber was pumped down to a base pressure of ~1.0×10^{-3} Pa at the temperature of 200 °C, (3) Ar^+ ion bombarding was performed for 30 min before deposition, (4) a strongly adherent a-C:H:Si interlayer of ~400 nm thickness was first deposited to improve the adhesion between the top layer

and the Si substrates, and (5) the top a-C:H:Si film was then deposited using a wide range of 25%duty-1kHz-pulsed bias voltages from 0.25 to 3.5 kV in the gas-ionization system (i.e., C_7H_8/TMS gas flow ratio of 1, pressure of 0.25 Pa, anode current of 0.5 A, filament current of 30 A, reflector voltage of 10 V). The total thickness of the samples was kept constant at 1.6~1.8 μm.

2.2.2 Dynamic Scaling Theory

The growth process for the structural evolution of ultrasmooth a-C:H:Si films can be revealed by the dynamic scaling theory [2.25-27]. By measuring the evolution of surface roughness w (interface width) through the scaling coefficients (roughness exponent α and growth exponent β), it is possible to derive the main growth mechanisms, such as a "ballistic deposition" or a "random deposition with surface diffusion relaxation" [2.28]. Based on this model, for a self-affine surface, the roughness w scales following the Family-Vicsec relation [2.26, 27].

$$w \sim L^{\alpha} f\left(t / L^{\alpha/\beta}\right) \qquad (2.1)$$

where t is the deposition time and L is the scale size of measurement. For a short deposition time, the growing surface gradually roughens: $w \sim t^{\beta}$. Over a certain time, the roughness reaches saturation: $w \sim L^{\alpha}$. The roughness exponent α ($0 \leq \alpha \leq 1$) is a static exponent describing the surface undulation at a certain time, while the growth exponent β is a dynamic exponent since it determines the initial stage of growth [2.28]. The scaling exponents can be derived from the evolution of roughness over time or by the height-height correlation function (HCF) through AFM measurements. The HCF function can be calculated from:

$$H(r) = \left\langle \left[h(x) - h(x+r) \right]^2 \right\rangle \qquad (2.2)$$

where $h(x)$ denotes the surface height at a position x on the surface at time t, r is the lateral distance and the angle brackets represents an average. The HCF function takes the form $H(r)=2w^2 f(r/\xi)$ with $H(r)=2w^2$ for $r >> \xi$ and $H(r)=(mr)^{2\alpha}$ for $r << \xi$ with local

slope $m = (\sqrt{2}w)^{1/\alpha} / \xi$ [2.28, 29]. From this function, a new term can be deduced, namely lateral correlation length ξ, which represents the critical lateral distance below which the surface heights are correlated and is defined as $\xi \sim t^{1/z}$. This new exponent z is called dynamic exponent and usually follows the relation: $z = \alpha/\beta$ [2.28]. For the purpose of AFM analysis in this work, another set of a-C:H:Si films with different deposition time from 1 min up to 3 h were directly deposited onto Si substrates at a bias voltage of 2 kV using the same coating parameters as described above.

2.2.3 Sample Characterization

The energetic radicals produced in the gas-ionization system during deposition were detected by a SRS RGA300 quadrupole mass spectrometer. The quadrupole probe was operated in residual gas analysis (RGA) mode, in which the ions were formed through electron impact ionization and classified by their mass/charge ratio (m/z). Due to the maximum working pressure for RGA being in the range of ~10^{-4} Torr (~10^{-2} Pa), a simple aperture-based pressure reduction unit was connected through a flange port to the vacuum chamber before the RGA monitor started to sample the composition in the vacuum. The location of the flange port was chosen in the central route directly facing the incoming ion flux for RGA sampling. The RGA sampling was carried out by re-producing the coating environments using the same deposition parameters. The upper part of sample holder was removed to avoid shielding of the ion flux. Note that the mass fragments detected by the RGA reflect the ionized species by the RGA rather than the in situ ion radicals produced by the ionization system. Nevertheless, it can still give some estimation of the actual growth species based on this setting up. The surface morphology of a-C:H:Si films was characterized by AFM (Digital Instruments NanoScope IIIa) with a Si_3N_4 tip of nominal 10 nm radius in contact mode. A square area of 2.5×2.5 μm^2 was scanned at a tip velocity of 5 μm/s for roughness evaluation. The captured AFM image consisted of 512 scanning lines and was converted to 512×512 z-height data points. Thereafter, the HCF curve was calculated using a

home-made code in MatLab. The hydrogen content was determined by an elastic recoil detection analysis (ERDA)/Rutherford backscattering spectroscopy (RBS) equipment. The spectra were acquired by using a 0.5 MeV N^+ beam impinging at an incident angle of 67.5° with respect to the surface normal. The experimental curves were then fitted using the SIMNRA simulation code. The elemental composition and chemical bonding state were derived from PHI Quantera II SXM X-ray photoelectron spectroscopy (XPS) after 2 min Ar^+ pre-sputtering. The Raman spectra were collected by a Renishaw System using an Ar^+ laser with a wavelength of 532 nm. The FTIR spectra were measured by a ThermoNicolet Nexus 470 system. Note that several sister samples were prepared for each characterization method under the same deposition conditions to guarantee reproducibility of the data.

The mechanical properties of a-C:H:Si films with respect to hydrogen content were characterized by nanoindentation. The viscoplastic behavior of a material was evaluated by a Norton-Hoff law [2.30-32]:

$$H = H_0 \cdot \dot{\varepsilon}^x \qquad (2.3)$$

where H is the hardness, H_0 is a constant, $\dot{\varepsilon}$ is the strain rate during loading and x is a constant called viscoplastic exponent. In general, the strain rate $\dot{\varepsilon}$ is proportional to the ratio of loading rate P' over load P during indentation [2.31]. For a plastic behavior, the exponent x equals 0, while for a Newtonian viscous behavior, the exponent x obtains 1. For detailed description, please see references [2.31, 32]. To derive the exponent x of a-C:H:Si films, six ratios of P'/P from 0.02 to 0.5 were chosen to measure the hardness with a maximum indentation load of 1 mN. The classical Stoney's equation was employed to calculate the residual stress of the films by measuring the Si wafer curvature before and after film deposition. The friction tests were performed on a CSM pin-on-disc tribometer. The film-coated SUJ2 ball of 6 mm in diameter was slide against film-coated Si substrate under 2 N at a sliding speed of 20 cm/s in dry N_2.

2.3 Results

2.3.1 Growth Mechanism and Dynamic Surface Smoothening

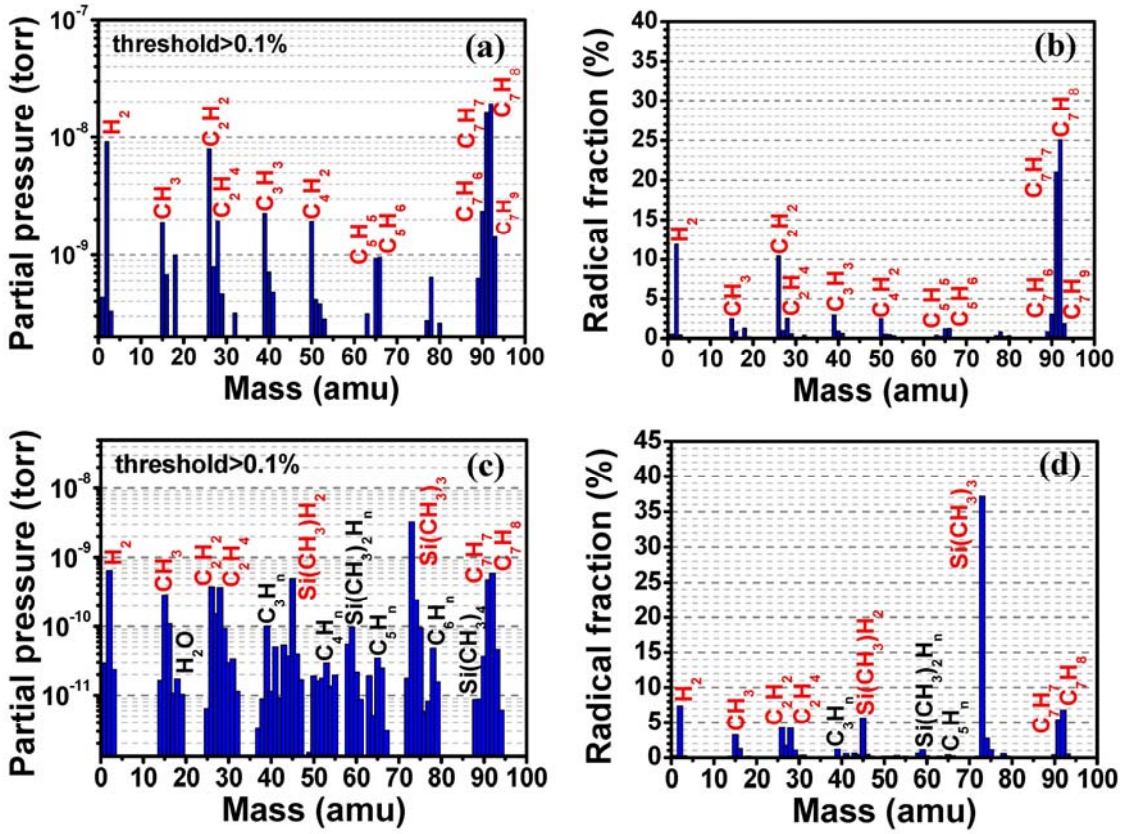

Figure 2.2 Mass spectra detected in the ionization system: (a) the partial pressure (detecting threshold>0.1%) of fragments ionized from C_7H_8 for growing a-C:H film and (b) the corresponding relative fraction of each component, (c) the partial pressure (detecting threshold>0.1%) of fragments ionized from C_7H_8+TMS mixture for growing a-C:H:Si film and (d) the corresponding relative fraction of each component.

The ionic radicals produced in the IVD system were detected by Mass Spectroscopy. Figure 2.2(a) shows the distinct ionic and neutral fragments produced from decomposition of C_7H_8 at a filament current of 30 A. It can be seen that there are three kinds of hydrogen-bearing fragments decomposed from C_7H_8 precursor, namely benzene-ring-containing fragments ($C_7H_{6\text{-}9}$), open-chain hydrocarbon fragments (C_5H_5, C_5H_6, C_4H_2, C_3H_3, C_2H_4, C_2H_2, CH_3) and molecular H_2. The corresponding relative

fraction of each fragment is indicated in Figure 2.2(b). The main growth clusters according to their percentage in the ionic flux are arranged as follows:

C_7H_8>C_7H_7>H_2>C_2H_2>C_7H_6>C_3H_3>C_2H_4>C_4H_2>CH_3.

Therefore, the pure a-C:H film was grown from the dissociation and condensation of these energetic ions upon impact on the substrate under applied bias voltage. Higher incident ion energy generally results in deep penetration, covalent linking and significant loss of hydrogen, while lower ion energy produces hydrogen-rich flexible bonding network.

The fragments produced from decomposition of TMS/C_7H_8 mixture through the ionization system at the same filament current during deposition are shown in Figure 2.2(c). It is observed that the ion flux consists of diverse energetic clusters including hydrogen aggregation (H, H_2, H_3), low-carbon clusters (C_1H_n, C_2H_n, C_3H_n), high-carbon clusters (C_4H_n, C_5H_n, C_6H_n, C_7H_n) and Si-containing radicals ($Si(CH_3)H_n$, $Si(CH_3)_2H_n$, $Si(CH_3)_3H_n$, $Si(CH_3)_4$). In addition, some contaminant species such as OH and H_2O can also be detected in the chamber. Note that the detecting species by RGA might be more or less different from the practical bombarding ions on the growing film. Nevertheless, the setting place of RGA (i.e., directly facing the incoming ion flux) and the pressure reduction system as described above give some estimation of the actual growth species. The corresponding relative fraction of each ion cluster is indicated in Figure 2.2(d). The main growth clusters based on their percentage in the ion flux during deposition are arranged as follows:

$Si(CH_3)_3$>H_2>C_7H_8> $Si(CH_3)H_2$>C_7H_7>C_2H_2>C_2H_4>CH_3.

It is thus reasonable to deduce that the TMS molecules were mainly fragmented into $Si(CH_3)_3$ and $Si(CH_3)H_2$, while the toluene molecules lost one hydrogen and were primarily ionized into C_7H_7, in addition to a noticeable quantity of survival C_7H_8 molecules. Note that some Si-H bonds were formed in the $Si(CH_3)H_2$ fragment due to hydrogen re-saturation of the Si atom. The second largest peak detected by the RGA of molecular H_2 cluster might be produced by recombination of hydrogen atom during

ionization of the gas precursor either in the ion beam system or in the RGA ion source. Special attention should also be paid to the concurrence of unsaturated carbon radicals C_2H_2 and C_2H_4, as well as the termination-forming group CH_3. These low-carbon species were most likely to be produced due to the deep decomposition of some precursor molecules. It should be noted that the present energetic ion growth of a-C:H:Si films involves three general stages including the production of ions from precursor molecules (dissociation, dehydrogenation, ionization etc.), the ion-surface interaction and the subsurface interactions in the film. The above RGA diagnosis belongs to the first stage, while the following second and third stages describe the growing process from energetic ions activated by the applied bias voltages (i.e., 0.25-3.5 kV used in this work). These accelerating ions are bombarding the growing film surface and will be dissociated into atoms upon penetration. The generated C, Si and H atoms will penetrate to a certain depth according to their distinct energy. All these interdependent factors determine the final stoichiometry and bonding structures of the growing a-C:H:Si films, as will be discussed below.

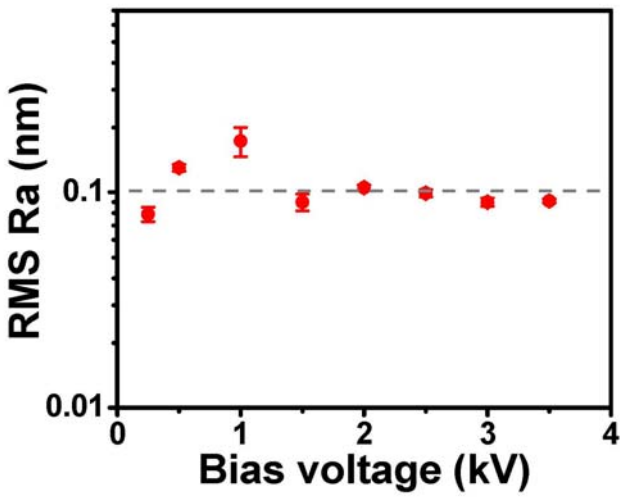

Figure 2.3 RMS-Ra evolution of a-C:H:Si films as a function of bias voltage.

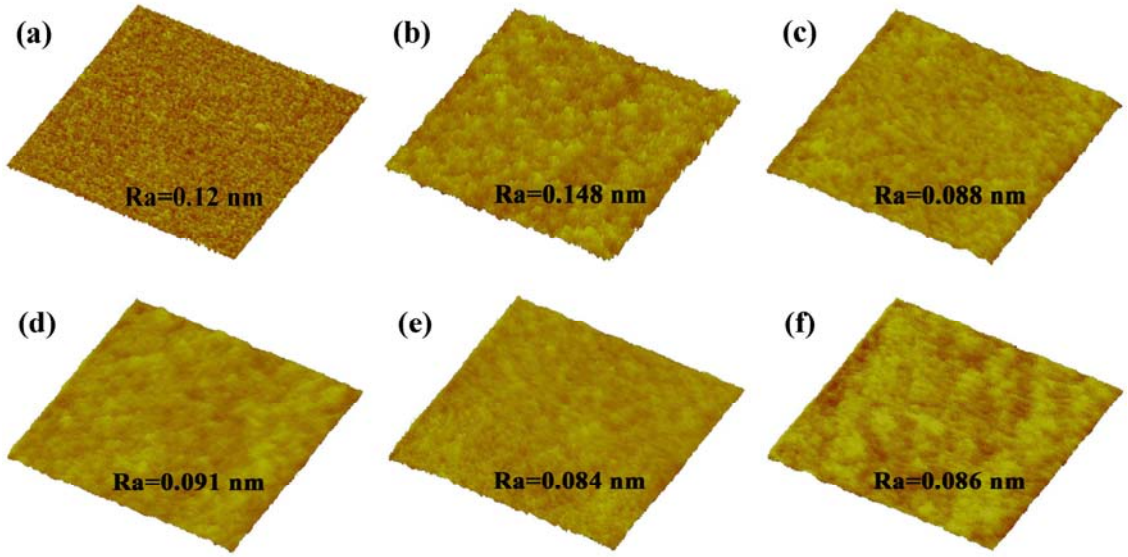

Figure 2.4 2.5×2.5 μm^2 AFM images indicating the surface morphology evolution of a-C:H:Si films grown at bias voltage of 2 kV for different deposition times: (a) 0 s, (b) 60 s, (c) 300 s, (d) 1800 s, (e) 3600 s and (f) 10800 s.

Figure 2.3 shows the logarithmic plot of the RMS roughness evolution of a-C:H:Si films with respect to the applied bias voltage. The results indicate that all the as-grown a-C:H:Si films possess atomically smooth surfaces, and the RMS roughness is approximately constant (~0.1 nm) except for some little scatter effect in the low bias voltage range. It seems that ultrasmooth surfaces of a-C:H:Si films can be grown from energetic ions in a wide range of ion energy. To disclose the time evolution of such an ultrasmooth interface, another set of a-C:H:Si films grown at bias voltage of 2 kV were prepared with different deposition times. The surface morphology evolution measured by AFM is shown in Figure 2.4. The mirror-polished Si wafer possesses an ultrasmooth surface with roughness of ~0.12 nm (Figure 2.4(a)). At the onset of film deposition (Figure 2.4(b)), some nanosized grainy aggregates are formed on the bare Si substrate, causing a relatively high roughness (*R*a~0.148 nm). However, after a short deposition time of 5 min (Figure 2.4(c)), these grainy structures appear to merge and flatten the surface (*R*a~0.088 nm). Further depositions (30 min in Figure 2.4(d) and 60 min in Figure 2.4(e)) hardly smoothen the growing surface, indicating a saturation of the

roughness (*R*a~0.09 nm). As a consequence, after 3 h deposition (Figure 2.4(f)), the grown surface exhibits a featureless and ultrasmooth morphology with a roughness of 0.086 nm. The above results demonstrate that a dynamic smoothening process occurred under concurrent ion impingement during deposition of a-C:H:Si films.

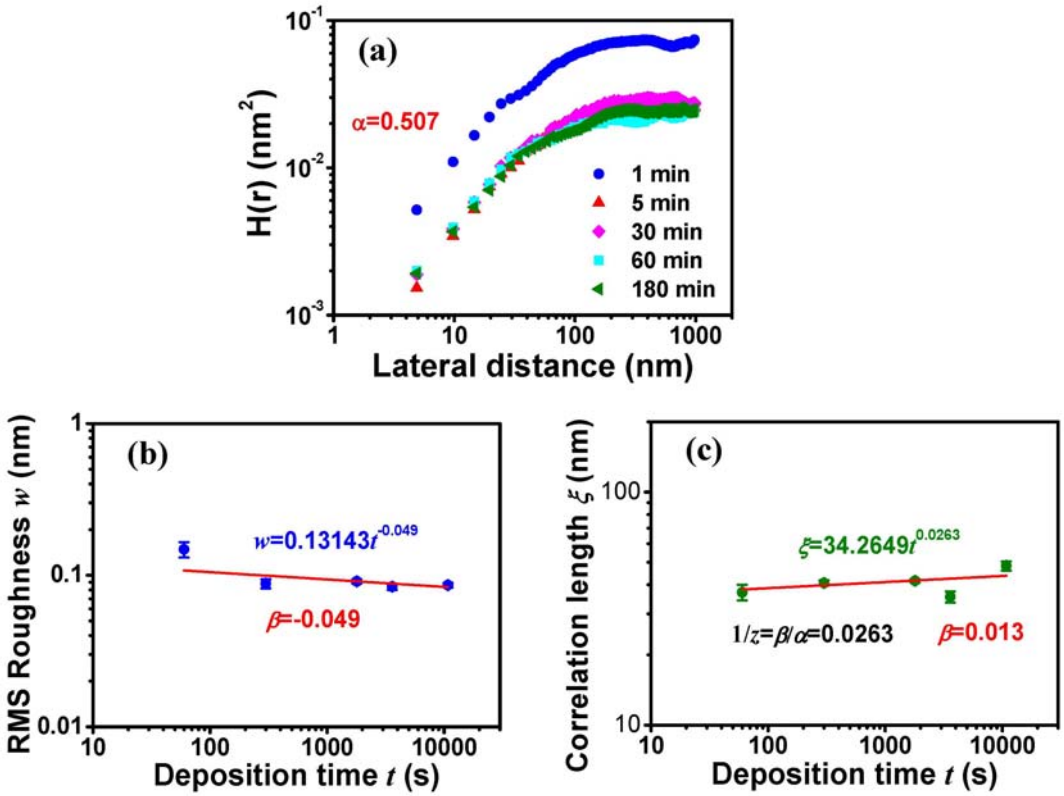

Figure 2.5 Dynamic scaling of a-C:H:Si films grown at bias voltage of 2 kV: (a) HCF curves for different deposition times, (b) RMS roughness w vs. deposition time t and the derived growth exponent β, and (c) lateral correlation length ξ vs. deposition time t and the derived growth exponent β.

The dynamic scaling behaviors of the as-grown a-C:H:Si surfaces are displayed in Figure 2.5. The downshift of HCF curve (Figure 2.5(a)) to a saturation position with respect to the deposition time confirms the dynamic smoothening process as observed in Figure 2.4. The corresponding calculated scaling parameters are presented in Table 2.1. The roughness exponent α gradually decreases from 0.516 to 0.471 as the deposition time increases, resulting in an average value of 0.507. The local slope m also shows a

decreasing trend from 0.00127 to 0.00027 with respect to the deposition time, originating from the elongated lateral correlation length ξ and the reduced interface width w. The dynamic evolutions of interface width w and correlation length ξ as a function of the deposition time are plotted in Figures 2.5(b) and 2.5(c), respectively. The corresponding calculated values for growth exponent β are -0.049 and 0.013, respectively. Thus, the scaling exponents for a representative ultrasmooth a-C:H:Si films grown form energetic ions at bias voltage of 2 kV are α~0.51 and β~0.

Table 2.1 Calculated scaling parameters of HCF curves as shown in Figure 2.5(a) and the RMS surface roughnesses of a-C:H:Si films grown at bias voltage of 2 kV for different deposition times.

Deposition time (s)	α	m	ξ (nm)	w (nm)	RMS (nm)
60	0.516	0.00127	37.1	0.148	0.148±0.002
300	0.538	0.00051	40.7	0.088	0.088±0.003
1800	0.516	0.00046	41.6	0.091	0.091±0.002
3600	0.494	0.00038	35.5	0.084	0.084±0.002
10800	0.471	0.00027	48.2	0.086	0.086±0.002

These exponents do not match any of the standard continuum growth models, such as Edwards-Wilkinson (EW, α=0, β=0) [2.33], Kardar-Parisi-Zhang (KPZ, α~0.38, β~0.24) [2.34] and Molecular Beam Epitaxy (MBE, α=1, β=0.25) [2.35]. However, a similar dynamic smoothening behavior has also been observed in ta-C films (α~0.39, β~0-0.1) deposited by filtered cathodic vacuum arc (FCVA) [2.29, 36, 37] or in TiC/a-C nanocomposite films (α~0.55, β~0) prepared by pulsed DC magnetron sputtering [2.38]. The former case assigns the smoothing mechanism of ta-C films to the carbon ion impact-induced downhill currents in the top layer of a growing film, while the latter condition proposes that the dynamic smoothening of TiC/a-C nanocomposite films arises from the shielding effect of 2 nm thick amorphous front layer. In both cases, the

authors emphasize the crucial influence of ion-impact induced surface diffusion and relaxation, which generally induces a growth exponent of β~0 [2.39]. Considering the present ion-dominating growth process, we expect that the dynamic smoothening behavior (β~0) of ultrasmooth a-C:H:Si films is also likely to be thermally activated by the energetic ion-impact induced subsurface 'polishing' process, i.e., local curvature flattening, surface diffusion and relaxation. However, special attention should be given to the considerable chemical etching effect during gas ionization deposition since it involves hydrogen, which does not exist for FCVA and non-reactive sputtering. Thus, the exact smoothening mechanism of a-C:H:Si films needs further experimental and simulation work to confirm.

2.3.2 Ion Energy Dependence of Structural Evolution of a-C:H:Si

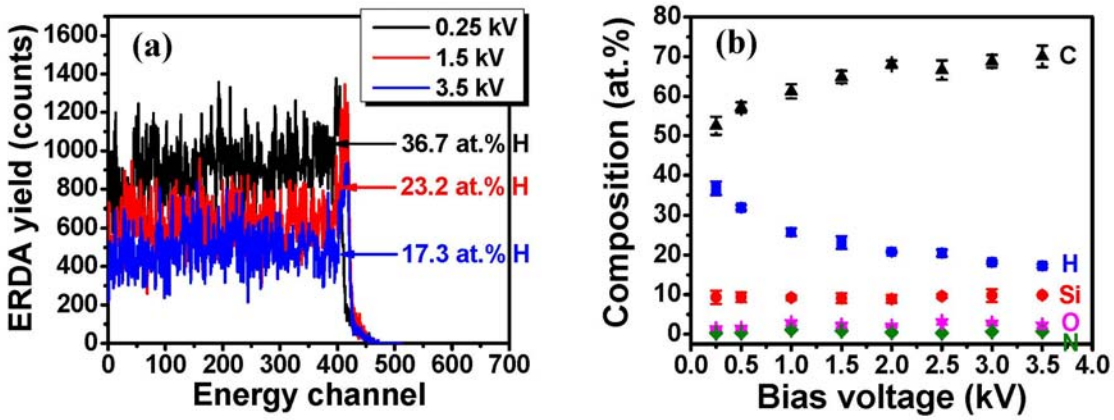

Figure 2.6 The composition of a-C:H:Si films: (a) representative ERDA spectra indicating the hydrogen content for different bias voltages, (b) evolution of elemental constitutions determined by ERDA and XPS, as a function of bias voltage.

The composition of as-grown a-C:H:Si films being dependent on bias voltage (i.e., incident ion energy) is indicated in Figure 2.6. The scatter yield of hydrogen recoils induced by 0.5 MeV N^+ irradiation from the samples prepared at three representative bias voltages of 0.25, 1.5 and 3.5 kV is shown in Figure 2.6(a). It can be seen that the

observed ERDA yield gradually decreases when increasing the bias voltage, and the derived average hydrogen contents in the films are 36.7 at.% (0.25 kV), 23.2 at.% (1.5 kV) and 17.3 at.% (3.5 kV), respectively. Figure 2.6(b) shows the evolution of overall constitutions determined by combining ERDA with XPS results as a function of bias voltage. The carbon content in the films gradually increases from 52.5 to 70.1 at.% when increasing the bias voltage from 0.25 to 3.5 kV, while the hydrogen content decreases significantly from 36.7 to 17.3 at.%. Meanwhile, the Si content is kept almost constant at ~9-10 at.%, irrespective of the bias voltage. It seems that the Si incorporation is only determined by the volume fraction of TMS in the mixture gas, reflecting that all the Si atoms from Si-containing fragments penetrate upon impact and are mostly incorporated into the growing film. In addition, a small amount of oxygen (i.e., 1-3 at.%) was present in all the as-grown a-C:H:Si films, as well as some traces of nitrogen remaining in the films. These results demonstrate that the loss of hydrogen atoms during deposition is promoted by higher incident ion energy, in which the light-element hydrogen is likely to be lost due to displaced desorption and/or re-sputtering of H by the incoming energetic ions.

The influence of ion energy on the evolution of bonding configurations of a-C:H:Si films can be analyzed from XPS C1s core level spectra. Before data collection, Ar^+ sputter was performed for 2 min to remove the contamination adsorbed on the surface. A relatively low accelerating voltage (i.e., 0.5 kV) was chosen to minimize the bombarding effect on the local atomic arrangement by Ar^+ ion sputtering. It is estimated that a sputter depth of ~10 nm could be achieved by this sputtering condition. Considering that the typical thickness of distinct subsurface layer of a-C:H film upon ion impact is just a few nanometer thick even in a high ion energy, the obtained XPS data after Ar^+ sputtering should reflect the bonding information of bulk layer. Note that Ar^+ bombardment might modify the bonding and the corresponding XPS spectra. Figure 2.7 shows the deconvoluted C1s peaks from three typical samples prepared at bias voltages of 0.25 kV (Figure 2.7(a)), 1.5 kV (Figure 2.7(b)) and 3.5 kV (Figure 2.7(c)),

and the corresponding evolution of each component as a function of bias voltage (Figure 2.7(d)). The deconvolution of spectra indicates that the broad C1s peaks consist of four well separated peaks corresponding respectively to C-Si (283.7±0.3 eV), C=C (284.5±0.1 eV), C-C (285.3±0.1 eV) and C-O (286.7±0.2 eV). The C=C peak positioned at 284.5 eV can be assigned to sp^2 bonding structure, while the sp^3 bonding configuration appears at lower binding energy of ~283.7 eV for C-Si bonds, or at higher binding energy of ~285.3 eV for C-C bonds.

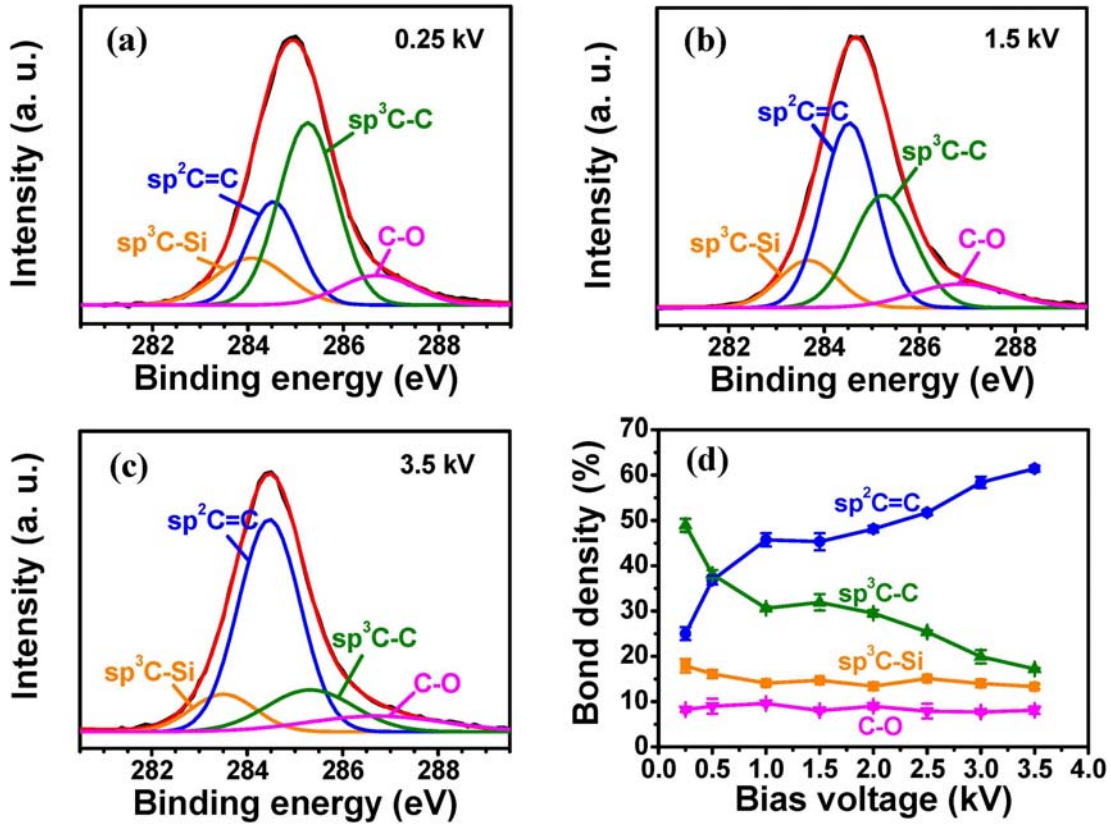

Figure 2.7 Deconvolution of the XPS C1s peaks obtained from a-C:H:Si films deposited at different bias voltages: (a) 0.25 kV, (b) 1.5 kV and (c) 3.5 kV, and (d) the corresponding evolution of carbon bonds as a function of bias voltage.

However, it should be pointed out that the sp^3 configuration located at ~285.3 eV stems from not only the C-C bonds but also the C-H covalent bonds. For instance, the C1s peak in Figure 2.7(a), from the sample grown at the lowest bias voltage of 0.25 kV,

displays a dominated sp^3 C-C peak among the four deconvoluted peaks. The formation of such a sp^3-rich structure is attributed to the high hydrogen content (36.7 at.%) in the film, which induces a polymeric carbon network containing a large fraction of C-H_n groups. In comparison, at an intermediate bias voltage of 1.5 kV (Figure 2.7(b)), the fraction of sp^3 C-C in the C1s peak is significantly reduced. Further increase in the bias voltage to 3.5 kV results in a sp^2-dominant structure in the film (Figure 2.7(c)). Figure 2.7(d) summarizes the evolution of each bond component in the C1s peaks as a function of bias voltage. As seen from this figure, the sp^2 C=C bond density continuously increases from ~25% to ~60% when increasing the bias voltage from 0.25 to 3.5 kV. This variation is in line with the Raman results (see discussion below). Meanwhile, the fraction of sp^3 C-C bond first decreases from ~50% to ~30% when increasing the bias voltage from 0.25 to 1.0 kV, and then maintains this fraction in the bias voltage range of 1.0-2.0 kV. Afterwards, it proceeds to decrease when further increasing the bias voltage up to 3.5 kV.

In the low bias voltage range, the decreasing of sp^3 C-C bond stems from the continuous hydrogen loss upon impact with increasing incident ion energy. The saturation of sp^3 C-C bond fraction in the intermediate bias voltage range is actually a compromising result from the decreasing of C-H bonds in the films and the formation of sp^3 C-C bonding under energetic ion impact. The reducing bond density of sp^3 C-C in the highly energetic conditions of ion bombardment (i.e., bias voltage of 2.5-3.5 kV) arises from the converting of sp^3 C-C to sp^2 C=C bonding structure. Furthermore, the sp^3-coordinated C-Si bond has a relatively high fraction of ~16-18% in low bias voltage range (i.e., 0.25-0.5 kV), and then maintains an almost constant fraction of ~13-14% in the raised bias voltage range (i.e., 1.0-3.5 kV). The occurrence of a noticeable higher fraction of Si-C bond at low bias voltages might be attributed to the lower content of C if considering the fact that C atoms are partly etched by H while Si atoms are not. This argument is confirmed, on one hand, by the almost constant Si content as shown in Figure 2.6(b), and on the other hand, by the FTIR results as will be discussed below. In

addition, a small amount of C-O bonds (i.e., 7-8%) are present in all the as-grown a-C:H:Si films, irrespective of the bias voltage.

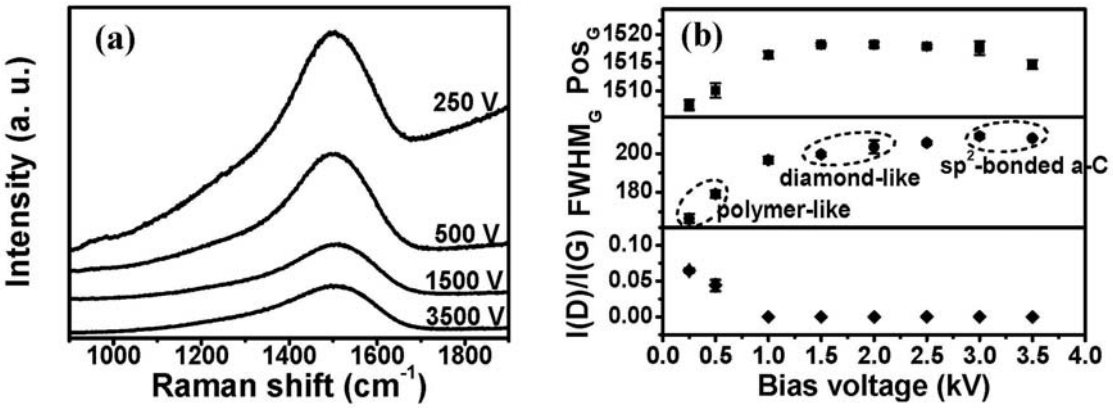

Figure 2.8 Visible Raman spectra indicating carbon bonding state of a-C:H:Si films: (a) representative Raman spectra for samples grown at different bias voltages, and (b) the corresponding evolution of deconvoluted Raman parameters including I(D)/I(G), FWHM(G) and Pos(G) as a function of bias voltage.

The carbon bonding state of a-C:H:Si films is further investigated by visible Raman spectroscopy, as shown in Figure 2.8. Raman spectroscopy can provide useful information mainly on the configuration of sp^2 sites and the size of sp^2 clusters [2.40]. Representative Raman spectra for samples grown at different bias voltages are displayed in Figure 2.8(a). The main spectral feature for all the measured spectra is typical of a-C:H films, with a broad band appearing in the range of 1300-1700 cm^{-1}. The most noticeable difference between these spectra is the gradually enhanced photoluminescence (PL) background with decreasing the bias voltage from 3.5 to 0.25 kV, implying a gradual increase of hydrogen content in the film and formation of more polymeric structure [2.41, 42]. A weak Si second-order peak at ~970 cm^{-1} observed for the sample grown at 0.25 kV is considered to originate from the increased transparency by hydrogen-induced polymeric structure. In general, the visible Raman spectrum can be deconvoluted into two modes, the *G*-peak around 1560 cm^{-1} and the *D*-peak around 1350 cm^{-1}. The *G*-peak is due to the stretching vibrations of all pairs of sp^2 atoms in

both rings and chains, while the *D*-peak is attributed to the breathing modes of sp^2 atoms from aromatic rings [2.40]. To derive further information from these spectra, we analyze them by fitting a Breit-Wigner-Fano (BWF) line shape for the *G*-peak, and a Lorentzian one for the *D*-peak. It should be pointed out that a single skewed BWF line shape is actually sufficient to obtain a reasonable fit for the films deposited at higher bias voltages (i.e., 1.0-3.5 kV) because the *D*-peak intensity is effectively zero for these films. However, it is necessary to include another Lorentzian one to derive the *D*-peak for the films deposited at lower bias voltages (i.e., 0.25-0.5 kV) due to a small residual in the region of about 1350 cm^{-1}. Details about this fitting procedure can be found in Refs. [2.43] and [2.44]. Figure 2.8(b) shows the derived *G*-peak position Pos(*G*), *G*-peak width FWHM(*G*) and relative intensity ratio of *D* and *G* peaks *I*(*D*)/*I*(*G*) as a function of bias voltage. It is observed that the intensity ratio *I*(*D*)/*I*(*G*) is small for low bias voltage, and it sharply falls to zero at bias voltage larger than 0.5 kV. Considering the continuous increase in the sp^2 bond density from XPS in Figure 2.7(d), it is thus concluded that the enhanced fraction of sp^2 phase mainly arises from the formation of sp^2-bonded olefinic chains instead of aromatic rings [2.40]. This phenomenon is thought to be derived from the suppression of ring-like sp^2 structure by Si atoms [2.1, 4, 5]. FWHM(*G*) is mainly sensitive to structural disorder, arising from bond angle and bond length distortions. FWHM(*G*) would be small if the sp^2 clusters are defect-free, unstrained (stress-free) or "molecular" [2.11, 40]. As seen in Figure 2.8(b), FWHM(*G*) increases gradually with bias voltage, indicating the structural evolution of a-C:H:Si films from low-disorder polymer-like grown from low-energy ions to diamond-like at intermediate ion energy, and finally to high-disordering sp^2-bonded a-C deposited at high ion energies. The shift of *G*-peak position is affected by several competing factors such as the presence of sp^2 chains or rings, clustering, bond disorder, sp^3 content and even stress state [2.40]. As shown in Figure 2.8(b), the derived *G*-peak position Pos(*G*) is much lower than that of a-C:H films (i.e., around ~1560 cm^{-1}), which is mainly attributed to the lowering of C=C vibration modes by the presence of heavier Si atoms

in the carbon network, and partially to the reduction in compressive stress since the longer de-strained C-Si bridging bonds vibrate at lower frequencies [2.2-4]. In addition, Pos(*G*) increases gradually with bias voltage, and shows a maximum at bias voltage of 1.5-2.5 kV, and then decreases slightly. Such a dependence of Pos(*G*) on bias voltage should be the competitive result from the increased fraction of sp^2 sites and the enhanced disordering with increasing bias voltage. Note that in general the visible Raman intensity of a-C:H films is proportional to the fraction of sp^2 phase. However, in the present case of a-C:H:Si films, the polymeric sample has higher intensity even if they have lower sp^2 content. The underlying origin is not clearly understood yet. Probably the excitation efficiency of laser is different in the distinct bonding structures such as polymeric, diamond-like or sp^2-bonded a-C in a-C:H:Si films.

FTIR is sensitive to hydrogen induced infrared vibration bands in amorphous carbon films in terms of energies and intensities of stretching and bending modes [2.45]. In general, three characteristic band regions can be detected in a-C:H:Si films: the $Si\text{-}H_n$ bending modes and Si-C stretching modes below 1300 cm^{-1}, the $Si\text{-}H_n$ stretching modes around 2125 cm^{-1}, as well as the $C\text{-}H_n$ stretching modes around 2900 cm^{-1} [2.2, 46]. Figure 2.9 shows the normalized FTIR spectra assigning to these three band regions from the representative samples grown at different bias voltages. As observed in Figure 2.9(a), the main spectral feature in the low wavenumber region is the two dominating absorption peaks from Si-C stretching modes located at 670 cm^{-1} and 780 cm^{-1}, respectively [2.46]. These two peaks are particularly significant when deposited at low bias voltage of 0.25 kV, and then become weakened as the bias voltage increases. A broad band around ~950-1050 cm^{-1} is attributed to the superimposition of the $Si\text{-}CH_3$ rocking or wagging mode (970 cm^{-1}) and $Si\text{-}(CH_2)_n\text{-}Si$ wagging mode (1000 cm^{-1}) [2.46]. The former mode is significant when the bias voltage is low (i.e., 0.25 kV), while the latter mode appears and becomes intensified as the bias voltage increases. The band observed at ~1260 cm^{-1} is ascribed to the symmetric bending mode of $Si\text{-}CH_3$ [2.47], which becomes featureless with increasing the bias voltage. Another noticeable

band attributed to the Si-H_n bending mode is observed around 650 cm^{-1} [2.47]. The presence of a peak at ~1100 cm^{-1} stems from the Si-O stretching vibration mode [2.48], which confirms the existence of oxygen in the a-C:H:Si films.

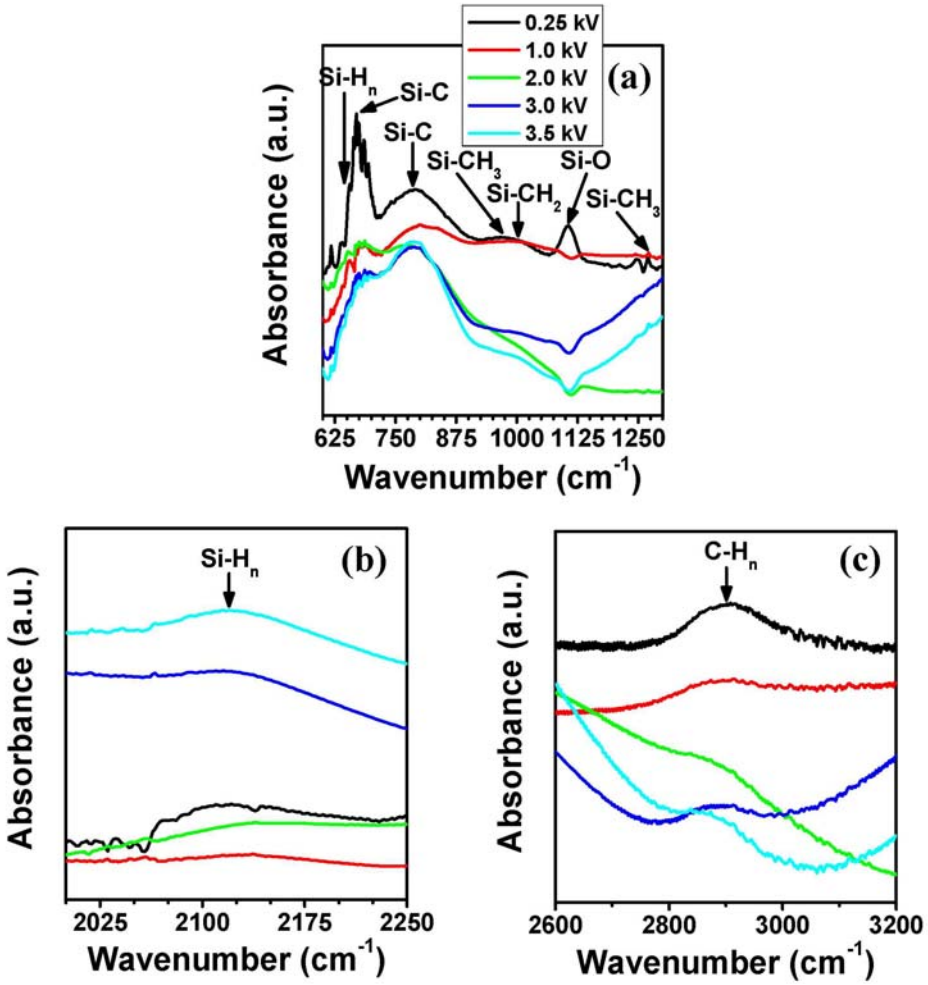

Figure 2.9 Normalized FTIR spectra indicating local chemical bonding state of a-C:H:Si films: (a) the Si-C stretching and Si-H_n bending modes below 1300 cm^{-1}, (b) the Si-H_n stretching modes around 2125 cm^{-1} and (c) the C-H_n bond stretching modes around 2900 cm^{-1}. Note that no reliable spectra could be measured in the 1300-2000 cm^{-1} range due to the strong noise effect from water vapor contribution.

The change trend observed in the Si-H_n stretching mode [2.46] around 2125 cm^{-1} provides additional information concerning the film's growth and structure, as shown in Figure 2.9(b). This band is obvious at bias voltage of 0.25 kV, and becomes featureless

when increasing the bias voltage to 1.0 kV. However, the band shape recovers and becomes more intense with increasing the bias voltage from 2.0 to 3.5 kV, indicating the high-energy ion bombardment promotes the re-saturation of Si atom by hydrogen. The C-H_n stretching mode around 2900 cm^{-1} shown in Figure 2.9(c) also confirms the gradual hydrogen loss process as the absorption band evolves from a distinctive shape to almost featureless curves as the bias voltage increases from 0.25 to 3.5 kV. The above analytical results demonstrate that the hydrogen incorporation or desorption upon ion bombarding and the produced carbon bonding network of the growing film are profoundly affected by the incident ion energy. At low bias voltage, the incident ions appear to be less energetic, leading to much less impacting effect, and thus produce films in which most dissociated hydrogen atoms upon penetration are bonding to or trapped in the growing film layer. For instance, the distinctive vibration bands such as Si-CH_3 and Si-H_n observed in the sample grown at 0.25 kV are likely to originate from the hydrogen bonding or re-saturation of the C and Si atoms during growth, while the enhanced Si-C band is derived from the decreasing C concentration due to chemical etching effect by abundant hydrogen. In comparison, high bias voltage increases the incident ion energy and promotes the replacement or re-sputtering of hydrogen by the incoming ions, resulting in a hydrogen deficient bonding network containing bridging, cross-linking or disordering units. Thus, depending on the ion energy, the grown film structure can exhibit more polymeric, diamond-like, or even sp^2-bonded a-C.

2.3.3 Nanomechanical and Viscoplastic Properties

Based on the above analysis, it is necessary to evaluate the nanomechanical properties of a-C:H:Si films and correlate their evolution with the structural and bonding characteristics. Figure 2.10 shows the dependence of nanoindentation hardness H, elastic modulus E, and residual stress σ on the applied bias voltage. As shown in Figure 2.10(a), the evolution of hardness has a close relationship with the carbon network structure as derived from XPS (Figure 2.7(d)), Raman (Figure 2.8(b)) and

FTIR (Figure 2.9). The relatively low hardness (~13.8 GPa) in polymeric structure produced at low bias voltage of 0.25 kV is due to the formation of H-terminated sp^3CH_n (n>1) bonding, which weakens the bonding constrains of tetrahedrally bonded C or Si atoms by bonding more H atoms, and thus reduces the hardness and relaxes the stress. Note that the hardness of polymeric sample (~13.8 GPa) is far larger than that of traditional organic polymers (i.e., ~0.5-2 GPa), but we still call it "polymer-like" due to their high H content and chain-developed bonding structure.

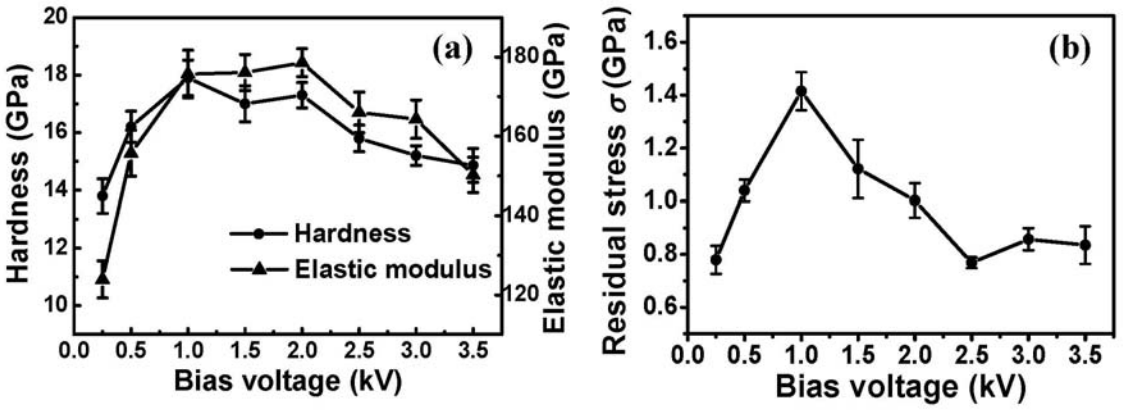

Figure 2.10 Nanomechanical properties of a-C:H:Si films: (a) variations of hardness *H* and elastic modulus *E* and (b) evolution of residual stress σ as a function of bias voltage.

On the other hand, the hardness gradually increases up to ~17-18 GPa with increasing the bias voltage to the range of 1.0-2.0 kV as the bonding structure evolves from soft polymeric to hard diamond-like. These hard a-C:H:Si films are deposited under intense ion bombardment where incident ions preferentially displace or re-sputter the hydrogen atoms, while subplantation of carbon ions increases the local C-C bond density and promotes the cross-linking of carbon network [2.10]. Meanwhile, the increase of sp^3 fraction due to subplantation process increases the internal stress since the quaternary bonding C-atoms result in over-constrained network as well as increased coordination number [2.10]. Further increasing in the bias voltage to a high value causes a continuous degradation of hardness as the film bonding structure becomes more

amorphous (Figure 2.8) due to the deep hydrogen deficiency and sp^3-to-sp^2 conversion under highly energetic ion bombardment. A similar variation trend depending on the bias voltage is also observed for the measured elastic modulus, as shown in Figure 2.10(a). The stress state presented in Figure 2.10(b) confirms the above argument, that is, the grown a-C:H:Si films display significantly low residual stresses (~0.8 GPa) in polymer-like and sp^2-bonded a-C structures while possessing a relatively high compressive stress (~1.4 GPa) inherent in hard diamond-like network.

The rheological properties of materials play important roles in determining the interfacial behaviors between two processing surfaces, for example, the sliding contact interface under pressure. Previous work has pointed out that hydrogen incorporation affects significantly the flexibility of carbon network (i.e., viscoplasticity) and the surface chemistry in a-C:H films, especially in hydrogen-rich polymeric structure [2.17, 32]. The capability of polymeric structures to deform depends on their ability to adjust their chain conformation on a molecular level, and the mobility of molecular units with their structural arrangements leads to a strain rate dependence of hardness in nanoindentation tests [2.49].

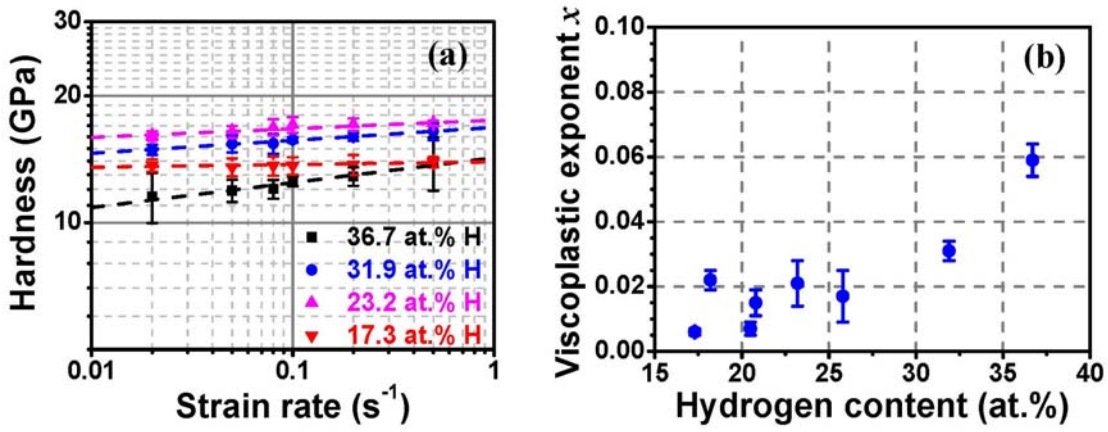

Figure 2.11 The viscoplastic behaviors of a-C:H:Si films: (a) evolution of hardness with respect to strain rate for representative samples with different hydrogen contents, and (b) correlation between the derived viscoplastic exponent x and the hydrogen content.

Figure 2.11 presents the viscoplastic behaviors of a-C:H:Si films with respect to the hydrogen content incorporated in the films. The log-log plots of the hardness vs. strain rate from four representative samples with different hydrogen contents are indicated in Figure 2.11(a). According to the Norton-Hoff law (a power law function) described previously, the viscoplastic exponent x could then be obtained by linear fitting on the log-log plot. There seems to be a rough tendency that the slope (viscoplastic exponent x) of these fitting lines increases with the hydrogen content, indicating an enhanced viscoplastic property. The derived viscoplastic exponent values as a function of hydrogen content for all the as-grown samples are summarized in Figure 2.11(b). It seems that the viscoplastic exponent falls into a low value range of around 0.005-0.02 when hydrogen content is lower than 30 at.%. No distinct correlation between them can be found. However, the viscoplastic exponent increases sharply when the hydrogen content exceeds 30 at.%, and obtains a value of ~0.06 for the sample with the maximum hydrogen content of 36.7 at.%. This variation is consistent with a more polymeric and less cross-linked structure as verified by XPS, Raman and FTIR results above.

2.3.4 Superlubricity in Dry Nitrogen

It has been well documented that the friction reduction effect of hydrogen in a-C:H films is attributed to the passivation of dangling bonds by the formation of C-H bonds at sliding contact interface [2.16, 17, 50]. The hydrogen passivation can dramatically change the direction of material transfer and largely inhibit adhesive interaction between two contact surfaces [2.51]. The friction force ranging from strikingly large to vanishingly small depends to a large extent on the hydrogen content as well as the carbon network organization such as ring-like structure [2.17]. Thus, a near-frictionless state, often referred as “superlubricity”, is obviously of high interest both from the basic scientific perspective of tribology and from the promising applications. However, the possibility to obtain such a superlubric state and the underlying mechanism being dependent on hydrogen content have not been investigated so far in a-C:H:Si films.

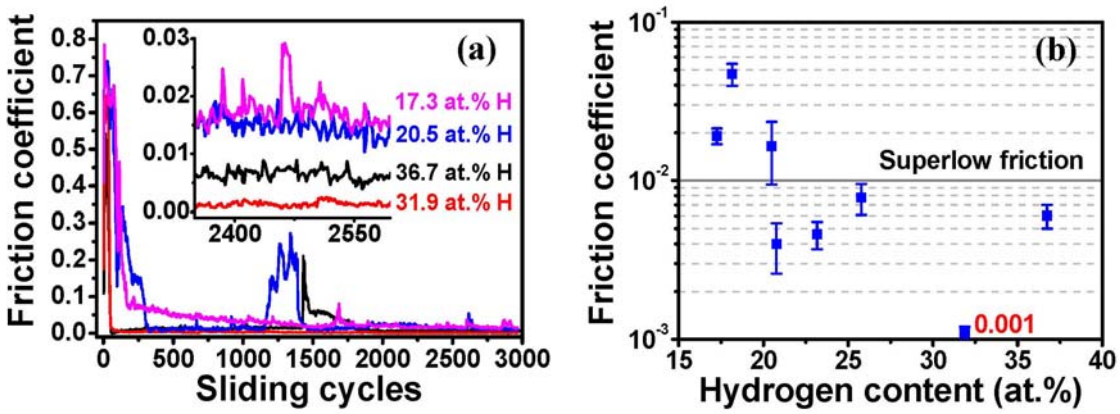

Figure 2.12 (a) Representative friction coefficient curves of a-C:H:Si films with different hydrogen contents tribotested in dry N_2. The inset figure shows the magnified friction curves in steady state. (b) Hydrogen dependence of average steady-state friction coefficient, indicating the existence of a superlow friction region when H>20 at.%.

Figure 2.12(a) shows the friction coefficient curves tribotested in dry N_2 atmosphere from four representative a-C:H:Si samples with different hydrogen contents. It can be obviously seen that for all the tested samples the friction coefficient evolves into a stable state after an intensive running-in period (i.e., initial friction coefficient around 0.5-0.8). Note that the running-in period differs significantly in the processing cycles with respect to the hydrogen content in the films: ~55 cycles (36.7 at.% H), ~75 cycles (31.9 at.% H), ~300 cycles (20.5 at.% H) and ~1500 cycles (17.3 at.% H), respectively. In addition to the prolonged running-in period, a considerable number of vibrations in friction coefficients are observed for hydrogen deficient samples, i.e., 20.5 at.% and 17.3 at.% hydrogen-containing films. The inset figure presents the magnified friction coefficient curves in the stable state. A superlow friction coefficient (~0.001) is recorded for the sample with hydrogen content of 31.9 at.%, indicating completely vanishing of friction. Note that the superlubricity is generated by the formation of a transfer layer. The initial friction of the original pristine layer is very large and thus running-in is required to obtain superlubricity. A somewhat increased but still extremely low friction coefficient (~0.006) is also observed for the sample hydrogenated to 36.7 at.%. This is beyond our expectation when considering the fact that more sufficient

hydrogen passivation on the contact surface should provide more effective lubricating effect. Further work is needed to clarify the underlying mechanism. In contrast, the friction coefficients obtained for hydrogen deficient samples just approach a quasi-superlubric state: 0.016 for 20.5 at.% H and 0.019 for 17.3 at.% H, respectively. In addition, the amplitude of fluctuations existed in the friction curves is strengthened with decreasing the hydrogen content in the films, which is indicative of worsening stability of superlubric state. Figure 2.12(b) summarizes the hydrogen dependence of average steady-state friction coefficient measured in dry N_2 for the as-grown a-C:H:Si films. There seems to be a hydrogen content threshold (H>20 at.%) for the energetic ion grown ultrasmooth a-C:H:Si films to exhibit superlow friction in dry inert gas atmosphere.

2.4 Discussion

Numerous work has emphasized the paramount role of incident ion energy during growth in determining the bonding structure and mechanical properties of amorphous carbon films [2.52-54]. Several theoretical models have been proposed for describing the growth process of amorphous carbons from energetic species, including subplantation [2.55, 56], thermal spike [2.57], compressive stress [2.58] and atomic peening [2.59]. The most widely accepted subplantation model attributes the formation of sp^3 bonding to an equilibrium process between densification (local density increment) and relaxation. Experimental and simulation results have predicted that surface penetration occurs for ions with energies larger than 30-40 eV (referred as threshold energy E_p) [2.10].

Here, we take the average kinetic energy per atom E_{at} as the controlling parameter for growth process in a-C:H:Si films. For an incident molecular ion m_0 with kinetic energy E_0, it will break up into atoms upon impact on the film surface and share their kinetic energy between the individual atoms. Each atom m_i will have energy: $E_i=(m_i/m_0)E_0$. Note that a small energy must be subtracted from E_0 to break each

individual bonding between atoms in the molecule [2.10]. Considering the bias voltages used in this work (0.25-3.5 kV), the calculated E_{at} for atoms in the dominant growth clusters such as $Si(CH_3)_3$ are as follows: E_{Si}≈96-1342 eV for Si, E_C≈41-575 eV for C and E_H≈3.4-48 eV for H, respectively. In addition, the E_H for H atom in the second abundant cluster H_2 can range from 125 to 1750 eV. Thus, a considerable number of impact atoms with different energy levels existed upon penetration even under the lowest accelerating voltage of 0.25 kV. It should be pointed out that most of the bombarding H atoms involved in film growth come from the impact dissociation of the $Si(CH_3)_3$ molecules (consisting of 9 H-atoms per molecule) due to their high fraction in the incoming ion flux (~37%, see Figure 2.2(b)). The H atoms deriving from H_2 molecules (~7%) in the ion flux upon impact just make a small contribution to the total bombarding H atoms. The incoming of these energetic clusters onto growing surface results in atomic penetration, sputtering of atoms and local structure arrangement due to the intensive bombardment effect.

Table 2.2 Summary of growth conditions and scaling exponents of ultrasmooth amorphous carbon or silicon based films grown from different energetic ion systems.

Film type	Growth method	Ion-accelerating system	Ion energy (eV)	RMS-*Ra* (nm)	α	β	Ref.
ta-C	FCVA	Self-bias	20-40	0.1	~0.39	~0-0.1	2.29, 36, 37
ta-C	HCA	Self-bias	20-40	0.12	~0.39	~0-0.1	2.36
a-C	MS	Bias	-	0.05-0.2	-	~0	2.36
ta-C:H	ECWR	Self-bias	~78	0.11	0.32	0.09	2.60
TiC/a-C	MS	Pulsed DC bias	40	0.2	~0.55	~0	2.38
a-C:H	ECR-CVD	DC bias	≥120	0.1-0.16	0.1	~0	2.61
a-C:H	MS	Pulsed bias	-	1.3	0.18	0.21	2.62
a-CN:H	ECR-CVD	DC bias	≥90	0.1-0.2	~0	-	2.63
a-Si:H	PECVD	-	-	0.3-2	-	0.28	2.64
a-C:H:Si	IVD	Pulsed bias	~30-~600	~0.1	0.51	~0	this work

Under this energetic bombardment, a dynamic smoothing behavior of growing interface is expected to correlate with the material redistribution in a localized region. The recent "atomistic impact-induced downhill current" model successfully explains the suppression of the surface roughening process by redeposition of atoms from hills into valleys due to the dominant lateral re-emission of atoms [2.37]. The tops of hills are sputtered more efficiently than slopes or valleys. Sufficient energy transferred to the re-emitted atoms motivates their enhanced surface diffusion and relaxation, thus, facilitating the flattening of the hills between the valleys [2.37].

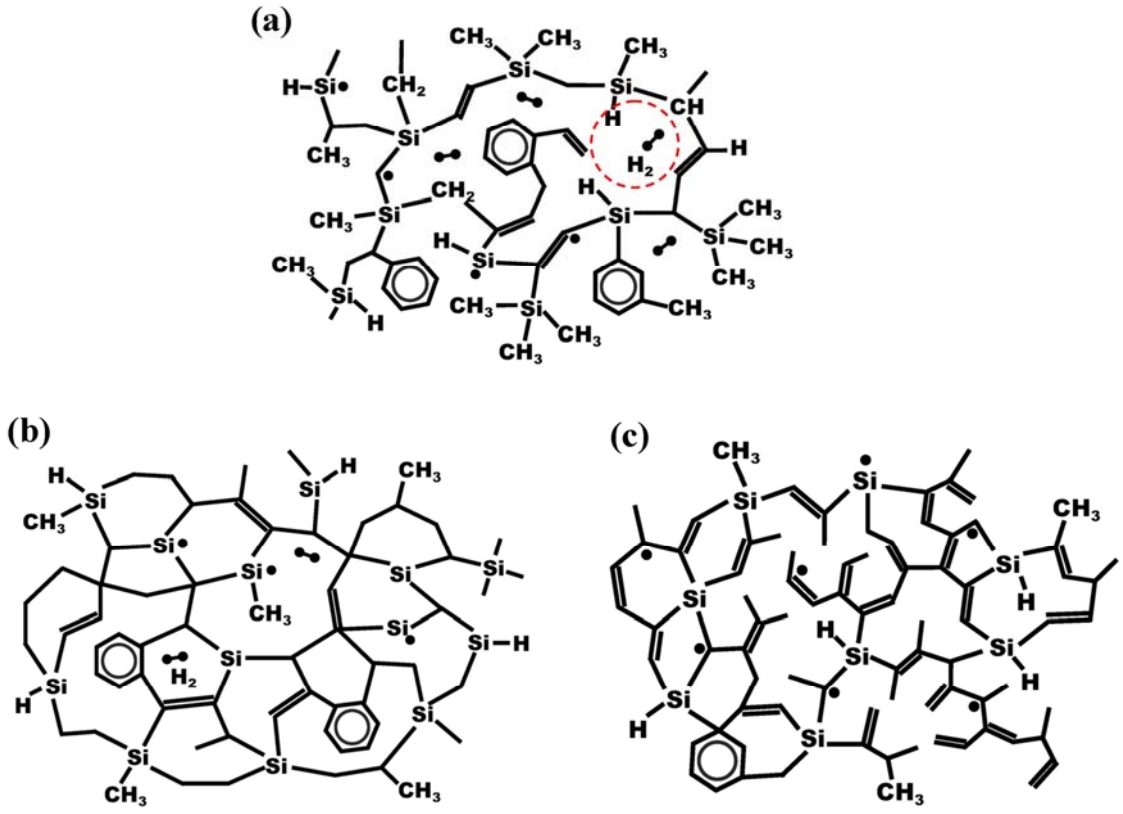

Figure 2.13 Structural models proposed for a-C:H:Si films grown from tetramethylsilane and toluene mixtures in different ion energy regions: (a) chain-developed polymer-like structure under low ion energy, (b) cross-linked diamond-like structure under moderate ion energy and (c) mainly-sp^2-bonded a-C structure under high ion energy.

The above speculation is also valid for the as-grown a-C:H:Si films by the observed ultrasmooth surface (Ra~0.1 nm) with an extremely small growth exponent β~0. Table 2.2 compares the present work with other ultrasmooth films concerning the growth conditions and scaling exponents reported in different energetic systems. Obviously, nano or even subnano-scale ultrasmoothness can be obtained in a wide range of ion energy irrespective of the growth method, indicating the existence of a universal mechanism underlying such smoothening process. Moreover, a minimum incident ion energy (i.e., 20-30 eV) seems to be required for activating such smoothening behaviors. This value is quite close to the threshold energy of surface penetration E_p=30-40 eV mentioned above. In addition, an extremely low or near-zero growth exponent β is always a distinctive feature for such ultrasmooth surfaces, which further confirms the smoothening effect of surface diffusion and relaxation during film deposition [2.39]. Molecular dynamics (MD) simulation of deposition progresses involving subplantation has predicted that surface processes are dominant for deposition at incident ion energy below 30 eV, while subsurface processes govern the structure formation at higher energies of ion impingement [2.65]. As noted in Figure 2.3, the RMS roughness of a-C:H:Si films saturates at ~0.1 nm except for some little scatter effect in the low bias voltage range. This observation points out the association of roughening to surface processes and smoothening nature to subsurface processes for carbon films grown from energetic ions irrespective of their structures (i.e., hydrogen content, sp^3 fraction). This is further interpreted by the downhill current model in amorphous carbon films that the impact-induced diffusion smoothening strength increases linearly with the energy of incoming ions up to ~120 eV, and then it saturates because for higher energies ions penetrate into the subsurface layer and release a part of the impact energy in the bulk [2.37]. Note that all amorphous carbon films deposited from energetic ions have an uppermost thin sp^2 layer so that the smooth layer is predominantly sp^2-rich even for ta-C films. This is particularly true for sp^2-rich films grown from high energy of ~keV, in which the bulk sp^3 fraction is less than 50% but their roughness is still very low and

similar to that of ta-C films [2.66]. However, as mentioned above, the chemical etching effect by hydrogen should also play a crucial role in modifying the growing interface during gas ionization deposition of a-C:H:Si films. Further work is needed to uncover the underlying mechanism.

Considering the determinative role of carbon atom in a-C film forming, we divide the ion-surface interaction processes according to the calculated carbon atom energy E_C in the main growth clusters into low- (dozens of eV), moderate- (around 100-250 eV) and high-energy (several hundreds of eV) ones as compared to the penetration energy threshold E_p. Depending on the accelerating energy, the ion-surface interactions during deposition of a-C:H:Si films can vary from shallow penetration to subplantation to deep implantation [2.65, 67, 68]. An interaction is considered to be low energy when E_C is below or just close to E_p under low bias voltage such as 0.25 kV, i.e., E_C~41 eV in cluster $Si(CH_3)_3$, E_C~33 eV in cluster C_7H_8. Such a growth pattern can be classified as shallow penetration, in which the impact carbon ions just penetrate the growing surface and make bonds within the film. Meanwhile, the Si atoms penetrate deeper and are trapped in the film due to their higher energy (i.e., E_{Si}~96 eV in main cluster $Si(CH_3)_3$) while the low energy hydrogen atoms (E_H~3.4 eV) mainly concentrate at the topmost layer. To large extent, these abundant hydrogen atoms saturate or even preferentially etch off the carbon atoms, which results in a relatively lower content of C (Figure 2.6(b)). In addition, considerable high energy hydrogen atoms (E_H~125 eV) from impact dissociation of H_2 clusters can penetrate deeper and re-saturate C and Si atoms along the penetration depth. Thus, the distribution profiles of C, Si and H overlap to a certain degree in this low energy interaction condition. Note that some atoms knocked into the film might displace back to the surface with voids left, creating a porous, low density region. Therefore, a chain-connected polymer-like structure is developed for a-C:H:Si films grown from low energetic ions, as illustrated in Figure 2.13(a). A large number of sp^3-bonded CH_3 groups along with considerable Si-H bonds are present in the film. These methyl terminations are connected through numerous Si-C bridging

bonds and/or C-C bonds to the backbones of the film bonding network. The capability to deform and the mobility of such a chain structure with their structural arrangements under contact pressure is the origin of a viscoplastic behavior in polymer-like material [2.49], as confirmed by a high viscoplastic exponent in Figure 2.11(b). In addition, quite a few unbound hydrogen molecules are probably to be formed and trapped in the lattice interstices in the case of hydrogen abundance at low bias voltage. The presence of such molecular hydrogen in polymeric a-C:H:Si films is considered to promote the formation of porous structure and a loss of connectivity in the host material. However, these polymeric a-C:H:Si films exhibit the most stable and lowest friction coefficients (Figure 2.12) in dry N_2, for which the sufficient existence of hydrogen-terminated C-H_n and Si-H_n groups along with the trapped molecular hydrogen should be the reason. A similar polymeric structure in a-SiC:H films grown form TMS under high gas pressure was reported by Rynders [2.69].

On the other hand, a moderate ion energy (E_C~100-250 eV, bias voltage range of 1-2 kV) results in intensive subplantation of the carbon ions into the growing subsurface. This interaction causes a significant loss of hydrogen atoms by preferential displacement of bonded hydrogen in a collision cascade: penetrating ions displace predominantly the bonded hydrogen due to the smaller threshold energy for displacement of hydrogen (2.5 eV) compared to that of carbon (25 eV) [2.70]. The displaced hydrogen atoms can recombine with a lattice defect or form H_2 molecules by recombination with another displaced H atom. These H_2 molecules are either trapped in internal voids or diffuse to the surface and desorb [2.70]. As a consequence, the hydrogen content decreases with increasing ion energy, which enhances the cross-linking of the film network by continuous formation of C-C and Si-C bonds (see Figure 2.13(b)). Meanwhile, the penetration and densification under this ion energy range increases the local density, compressive stress and sp^3-carbon fraction, thus, increasing the hardness as shown in Figure 2.10. It should be noted that these diamond-like a-C:H:Si films can still exhibit superlow friction in dry N_2 but the stability

of superlubricity is degraded to some extent due to hydrogen deficiency, which is reflected by lots of fluctuations in the friction curves as shown in Figure 2.12(a). When carbon ion energy is in the range from several hundreds of up to ~600 eV (i.e., 3.5 kV), much higher than E_p, the incoming ion clusters undergo severe collisions with the growing surface and the dissociated atoms implant into much deeper subsurface. The excess energy is dissipated and this causes a relaxation of sp^3 bonding back to sp^2 [2.71]. Meanwhile, hydrogen atoms are continuously lost due to displaced desorption or even re-sputtering of H by the incoming energetic ions. A more sp^2-bonded amorphous structure is thus developed under this high ion energy condition, as shown in Figure 2.13(c). Note that this sp^2-bonded structure of a-C:H:Si is dominantly rich in sp^2 olefinic bonds (Figure 2.8) instead of graphitic ones, which are frequently observed in pure a-C:H films deposited under high ion energy. The present case is mainly attributed to the suppression of ring-like structure by Si atoms incorporated in the films, as confirmed by MD simulation [2.5]. As noticed in Figure 2.12, these hydrogen-deficient a-C:H:Si films are unable to present superlubric state but still can exhibit ultralow friction coefficient, i.e., ~0.02-0.05.

2.5 Summary

Using ion vapor deposition system, a series of a-C:H and a-C:H:Si films have been grown from ionization of toluene and toluene/tetramethylsilane mixture, respectively, to investigate the growth mechanism and structural evolution being dependent on the ion energy (bias voltage). The roughness of the as-grown a-C:H:Si films is extremely low (~0.1 nm), and the derived roughness exponent and growth exponent are α~0.51 and β~0, respectively. The extremely small growth exponent during ion dominated deposition requires the presence of energetic ion-impact induced subsurface “polishing” process, i.e., local curvature flattening, surface diffusion and relaxation. With increasing the bias voltage from 0.25 to 3.5 kV, the hydrogen content in a-C:H:Si films decreases gradually from 36.7 to 17.3 at.%, while the carbon content in the films increases

correspondingly from 52.5 to 70.1 at.%. Meanwhile, the Si content is kept almost constant at ~9-10 at.% for a fixed gas ratio of TMS/C_7H_8, irrespective of the bias voltage. Depending on the incident ion energy, the bonding structure of a-C:H:Si films evolves from hydrogen-rich chain-developed polymer-like, to hard cross-linked diamond-like, and finally to hydrogen-deficient sp^2-bonded a-C. The measured nanomechanical properties confirm the structural characteristics of the above a-C:H:Si films grown in different ion energy regions. An enhanced viscoplastic behavior is observed for polymeric a-C:H:Si films. A threshold in hydrogen content at around ~20 at.% seems to be necessary for achieving superlow friction in dry N_2 atmosphere. However, more stable and durable superlubric state is feasible when hydrogen content is higher than 30 at.%, i.e., extremely low friction coefficient of ~0.001 for polymer-like a-C:H:Si film.

References

[2.1] X. M. He, K. C. Walter, M. Nastasi, S.-T. Lee, M. k. Fung. Investigation of Si-doped diamond-like carbon films synthesized by plasma immersion ion processing. *J. Vac. Sci. Technol. A* **2000**, 18, 2143-2148.

[2.2] B. Racine, A. C. Ferrari, N. A. Morrison, I. Hutchings, W. I. Milne, J. Robertson. Properties of amorphous carbon–silicon alloys deposited by a high plasma density source. *J. Appl. Phys.* **2001**, 90, 5002-5012.

[2.3] J. F. Zhao, P. Lemoine, Z. H. Liu, J. P. Quinn, P. Maguire, J. A. McLaughlin. A study of microstructure and nanomechanical properties of silicon incorporated DLC films deposited on silicon substrates. *Diamond Relat. Mater.* **2001**, 10, 1070-1075.

[2.4] P. Papakonstantinou, J. F. Zhao, P. Lemoine, E. T. McAdams, J. A. McLaughlin. The effects of Si incorporation on the electrochemical and nanomechanical properties of DLC thin films. *Diamond Relat. Mater.* **2002**, 11, 1074-1080.

[2.5] T. Kumagai, S. Sawai, J. Choi, S. Izumi, T. Kato. Nanostructural interpretation for elastic softening of amorphous carbon induced by the incorporation of silicon and hydrogen atoms. *J. Appl.*

Phys. **2010**, 107, 124315.

[2.6] A. Varma, V. Palshin, E. I. Meletis. Structure–property relationship of Si-DLC films. *Surf. Coat. Technol.* **2001**, 148, 305-314.

[2.7] S. C. Ray, C. W. Bao, H. M. Tsai, J. W. Chiou, J. C. Jan, K. P. Krishna Kumar, W. F. Pong, M.-H. Tsai, W.-J. Wang, C.-J. Hsu, T. I. T. Okpalugo, P. Papakonstantinou, J. A. McLaughlin. Electronic structure and bonding properties of Si-doped hydrogenated amorphous carbon films. *Appl. Phys. Lett.* **2004**, 85, 4022-4024.

[2.8] G. A. Abbas, P. Papakonstantinou, J. A. McLaughlin, T. D. M. Weijers-Dall, R. G. Elliman, J. Filik. Hydrogen softening and optical transparency in Si-incorporated hydrogenated amorphous carbon films. *J. Appl. Phys.* **2005**, 98, 103505.

[2.9] H. Nakazawa, R. Osozawa, T. Okuzaki, N. Sato, M. Suemitsu, T. Abe. Effects of hydrogen on the properties of Si-incorporated diamond-like carbon films prepared by pulsed laser deposition. *Diamond Relat. Mater.* **2011**, 20, 485-491.

[2.10] J. Robertson. Diamond-like amorphous carbon. *Mater. Sci. Eng. R* **2002**, 37, 129-281.

[2.11] C. Casiraghi, A. C. Ferrari, J. Robertson. Raman spectroscopy of hydrogenated amorphous carbons. *Phys. Rev. B* **2005**, 72, 085401.

[2.12] Y. T. Pei, N. G. Chechenin, P. N. Chernykh, A. A. Turkin, D. Vainshtein, J. Th. M. De Hosson. On the quantification of unbound hydrogen in diamond-like carbon-based thin films. *Scripta Mater.* **2009**, 61, 320-323.

[2.13] V. I. Ivanov-Omskii, M. P. Korobkov, B. R. Namozov, E. A. Smorgonskaya, S. G. Yastrebov. Optical observation of bonded and quasi-free hydrogen in diamond-like carbon. *Diamond Relat. Mater.* **1999**, 8, 545-548.

[2.14] A. C. Y. Liu, R. Arenal, D. J. Miller, X. Chen, J. A. Johnson, O. L. Eryilmaz, A. Erdemir, J. B. Woodford. Structural order in near-frictionless hydrogenated diamondlike carbon films probed at three length scales via transmission electron microscopy. *Phys. Rev. B* **2007**, 75, 205402.

[2.15] J. Houska, J. E. Klemberg-Sapieha, L. Martinu. Formation and behavior of unbonded hydrogen in a-C:H of various compositions and densities. *Surf. Coat. Technol.* **2009**, 203, 3770-3776.

[2.16] A. Erdemir, O. L. Eryilmaz, G. Fenske. Synthesis of diamondlike carbon films with superlow friction and wear properties. *J. Vac. Sci. Technol. A* **2000**, 18, 1987-1992.

[2.17] A. Erdemir, C. Donnet. Tribology of diamond-like carbon films: recent progress and future prospects. *J. Phys. D Appl. Phys.* **2006**, 39, R311-R327.

[2.18] E. Braca, J. M. Kenny, D. Korzec, J. Engemann. Transition from polymer-like to diamond-like carbon coatings synthesized by a hybrid radiofrequency microwave plasma source. *Thin Solid Films* **2001**, 394, 29-38.

[2.19] K.-R. Lee, M.-G. Kim, S.-J. Cho, K. Y. Eun, T.-Y. Seong. Structural dependence of mechanical properties of Si incorporated diamondlike carbon films deposited by RF plasma-assisted chemical vapour deposition. *Thin Solid Films* **1997**, 308-309, 263-267.

[2.20] A. L. Baia Neto, R. A. Santos, F. L. Freire Jr., S. S. Camargo Jr., R. Carius, F. Finger, W. Beyer Relation between mechanical and structural properties of silicon-incorporated hard a-C:H films. *Thin Solid Films* **1997**, 293, 206-211.

[2.21] Y. J. Chabal, C. K. N. Patel. Molecular hydrogen in a-Si:H. *Rev. Mod. Phys.* **1987**, 59, 835-844.

[2.22] C. Weissmantel, H.-J. Erler, G. Reisse. Ion beam techniques for thin and hard film deposition. *Surf. Coat.* **1979**, 86, 207-221.

[2.23] C. Weissmantel, G. Reisse, H.-J. Erler, F. Henny, K. Bewilogua, U. Ebersbach, C. Schürer, *Thin Solid Films* **1979**, 63, 315-325.

[2.24] C. Weissmantel. Preparation, structure, and properties of hard coatings on the basis of i-C and i-BN. In *Thin Films From Free atoms and Particles*, edited by K. J. Klabunde, Academic Press, Orlando, 1985, pp. 153-201.

[2.25] A.-L. Barabasi, H. E. Stanley. *Fractal Concepts in Surface Growth*, Cambridge University Press, New York, 1995.

[2.26] F. Family, T. Vicsek. Scaling of the active zone in the Eden process on percolation networks and the ballistic deposition model. *J. Phys. A Math Gen* **1985**, 18, L75-L81.

[2.27] F. Family, T. Vicsek. *Dynamics of Fractal Surfaces*, Cambridge University Press, New York, 1995.

[2.28] Y. P. Zhao, G.-C. Wang, T.-M. Lu. *Characterization of amorphous and crystalline rough surface: principles and applications*, Academic Press, London, 2001.

[2.29] C. Casiraghi, A. C. Ferrari, R Ohr, A. J. Flewitt, D. P. Chu, J. Robertson. Dynamic roughening of tetrahedral amorphous carbon. *Phys. Rev. Lett.* **2003**, 91, 226104.

[2.30] V. D. Jardret, W. C. Oliver. Viscoelastic behavior of polymer films during scratch test: a quantitative analysis. In *Thin Films: Stress and Mechanical Properties VIII, Materials Research Society Symposium Proceedings*, edited by P. Besser, E. Shaffer II, O. Kraft, N. Moody and R. Vinci, Materials Research Society, Pennsylvania, 2000, Vol. 594, pp. 251-256.

[2.31] G. Hochstetter, A. Jimenez, J. L. Loubet. Strain-rate effects on hardness of glassy polymers in the nanoscale range. Comparison between quasi-static and continuous stiffness measurements. *J. Macromol. Sci. B* **1999**, 38, 681-692.

[2.32] J. Fontaine, J. L. Loubet, T. Le Mogne, A. Grill. Superlow friction of diamond-like carbon films: a relation to viscoplastic properties. *Tribol. Lett.* **2004**, 17, 709-714.

[2.33] S. F. Edwards, D. R. Wilkinson. The surface statistics of a granular aggregate. *Proc. R. Soc. Lond. A* **1982**, 381, 17-31.

[2.34] M. Kardar, G. Parisi, Y.-C. Zhang. Dynamic Scaling of Growing Interfaces. *Phys. Rev. Lett.* **1986**, 56, 889-892.

[2.35] S. Das Sarma, P. Tamborenea. A new universality class for kinetic growth: one-dimensional molecular-beam epitaxy. *Phys. Rev. Lett.* **1991**, 66, 325-328.

[2.36] C. Casiraghi, A. C. Ferrari, J. Robertson. The smoothness of tetrahedral amorphous carbon. *Diamond Relat. Mater.* **2005**, 14, 913-920.

[2.37] M. Moseler, P. Gumbsch, C. Casiraghi, A. C. Ferrari, J. Robertson. The ultrasmoothness of diamond-like carbon surfaces. *Science* **2005**, 309, 1545-1548.

[2.38] Y. T. Pei, K. P. Shaha, C. Q. Chen, R. van der Hulst, A. A. Turkin, D. I. Vainshtein, J. Th. M. De Hosson. Growth of nanocomposite films: from dynamic roughening to dynamic smoothening. *Acta Mater.* **2009**, 57, 5156-5164.

[2.39] P. Tamborenea, S. Das Sarma. Surface-diffusion-driven kinetic growth on one-dimensional substrates. *Phys. Rev. E* **1993**, 48, 2575-2594.

[2.40] A. C. Ferrari, J. Robertson. Interpretation of Raman spectra of disordered and amorphous carbon. *Phys. Rev. B* **2000**, 61, 14095-14106.

[2.41] T. Heitz, C. Godet, J. E. Bourée, B. Drévillon, J. P. Conde. Radiative and nonradiative recombination in polymerlike a-C:H films. *Phys. Rev. B* **1999**, 60, 6045-6052.

[2.42] J. Robertson. Recombination and photoluminescence mechanism in hydrogenated amorphous carbon. *Phys. Rev. B* **1996**, 53, 16302-16305.

[2.43] S. Prawer, K. W. Nugent, Y. Lifshitz, G. D. Lempert, E. Grossman, J. Kulik, I. Avigal, R. Kalish. Systematic variation of the Raman spectra of DLC films as a function of sp^2:sp^3 composition. *Diamond Relat. Mater.* **1996**, 5, 433-438.

[2.44] R. Kalish, Y. Lifshitz, K. Nugent, S. Prawer. Thermal stability and relaxation in diamond-like-carbon. A Raman study of films with different sp^3 fractions (ta-C to a-C). *Appl. Phys. Lett.* **1999**, 74, 2936-2938.

[2.45] J. Ristein, R. T. Stief, L. Ley, W. Beyer. A comparative analysis of a-C:H by infrared spectroscopy and mass selected thermal effusion. *J. Appl. Phys.* **1998**, 84, 3836-3847.

[2.46] A. Soum Glaude, L. Thomas, E. Tomasella, J. M. Badie, R. Berjoan. Selective effect of ion/surface interaction in low frequency PACVD of SiC:H films: Part B. Microstructural study. *Surf. Coat. Technol.* **2006**, 201, 174-181.

[2.47] W.-J. Wu, M.-H. Hon. The effect of residual stress on adhesion of silicon-containing diamond-like carbon coatings. *Thin Solid Films* **1999**, 345, 200-207.

[2.48] M. Ban, T. Hasegawa. Internal stress reduction by incorporation of silicon in diamond-like carbon films. *Surf. Coat. Technol.* **2003**, 162, 1-5.

[2.49] V. N. Pokrovskii. The mesoscopic theory of the slow relaxation of linear macromolecules. *Adv. Polym. Sci.* **2001**, 154, 143-219.

[2.50] C. Donnet, J. Fontaine, A. Grill, T. Le Mogne. The role of hydrogen on the friction mechanism of diamond-like carbon films. *Tribol. Lett.* **2001**, 9, 137-142.

[2.51] Y. Qi, E. Konca, A. T. Alpas. Atmospheric effects on the adhesion and friction between non-hydrogenated diamond-like carbon (DLC) coating and aluminum - A first principles investigation. *Surf. Sci.* **2006**, 600, 2955-2965.

[2.52] M. Weiler, S. Sattel, T. Giessen, K. Jung, H. Ehrhardt, V. S. Veerasamy, J. Robertson. Preparation and properties of highly tetrahedral hydrogenated amorphous carbon. *Phys. Rev. B* **1996**, 53, 1594-1608.

[2.53] M. A. Tamor, W. C. Vassell, R. Carduner. Atomic constraint in hydrogenated ‘‘diamondlike’’ carbon. *Appl. Phys. Lett.* **1991**, 58, 592-594.

[2.54] N. A. Marks, J. M. Bell, G. K. Pearce, D. R. McKenzie, M. M. M. Bilek. Atomistic simulation of energy and temperature effects in the deposition and implantation of amorphous carbon thin films. *Diamond Relat. Mater.* **2003**, 12, 2003-2010.

[2.55] Y. Lifshitz, S. R. Kasi, J. W. Rabalais. Subplantation model for film growth from hyperthermal species: application to diamond. *Phys. Rev. Lett.* **1999**, 62, 1290-1293.

[2.56] J. Robertson. Deposition mechanisms for promoting sp^3 bonding in diamond-like carbon. *Diamond Relat. Mater.* **1993**, 2, 984-989.

[2.57] H. Hofsäss, H. Feldermann, R. Merk, M. Sebastian, C. Ronning. Cylindrical spike model for the formation of diamondlike thin films by ion deposition. *Appl. Phys. A* **1998**, 66, 153-181.

[2.58] D. R. McKenzie. Tetrahedral bonding in amorphous carbon. *Rep. Prog. Phys.* **1996**, 59, 1611-1664.

[2.59] I. Koponen, M. Hakovirta, R. Lappalainen. Modeling the ion energy dependence of the sp^3/sp^2 bonding ratio in amorphous diamondlike films produced with a mass-separated ion beam. *J. Appl. Phys.* **1995**, 78, 5837-5839.

[2.60] S. Pisana, C. Casiraghi, A. C. Ferrari, J. Robertson. Roughness evolution during growth of hydrogenated tetrahedral amorphous carbon. *Diamond Relat. Mater.* **2006**, 15, 898-903.

[2.61] J. G. Buijnsters, M. Camero, L. Vázquez. Growth dynamics of ultrasmooth hydrogenated amorphous carbon films. *Phys. Rev. B* **2006**, 74, 155417.

[2.62] C. Lopez-Santos, J. L. Colaux, J. C. Gonzalez, S. Lucas. Investigation of the growth mechanisms of a-CH_x coatings deposited by pulsed reactive magnetron sputtering *J. Phys. Chem. C* **2012**, 116, 12017-12026.

[2.63] L. Vázquez, J. G. Buijnsters. Chemical and physical sputtering effects on the surface morphology of carbon films grown by plasma chemical vapor deposition. *J. Appl. Phys.* **2009**, 106,

033504.

[2.64] A. J. Flewitt, J. Robertson, W. I. Milne. Growth mechanism of hydrogenated amorphous silicon studied by in situ scanning tunneling microscopy. *J. Appl. Phys.* **1999**, 85, 8032-8039.

[2.65] S. Uhlmann, Th. Frauenheim, Y. Lifshitz. Molecular-dynamics study of the fundamental processes involved in subplantation of diamondlike carbon. *Phys. Rev. Lett.* **1998**, 81, 641-644.

[2.66] Y. Lifshitz, R. Edrei, A. Hoffman, E. Grossman, G. D. Lempert, J. Berthold, B. Schultrich, H. U. Jäger. Surface roughness evolution and growth mechanism of carbon films from hyperthermal species. *Diamond Relat. Mater.* **2007**, 16, 1771-1776.

[2.67] Y. Lifshitz, G. D. Lempert, E. Grossman, I. Avigal, C. Uzan-Saguy, R. Kalish, J. Kulik, D. Marton, J. W. Rabalais. Growth mechanisms of DLC films from C^+ ions: experimental studies. *Diamond Relat. Mater.* **1995**, 4, 318-323.

[2.68] V. N. Popok, I. Barke, E. E. B. Campbell, K.-H. Meiwes-Broer. Cluster–surface interaction: from soft landing to implantation. *Surf. Sci. Rep.* **2011**, 66, 347-377.

[2.69] S. W. Rynders, A. Scheeline, P. W. Bohn. Structure evolution in a-SiC:H films prepared from tetramethylsilane. *J. Appl. Phys.* **1991**, 69, 2951-2960.

[2.70] A. von Keudell, M. Meier, C. Hopf. Growth mechanism of amorphous hydrogenated carbon. *Diamond Relat. Mater.* **2002**, 11, 969-975.

[2.71] J. Robertson. Mechanism of sp^3 bond formation in the growth of diamond-like carbon. *Diamond Relat. Mater.* **2005**, 14, 942-948.

Chapter 3

Superlow Friction of a-C:H Film: Some Core Factors

In this chapter, attention mainly focuses on the tribological properties of a hydrogen-rich a-C:H film prepared by ion vapor deposition, as discussed in Chapter 2. The influences of film structure, counterpart material, environmental condition and contact pressure on the occurrence and durability of superlow friction for a-C:H film are presented in detail. The underlying lubrication mechanisms in specific conditions are discussed along with other comparable work reported in literatures.

3.1 Background

Hydrogenated amorphous carbon (a-C:H) film is one of the most investigated a-C materials, as described in Chapters I and II, due to their exceptional structure diversity and excellent mechanical and tribological properties. Numerous studies [3.1-5] have been devoted to exploiting a-C:H films as solid lubricants providing extremely low friction and outstanding durability for specific tribological applications such as microelectromechanical systems (MEMS) and aerospace instruments. It is emphasized that the friction and wear performances of a-C:H films are remarkably affected by the structural nature of the films (e.g., sp^3/sp^2 hybridization [3.6], density [3.7], hydrogen content [3.1, 2, 8], surface energy [3.9], roughness [3.10]), and by the tribotesting conditions (e.g., gaseous atmosphere surrounding contact [3.11-13], sliding velocity [3.14], contact pressure [3.15], surface chemistry of counterface [3.16]). Ultralow ($0.01<\mu<0.1$) or superlow ($0.001<\mu<0.01$) friction coefficient of a-C:H films can be

achieved under ultra-high vacuum (UHV) [3.2, 3, 11, 12], gas lubrication condition (H_2 atmosphere) [3.2, 11] or dry inert gas environment (such as dry Ar and dry N_2) [3.1, 12, 13] for some structure-tailored a-C:H films. For instance, Donnet et al. reported a superlow friction of 0.002 for PECVD-deposited a-C:H film with hydrogen content of ~40 at.% in UHV. A same near-frictionless state is also feasible for another a-C:H sample with relatively low hydrogen content of ~34 at.% when tribotested in an atmosphere of pure hydrogen (10 hPa) [3.2]. Meanwhile, Erdemir et al. made a breakthrough in realizing superlow friction and wear of a-C:H films grown from a hydrogen-rich plasma (i.e., H/C ratio of 10) in PECVD when these films were tested in dry N_2 [3.1]. It has been confirmed that hydrogen is the most paramount factor to achieve superlow friction for a-C:H films. A chemical surface inertness is expected through hydrogen-passivation of carbon dangling bonds, which results in little adhesive force across the contact interface and thus superlow friction [3.1]. However, some crucial issues concerning the superlubric properties of hydrogen-rich a-C:H films such as the influences of film structure, counterpart material, gaseous environment and contact pressure still remain unclear.

Therefore, in this chapter, we are trying to conduct a systematic investigation on the superlubric properties of a hydrogen-rich a-C:H film grown from IVD system. Special efforts are given to disclose the lubrication mechanism underlying this anti-friction carbon material. The present results are discussed with other relevant cases reported in literatures.

3.2 Experimental Methodology

3.2.1 Film Synthesis and Structure Characterization

The hydrogen-rich a-C:H film, namely PLCH, was prepared by ion vapor deposition (IVD) system, as described in Chapter 2. Liquid toluene (C_7H_8) was thermally heated to evaporate into the chamber serving as the reactive gas precursor. The film was designed

to possess a bilayer structure, in which an adherent a-C:H:Si film served as the basement layer to improve the adhesion strength and load capacity of the top a-C:H layer due to its relatively low hardness. The detailed synthesis procedures are shortly summarized as follows: (1) Si (100) wafers (*R*a=0.12 nm) and SUJ2 balls (for friction test) after ultrasonic cleaning were selected as coating substrates, (2) the chamber was pumped down to a base pressure of ~3.0×10^{-3} Pa at the temperature of 200 °C, (3) Ar^+ ion bombarding was performed for 30 min before deposition, (4) a strongly adherent a-C:H:Si interlayer of ~400 nm thickness was first deposited on the Si substrates, and (5) the top polymeric a-C:H film was then deposited under a relatively low bias voltage of 0.25 kV in the gas-ionization system (i.e., pressure of 0.25 Pa, anode current of 0.75 A, filament current of 30 A, reflector voltage of 10 V). The film morphology and thickness were characterized by cross-sectional observations in a scanning electron microscopy (SEM, Hitachi S-4800). The hydrogen content was determined by elastic recoil detection analysis (ERDA) using a 0.5 MeV N^+ beam impinging at an incident angle of 67.5° with respect to the surface normal. The chemical bonding state was derived from X-ray photoelectron spectroscopy (XPS, PHI Quantera II SXM) after 3 min Ar^+ pre-sputter. The Raman spectrum was recorded by a Renishaw System using an Ar^+ laser with a wavelength of 532 nm.

3.2.2 Friction Test

The friction tests were carried out in a pin-on-disk CSM tribometer. Specific tribotesting atmospheres with controlled pressures were produced by purging distinct gases such as humid air (20-30% RH), dry N_2, dry Ar, 40% H_2 + 60% He mixture and pure O_2 into the chamber until stability. Silicon nitride (Si_3N_4), bare or film-coated SUJ2 balls were selected as counterparts slide against film-coated Si wafers. Normal load in the range of 1-10 N and sliding velocity in the range of 0-25 cm/s are available for different tribotesting conditions. The sliding radius was set at 3.5 cm. A Nikon optical microscope was used to observe the wear morphologies after friction tests.

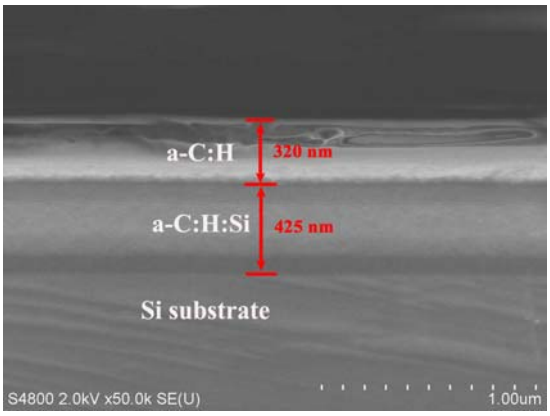

Figure 3.1 SEM cross-sectional morphology of the IVD-deposited hydrogen-rich a-C:H film showing a bilayer structure.

3.3 Results and Discussion

3.3.1 Basic Properties of Hydrogen-Rich a-C:H Film

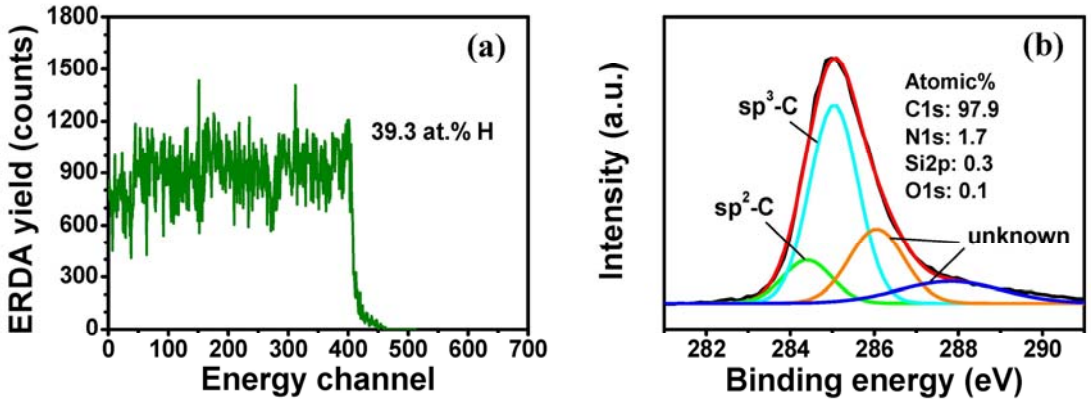

Figure 3.2 Constitute of a-C:H film: (a) hydrogen content measured by ERDA and (b) elemental composition and carbon bonding structure derived from XPS.

The SEM cross-sectional morphology of the as-grown a-C:H film is shown in Figure 3.1. It can be seen that the film possesses a bilayer structure, in which a a-C:H layer is on top of a dense a-C:H:Si interlayer. The thicknesses of these two individual layers are 320 and 425 nm, respectively. The hydrogen content and elemental composition of the top a-C:H layer were measured by ERDA and XPS, respectively, as

shown in Figure 3.2. The average hydrogen content is 39.3 at.% (Figure 3.2(a)), indicating a hydrogen-rich polymer-like structure is obtained at a low bias voltage of 250 V. The XPS spectrum (Figure 3.2(b)) depicts that the a-C:H film is mainly composed of carbon (97.9 at.%), while only a small amount of nitrogen (1.7 at.%), silicon (0.3 at.%) and oxygen (0.1 at.%) exist in the film. The peak deconvolution of C1s broad band shows a high fraction (~82%) of sp^3-bonded carbon configuration. Note that the sp^3-bond located at ~285.1 eV stems from not only the C-C bonds but also the hydrogen-terminated C-H bonds. The formation of such a sp^3-rich structure is thus attributed to the high hydrogen content in the a-C:H film, which induces a chain-developed polymeric network containing a large number of $C\text{-}H_n$ units. It should be mentioned additionally that there are two unknown peaks in the high binding energy region of ~286-288 eV. Considering the almost absence of oxygen in the film, these two peaks cannot be designed to C-O or C=O bonds. The most likely scenario is that these two peaks come from the argon-related chemical structures formed during the Ar^+ pre-sputtering process. Therefore, Ar^+ sputter may modify the film structure to some extent, i.e., hydrogen loss or sp^3-to-sp^2 transformation. Despite this, the above results are still sufficient to verify the polymeric characteristic of the as-grown a-C:H film. The Raman spectrum was further recorded to provide carbon bonding state of the as-grown a-C:H film, as shown in Figure 3.3. The steep photoluminescence background confirms the hydrogen-rich polymer-like structure, which is consistent with the Raman results from Casiraghi et al [3.17]. The deconvoluted *D* and *G* peaks signify the presence of both ring-like and chain-like sp^2-bonded configurations in the sp^3-rich carbon matrix. The I(*D*)/I(*G*) value, 0.56, further confirms the mainly amorphous nature of the as-grown a-C:H film according to the three-stage model by Ferrari [3.18]. Overall, the as-grown a-C:H film from toluene under a low bias voltage possesses a high H content, and a sp^3-C dominating amorphous network where some sp^2-bonded clusters or disordering units are present.

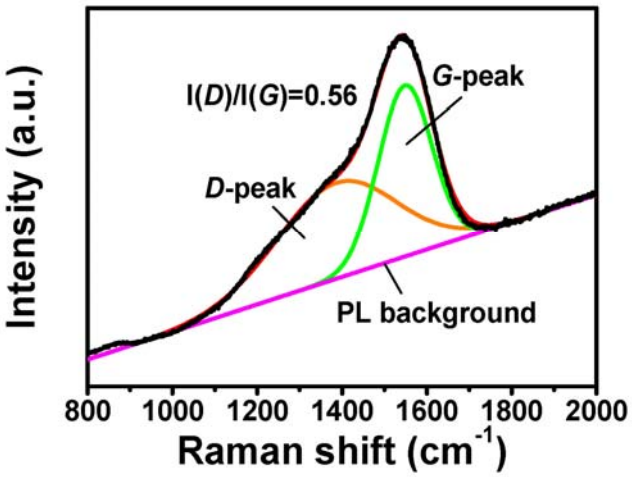

Figure 3.3 Raman spectrum showing an amorphous carbon bonding structure of a-C:H film: deconvolution of *D* and *G* peaks along with the photoluminescence background.

3.3.2 Comparison of Frictional Behaviors in Humid Air and Dry N_2

Ambient air is the most common service environment for tribological system. Therefore, we first tribotested the as-grown a-C:H film in humid environment, as shown in Figure 3.4. It is obviously seen that the friction coefficient is quite high in humid air (Figure 3.4(a)). It quickly increases from the initial value of ~0.2 to a peak value of ~0.5. Afterwards, it gradually decreases with further proceeding of slide, and finally stabilizes at around 0.3. A severe wear scar was produced on the bare SUJ2 ball surface (Figure 3.4(b)), indicating an insufficient protection effect due to intensive tribochemical interactions between the contact surfaces. Correspondingly, a noticeable wear track was formed on the film surface (Figure 3.4(c)). The present results once again confirm the previous findings by other researchers that friction is high for a-C:H film slide against steel counterpart in ambient air, which is mainly attributed to the continuous corrosive reactions between the carbon film surfaces and environmental gaseous molecules and the formation of covalent dangling bonds across the sliding interface [3.11, 12].

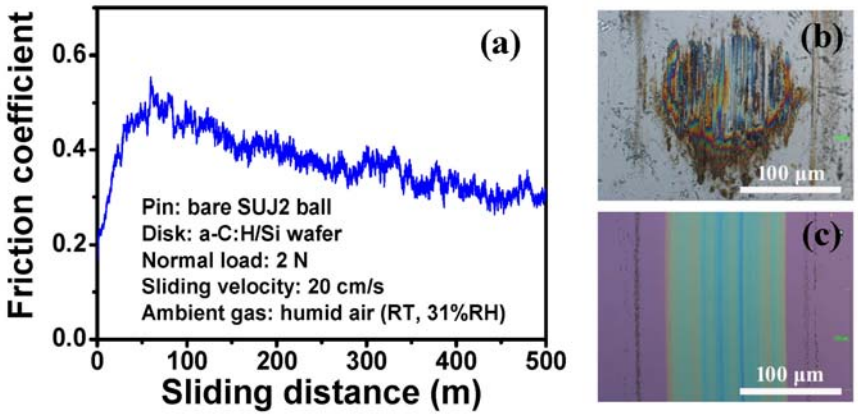

Figure 3.4 Frictional behavior of the hydrogen-rich a-C:H film in humid air: (a) friction coefficient vs. sliding distance, (b) wear scar on pin and (c) wear track on disk.

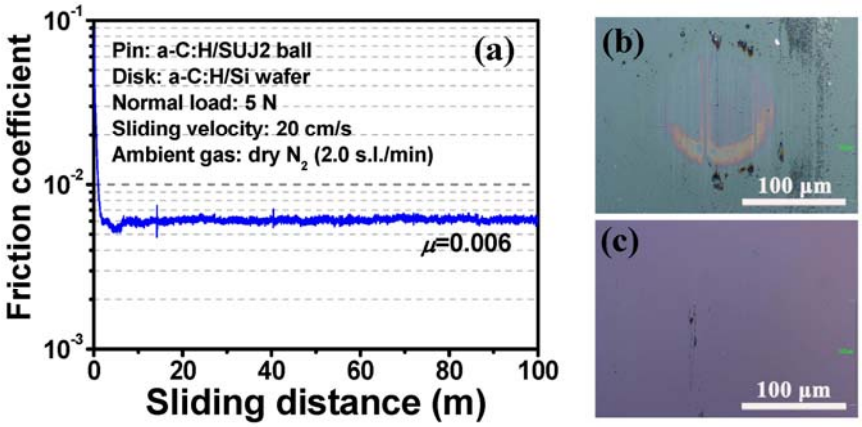

Figure 3.5 Frictional behavior of the hydrogen-rich a-C:H film in dry N_2: (a) friction coefficient vs. sliding distance, (b) wear scar on pin and (c) wear track on disk.

In comparison, the frictional behavior of the as-grown a-C:H film in dry N_2 is shown in Figure 3.5. Note that the SUJ2 ball was coated by the same a-C:H film in this condition. Contrary to the case in humid air, the friction coefficient quickly evolves into a quite stable state and achieves an extremely low value of ~0.006 (Figure 3.5(a)). The amplitude of variation in the steady-state friction coefficient is ±0.0003, implying an ultrasmooth rubbing process in the superlubric state for the self-mated a-C:H films. The wear scar produced on the film-coated SUJ2 ball is quite shallow and smooth (Figure 3.5(b)). In addition, scar surface with a color in purple or pale yellow can be observed

around the contact edge, implying the chemical bonding state at the sliding interface is different from the pristine film structure. Correspondingly, almost no wear occurred for the film-coated Si wafer, as observed in Figure 3.5(c). This result demonstrates that near-frictionless and near-wearless rubbing process can be achieved for the IVD-deposited a-C:H film in dry N_2 when tailoring the film structure to a hydrogen-rich polymeric configuration.

3.3.3 Effect of Counterpart Material on Superlubricity in Dry N_2

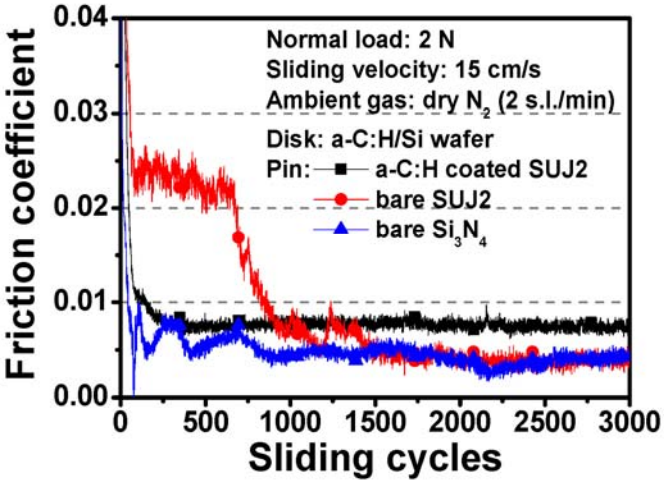

Figure 3.6 Frictional behaviors of the hydrogen-rich a-C:H film in dry N_2 slide against different counterpart materials including same-film-coated SUJ2 ball, bare SUJ2 ball and bare Si_3N_4 ball.

Counterpart material is a paramount factor affecting the frictional behaviors of a-C:H films, especially the build-up of tribolayer on the contact surface. For this purpose, we chose same-film-coated SUJ2 ball, bare SUJ2 ball and bare Si_3N_4 ball as the counterparts for friction tests in dry N_2. The results are shown in Figure 3.6. For self-mated sliding, the frictional behavior of a-C:H film resembles the result in Figure 3.5(a). The friction coefficient quickly evolves into an extremely low and stable value of ~0.008. For bare Si_3N_4 counterpart, superlow friction is also readily achieved after a short running-in period. However, the friction coefficient initially exhibits some

fluctuations, and gradually stabilizes at an average value of ~0.004. For bare SUJ2 ball, the rubbing process can be divided into two stages. Firstly, the friction coefficient is evolving smoothly in the region of 0.02-0.03 for about ~700 cycles. Subsequently, the friction coefficient abruptly drops to a superlow region (<0.01), and it gradually stabilizes at around 0.004 from ~1500 cycles to the end. The present result implies that running-in process is necessary for the occurrence of superlow friction when rubbing against bare steel surface. It is speculated that the removal of oxide layer on the steel surface and the continuous build-up of a carbon-rich tribolayer through material transformation from the film-coated disk is the most likely scenario for explaining this friction vanishing performance as observed in Figure 3.6.

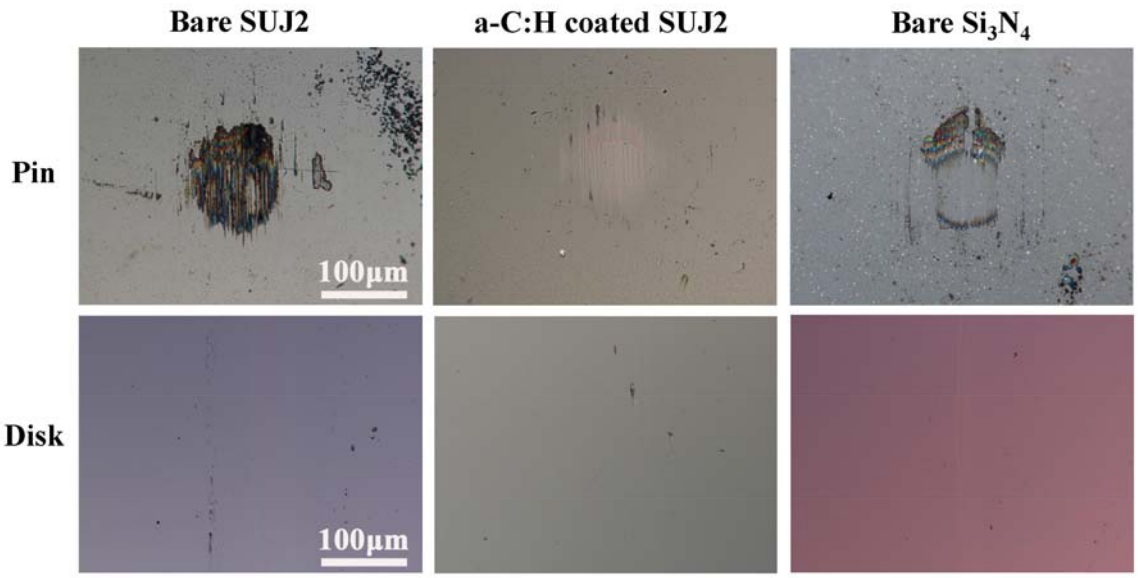

Figure 3.7 Wear morphologies on the pin and disk surfaces for the as-grown hydrogen-rich a-C:H film after the friction tests against different counterpart materials including same-film-coated SUJ2 ball, bare SUJ2 ball and bare Si_3N_4 ball.

The corresponding wear morphologies produced on the pin and disk surfaces are shown in Figure 3.7. For bare SUJ2 ball, a noticeable wear scar can be found in the contact area. Considering the final establishment of superlubric state, the abrasion of SUJ2 ball surface should mainly occur in the first stage, namely running-in period. In

addition, it is surprising to notice that no plentiful transferred materials can be found on the scar surface. However, this finding does not mean that there is no tribolayer formed on the contact surface. Recent study on carbon nitride (CN_x) has pointed that a quite thin (~10 nm) invisible-to-eye tribolayer produced on the Si_3N_4 ball surface is sufficient to achieve stable and durable ultralow friction in dry N_2 [3.19]. The present result also provides some evidence that the tribolayer established on the steel ball surface is quite thin, but highly capable of lubricating the sliding interface to eliminate friction. Correspondingly, a very mild wear track is observed on the film-coated disk. For a-C:H coated SUJ2 ball (self-mated), it shows the similar wear morphologies as observed in Figure 3.5, where very wild wear on ball surface and nearly no wear on film-coated disk are found. For bare Si_3N_4 ball, some tribodebris is found in front and behind of the contact area along the sliding direction, which is thought to be mainly transferred from the film material on the disk. Correspondingly, a near-invisible wear track is found to be formed on the film-coated disk.

3.3.4 Effect of N_2 Flow Rate on Achieving Superlubricity

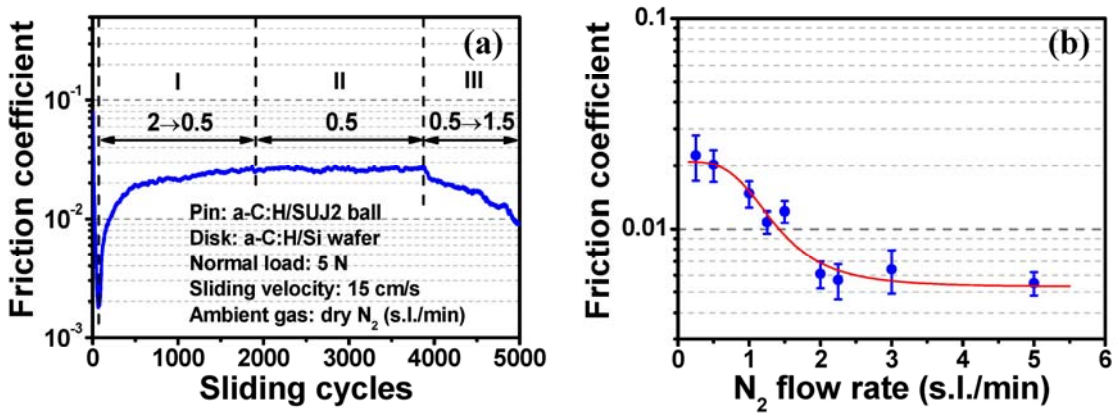

Figure 3.8 (a) Dynamic evolution of frictional behavior of the as-grown hydrogen-rich a-C:H film with gradually variable N_2 flow rate: 2→0.5 s.l./min (I), 0.5 s.l./min (II) and 0.5→1.5 s.l./min. (b) Evolution of steady-state friction coefficient as a function of N_2 flow rate.

Dry N_2 atmosphere has been frequently emphasized for its critical effect to achieve superlow friction in hydrogenated a-C films [3.1, 8, 12]. Therefore, it is highly necessary to investigate the correlation between flow rate or partial pressure of dry N_2 and friction-reducing performance of a-C:H films. For this purpose, we designed another friction test to track the effect of dry N_2 in real time, as shown in Figure 3.8(a). The outlet rate of dry N_2 flowing around the contact area was initially set at 2.0 s.l./min and then gradually decreased from 2.0 to 0.5 s.l./min once the onset of the sliding test. It can be seen that the friction coefficient first dropped to ~0.002, and it gradually increased to 0.02-0.03 with progressively decreasing the flow rate of dry N_2 to 0.5 s.l./min (stage I). Afterwards, it stabilized in the region of 0.02-0.03 when the flow rate of dry N_2 was kept constant at 0.5 s.l./min (stage II). However, the friction coefficient once again decreased when gradually increased the N_2 flow rate, and it re-entered into the superlow friction region as the flow rate of N_2 reached 1.5 s.l./min. Figure 3.8(b) summarizes the correlation between the steady-state friction coefficient and the flow rate of dry N_2. It can be obviously seen that a threshold of N_2 flow rate, namely 2.0 s.l./min, exists for the hydrogen-rich a-C:H film to achieve superlow friction (μ<0.01). However, further increase in the flow rate of dry N_2 has only a subtle effect on the steady-state friction coefficient. The above results demonstrate that N_2 molecules are involved in sustaining superlubric state during the rubbing process, in which sufficient inert N_2 molecules can effectively shield the contact surfaces from other reactive gases such as O_2 and H_2O, or may even provide extra lubrication effect by physical adsorption at the sliding interface [3.13].

3.3.5 Effect of Gaseous Atmosphere

To further evaluate the effect of gaseous atmosphere on frictional behavior, we tribotested the self-mated a-C:H films in more wide environments including humid air, dry O_2, dry Ar, H_2+He mixture and dry N_2. The results are shown in Figure 3.9. It is obviously seen that the friction responses of the hydrogen-rich a-C:H film is strongly

dependent on the molecular characteristic of the surrounding gases. In dry O_2, the friction coefficient gradually increases from 0.02 to 0.1, confirming the destruction of the hydrogen passivation state by oxygen atom. In humid air, however, the friction coefficient for this self-mated sliding also increases as the rubbing progresses but maintains an ultralow region of ~0.01-0.02, which is much lower than that of sliding against bare SUJ2 ball as observed in Figure 3.4. This is mainly due to intensive bonds break and material transfer occurred during build-up of tribolayers at the sliding interface, and to the mild interactions between the sliding interface and the gaseous molecules.

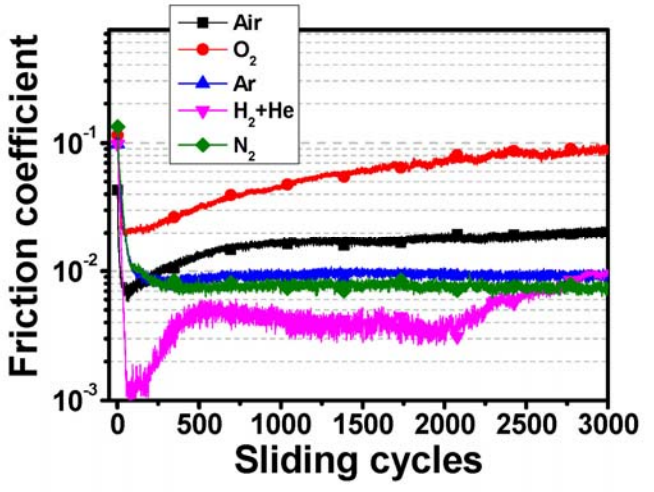

Figure 3.9 Comparison of frictional behaviors of self-mated a-C:H films in various atmospheres including humid air (20%RH), dry O_2, Ar, H_2+He mixture and N_2. The tribotesting conditions are as follows: normal load of 2 N, sliding velocity of 15 cm/s, individual gas flow rate of 2.0 s.l./min.

The frictional behaviors of the hydrogen-rich a-C:H film in dry N_2 and Ar exhibit quite similar responses, in which the friction coefficient evolves into an extremely low and stable region after a short running-in period as already observed in Figures 3.5(a) and 3.6. However, the steady-state friction coefficient in dry Ar (~0.01) is slightly higher than that of in dry N_2 (0.008). The underlying lubrication mechanism concerning this difference has not been well understood yet. Some researchers have proposed that

the formation of a perpendicularly oriented monolayer adsorbed on the contact interface by physical interactions between π orbital of sp^2-C atoms and lone pair electrons of N_2 is probably the reason for superior friction-reduction behavior in dry N_2 [3.13]. In H_2 + He mixture gas, the friction coefficient is lower than that of the other conditions, which clearly manifests the lubrication effect of hydrogen. However, it is also found that the rubbing process in H_2 + He mixture gas is not as stable as that in dry N_2 or Ar. The friction coefficient first sharply drops to ~0.001 onset of the sliding, and then gradually increases to the region of ~0.003-0.004, which lasts for about 1500~ sliding cycles. Afterwards, the friction coefficient increases again and finally reaches the value of ~0.01. It is quite difficult to fully understand the origin of the above phenomenon. It might be correlated with the reactive nature of molecular H_2, which always changes the tribochemical state at the sliding interface during sliding. In addition, the presence of inert He may also contribute to the complexity of this rubbing process.

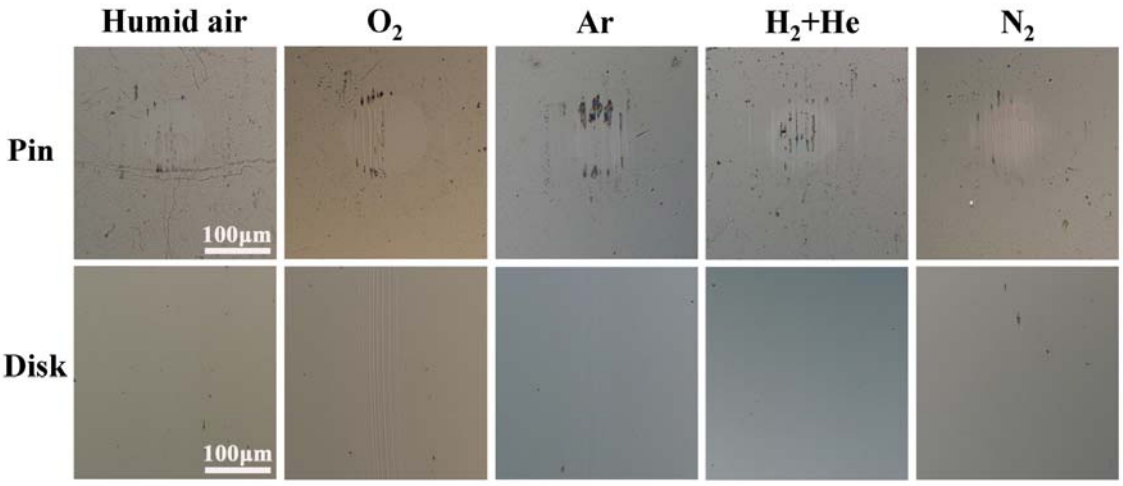

Figure 3.10 Wear morphologies on the pin and disk surfaces for the as-grown hydrogen-rich a-C:H film after the friction tests in different gaseous atmospheres as shown in Figure 3.9.

The corresponding wear morphologies produced on the pin and disk surfaces for the hydrogen-rich a-C:H film after the friction tests in different gaseous atmospheres are

shown in Figure 3.10. It can be seen that the wear scars formed on the film-coated pin surfaces are very mild and smooth for all the gaseous atmospheres. Among them, the diameter of wear scar in dry O_2 is larger than that of other conditions, confirming the relatively higher friction coefficient in this condition (Figure 3.9). Accordingly, no obvious wear tracks can be found on the film surfaces for the film-coated disks, especially in the atmospheres of dry N_2, Ar and H_2+He mixture, implying a near-wearless state for the self-mated a-C:H films upon sliding.

3.3.6 Effect of Contact Pressure

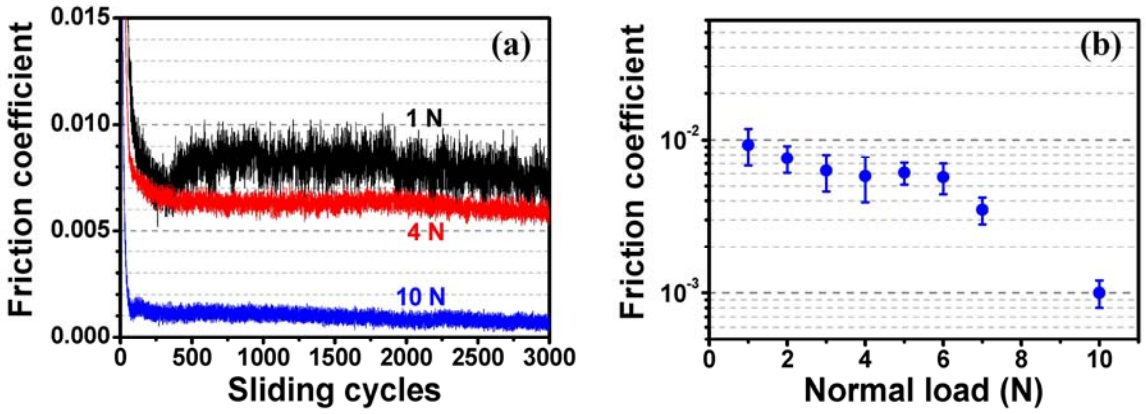

Figure 3.11 (a) Comparison of frictional behaviors of the hydrogen-rich a-C:H films in dry N_2 under three applied normal load: 1, 4, and 10 N. (b) The evolution of average steady-state friction coefficient as a function of applied normal load.

The contact pressure or applied normal load is another important factor controlling the frictional behaviors at the sliding interface. In general, high contact pressure induces intensive intra- and inter-film bonds break and formation and tribochemical interactions with the surrounding gaseous molecules [3.20, 21]. The friction force therefore depends on the final chemical state across the sliding interface. Figure 3.11 shows the influence of applied normal load on the frictional responses of the hydrogen-rich a-C:H films in dry N_2. As seen in Figure 3.11(a), the steady-state friction coefficient decreases from 0.009 to 0.006 to 0.001 with increasing the applied normal load from 1 to 4 to 10 N.

Meanwhile, the friction curve becomes increasingly smooth, with gradual decreasing vibration amplitude from ±0.0015 under 1 N to ±0.0003 under 10 N. Figure 3.11(b) depicts the correlation between the average steady-state friction coefficient and the applied normal load. Obviously, the friction coefficient gradually decreases with the increase of the normal load, implying a high contact pressure favoring the occurrence of friction-vanishing contact for the self-mated hydrogen-rich a-C:H films.

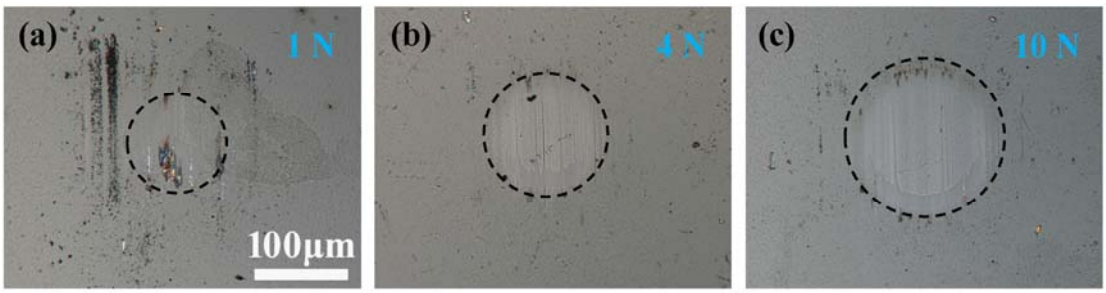

Figure 3.12 Wear scars produced on the film-coated pins after the friction tests at three normal loads of 1, 4 and 10 N in dry N_2. The dotted circles indicate the contact areas.

Figure 3.12 shows the produced wear scars on film-coated SUJ2 pin after the friction tests at the above three normal loads. The diameter of the wear scar increases from 95.2 to 136.3 to 155.6 μm as the normal load increases from 1 to 4 to 10 N. Therefore, we can roughly calculate the apparent contact pressure at the steady state according to the equation: $P_a=W/\pi r^2$. The corresponding parameters are as follows: W_1=1 N, r_1=95.2 μm; W_2=4 N, r_2=136.3 μm; W_3=10 N, r_3=155.6 μm. The calculated contact pressures are 0.14, 0.27, 0.53 GPa for the normal loads of 1, 4, 10 N, respectively. The traditional Bowden and Tabor model assumes that for solid lubricant the friction coefficient depends on the shear strength S of the interfacial tribofilm, the real contact area A and the normal load W, described as follows [3.22]:

$$\mu = S\frac{A}{W} \qquad (3.1)$$

If we assume that the real contact pressure is proportional to the apparent contact pressure and the shear strength S is almost constant, thus higher contact pressure will

result in lower friction coefficient. The present result indicates that the self-mated hydrocarbon surfaces under higher normal load (i.e., 10 N) are rubbing at higher contact pressure even though the contact area is enlarged as compared with the cases of lower normal loads (i.e., 4 and 10 N). It seems that the hydrocarbon network can at least stand a normal pressure of 0.5 GPa to maintain this near-frictionless state (i.e., μ~0.001). In addition, a higher contact pressure is more effective in smoothening the rubbing process, i.e, extremely small vibration amplitude of ±0.0003 under 10 N as observed in Figure 3.11(a).

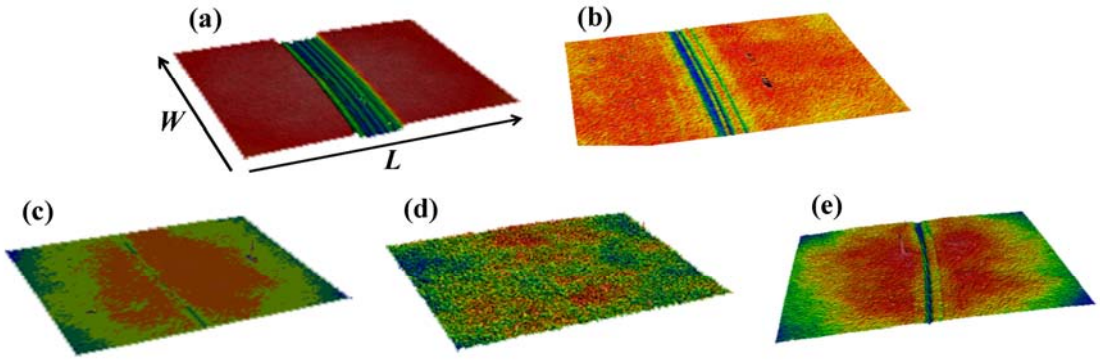

Figure 3.13 3D wear morphologies of the hydrogen-rich a-C:H films after the friction tests under different tribotesting conditions: (a) bare SUJ2, humid air, (b) bare SUJ2, dry N_2, (c) bare Si_3N_4, dry N_2, (d) self-mated, dry N_2, 5 N and (e) self-mated, dry N_2, 10 N. Note: W=520 μm, L=690 μm.

White-light surface interferometer was further employed to characterize the wear morphologies formed on the film-coated disk surface, as shown in Figure 3.13. Obviously, sliding against bare SUJ2 ball in humid air caused the most severe wear on the film surface (Figure 3.13(a)), as observed in Figure 3.4(c). However, the dry N_2 atmosphere significantly reduced the wear of film for the same counterparts (Figure 3.13(b)). In comparison, sliding against bare Si_3N_4 just caused very mild wear on the film surface (Figure 3.13(c)). The most wear-resistant behavior was found for the self-mated sliding in dry N_2, as confirmed by the indistinguishable wear track on the

film under 5 N (Figure 3.13(d)). The increase of normal load to 10 N also just resulted in very mild wear topography (Figure 3.13(e)).

3.4 Summary

A hydrogen-rich a-C:H film was grown by ion vapor deposition system using toluene as the precursor gas under a relatively low bias voltage of 250 V. The as-grown film has a high hydrogen content of 39.3 at.%, from which a sp^3-rich hydrocarbon network is developed. High friction coefficient and severe wear were observed for this film in humid air when sliding against bare SUJ2 ball, while superlow friction could be achieved in dry N_2 regardless of the counterpart material. However, self-mated contact or sliding against ceramic ball is the most favorable way for quick establishment of superlubric state in dry N_2. In comparison, an obvious running-in period is necessary to build up the anti-friction tribolayers before achieving superlow friction for bare SUJ2 ball. The atmospheric environment has a paramount influence on the frictional performances of the hydrogen-rich a-C:H film, where dry inert gas or hydrogen-bearing gas is more favorable for friction vanishing. In dry O_2, the increase of friction coefficient is due to the destruction of the hydrogen passivation state by oxygen atom. However, the friction coefficient can maintain a ultralow region in humid air for self-mated a-C:H film, which is much lower than that of sliding against bare SUJ2 ball. The steady-state friction coefficient in dry N_2 decreases as the normal load increases, which shows a non-Amontonian friction behavior. An extremely low friction coefficient of ~0.001 can be obtained at normal load of 10 N. Such a near-frictionless rubbing hardly results in any wear and loss of material.

References

[3.1] A. Erdemir, O. L. Eryilmaz, G. Fenske. Synthesis of diamondlike carbon films with superlow friction and wear properties. *J. Vac. Sci. Technol. A* **2000**, 18, 1987-1992.

[3.2] C. Donnet, J. Fontaine, A. Grill, T. Le Mogne. The role of hydrogen on the friction mechanism of diamond-like carbon films. *Tribol. Lett.* **2000**, 9, 137-142.

[3.3] X. Liu, J. Yang, J. Hao, J. Zheng, Q. Gong, W. Liu. A near-frictionless and extremely elastic hydrogenated amorphous carbon film with self-assembled dual nanostructure. *Adv. Mater.* **2012**, 24, 4614-4617.

[3.4] W. Tillmann, E. Vogli, F. Hoffmann. Wear-resistant and low-friction diamond-like-carbon (DLC)-layers for industrial tribological applications under humid conditions. *Surf. Coat. Technol.* **2009**, 204, 1040-1045.

[3.5] C. Wang, S. Yang, Q. Wang, Z. Wang, J. Zhang. Comparative study of hydrogenated diamondlike carbon film and hard hydrogenated graphitelike carbon film. *J. Appl. Phys.* **2008**, 103, 123531.

[3.6] Y. Wang, Y. Ye, H. Li, L .Ji, Y. Wang, X. Liu, J. Chen, H. Zhou. Microstructure and tribological properties of the a-C:H films deposited by magnetron sputtering with CH_4/Ar mixture. *Surf. Coat. Technol.* **2011**, 205, 4577-4581.

[3.7] H. Yasui, M. Taki, Y. Hasegawa, S. Takago. Mechanical properties of high-density diamond like carbon (HD-DLC) films prepared using filtered arc deposition. *Surf. Coat. Technol.* **2011**, 206, 1003-1006.

[3.8] F. Rabbani, B. M. Vogelaar. The importance of unbound hydrogen and increased aromatic structure on the friction and wear behaviour of amorphous hydrogenated carbon (a-C:H) coatings. *Diamond Relat. Mater.* **2004**, 13, 170-179.

[3.9] W. Navarrini, C. L. Bianchi, L. Magagnin, L. Nobili, G. Carignano, P. Metrangolo, G. Resnati, M. Sansoter. Low surface energy coatings covalently bonded on diamond-like carbon films. *Diamond Relat. Mater.* **2010**, 19, 336-341.

[3.10] T. Ohana, X. Wu, T. Nakamura, A. Tanaka. Roughness effect of mating ball on friction of diamond-like carbon film and friction mechanism in water and air environment. *Diamond Relat. Mater.* **2008**, 179, 860-863.

[3.11] J. Andersson, R. A. Erck, A. Erdemir. Friction of diamond-like carbon films in different atmospheres. *Wear* **2003**, 254, 1070-1075.

[3.12] H. I. Kim, J. R. Lince, O. L. Eryilmaz, A. Erdemir. Environmental effects on the friction of hydrogenated DLC films. *Tribol. Lett.* **2006**, 21, 53-58.

[3.13] L .Ji, H. Li, F. Zhao, W. Quan, J. Chen, H. Zhou. Effects of environmental molecular characteristics and gas–surface interaction on friction behaviour of diamond-like carbon films. *J. Phys. D Appl. Phys.* **2009**, 42, 135301.

[3.14] J. A. Heimberg, K. J. Wahl, I. L. Singer, A. Erdemir. Superlow friction behavior of diamond-like carbon coatings: time and speed effects. *Appl. Phys. Lett.* **2001**, 78, 2449-2501.

[3.15] F. Platon, P. Fournier, S. Rouxel. Tribological behaviour of DLC coatings compared to different materials used in hip joint prostheses. *Wear* **2001**, 250, 227-236.

[3.16] J. Fontaine, T. Le Mogne, J. L. Loubet, M. Belin. Achieving superlow friction with hydrogenated amorphous carbon: some key requirements *Thin Solid Films* **2005**, 482, 99-108.

[3.17] C. Casiraghi, A. C. Ferrari, J. Robertson. Raman spectroscopy of hydrogenated amorphous carbons. *Phys. Rev. B* **2005**, 72, 085401.

[3.18] A. C. Ferrari, J. Robertson. Interpretation of Raman spectra of disordered and amorphous carbon. *Phys. Rev. B* **2000**, 61, 14095-14107.

[3.19] P. Wang, M. Hirose, Y. Suzuki, K. Adachi. Carbon tribo-layer for super-low friction of amorphous carbon nitride coatings in inert gas environments. *Surf. Coat. Technol.* **2013**, 221, 163-172.

[3.20] G. T. Gao, P. T. Mikulski, G. M. Chateauneuf, J. A. Harrison. The effects of film structure and surface hydrogen on the properties of amorphous carbon films. *J. Phys. Chem. B* 2003, 107, 11082-11090.

[3.21] A. R. Konicek, D. S. Grierson, A. V. Sumant, T. A. Friedmann, J. P. Sullivan, P. U. P. A. Gilbert, W. G. Sawyer, R. W. Carpick. Influence of surface passivation on the friction and wear behavior of ultrananocrystalline diamond and tetrahedral amorphous carbon thin films. *Phys. Rev. B* **2012**, 85, 155448.

[3.22] F. P. Bowden, D. Tabor. *The Friction and Lubrication of Solids*, Clarendon Press, Oxford, 1964.

Chapter 4

Suppression of Moisture Sensitivity of Friction by Si Incorporation

In this chapter, the effect of silicon incorporation on suppressing the moisture sensitivity of a-C:H film in humid environment is systematically investigated. Different Si contents in the a-C:H:Si films were obtained by varying the gas flow ratio of TMS/C_7H_8. The pressure-induced tribochemical interaction of water molecules with carbonaceous film surfaces, especially the hydrophilic Si-OH surface, is highlighted for its paramount role in reducing the friction. A boundary water lubrication model depending on humidity level is proposed for explaining the ultralow friction of Si–OH surface in humid condition.

4.1 Background

As shown in Chapter 3, hydrogen-rich a-C:H films can exhibit extremely low friction and outstanding durability in dry inert gas and H_2 atmosphere, which is consistent with previous studies by other researchers [4.1-7]. However, these exotic superlubric behaviours disappear when the same a-C:H films are tribotested in ambient air. High friction was observed for this hydrogen-rich a-C:H film, especially in the case of sliding against bare steel pins. It is emphasized that the gaseous species such as water, oxygen and hydrocarbons in the ambient surroundings can have strong interactions with the surface carbon network of the a-C:H films, which cause high friction during sliding [4.8-10].

In order to reduce the tribological moisture sensitivity in ambient air and expand the application of a-C:H films to a more wide range, inclusions of metal elements (e.g.,

Ti, W, Cr) or non-metal elements (e.g., Si, F, N) into carbon matrix to form nanostructured or nanocomposite films are proposed [4.11-14]. Due to the unique chemical characters of silicon atom, silicon-containing hydrogenated amorphous carbon (a-C:H:Si) films have been proven to possess low residual stress [4.15], strong adhesion to various substrates [4.16], high hardness [4.17], high thermal stability [4.18] and especially the ultralow friction in humid air [4.19, 20]. Many authors have reported on the reproducibility of ultralow friction coefficients of approximately 0.02-0.1 in ambient humid environment as well as on the limited deterioration of wear resistance of a-C:H:Si films [4.20, 21]. It has been commonly suggested that the formation of low shear strength colloidal silica or silicon hydroxides (namely hydrophilic Si-OH structure) at sliding interface is the major cause of low friction [4.19, 22]. For instance, Choi and coworkers employed oxygen plasma treatment to produce a silicon oxide layer on the top surface of Si-DLC films. They confirmed that the transferred silicon oxide tribofilm effectively protected the contact area between the steel and DLC surfaces when sliding, which resulted in a low friction coefficient [4.23]. Recently, some researchers have already recognized that hydrophilic OH-terminated carbon surface can provide ultralow friction. Martin et al. found that ta-C films exhibited ultralow friction under boundary lubrication in presence of OH-containing molecules such as glycerol and hydrogen peroxide [4.24]. Both experimental and simulation results strongly suggested that the hydroxylation of carbon surface together with the formation of water-rich film at sliding interface was the origin of ultralow friction [4.24]. Konicek et al. also reported that the ultralow friction and wear of ultrananocrystalline diamond originated from the H_2O dissociative passivation of surface dangling bonds during sliding [4.25]. However, up to now, little attention was paid to the prominent role of water molecule adsorption (which depends on relative humidity and reciprocation frequency during sliding) on the hydrophilic Si-OH surface that cannot be ignored during frictional sliding.

The present work considers the potential for extending the tribological performance from ultralow to superlow friction in ambient atmosphere by accurately

tailoring the structural properties of a-C:H:Si films and by controlling the environmental tribotesting conditions (e.g., humidity, contact pressure), as well as the possibility to illuminate the underlying lubrication mechanism involving interfacial water adsorption on hydrophilic silicon hydroxide (Si-OH) surface. In addition, some interesting findings of superlubric behaviour in dry N_2 were also indicated as favorable results to understand the low friction mechanism of a-C:H:Si films.

4.2 Experimental Methodology

4.2.1 Sample Preparation

Table 4.1 Gas flows and elemental composition of a-C:H:Si films.

Sample	Gas flow (sccm)		XPS-composition (at.%)			
	TMS	C_7H_8	C	Si	O	N
No.1	0	5	97.3	0	2.6	0.1
No.2	1	4	90.2	3.6	6.2	0
No.3	2	3	85.5	6.8	6.9	0.8
No.4	2.5	2.5	82.9	8.4	8.7	0
No.5	3	2	79.1	11.4	8.2	1.3
No.6	4	1	72.7	18.5	8.7	0.1
No.7	5	0	62.1	35.6	1.9	0.4

The silicon-containing hydrogenated amorphous carbon (a-C:H:Si) films were prepared by ion vapor deposition system using tetramethylsilane (TMS) and toluene (C_7H_8) as gas source, as shown in Chapter 2. Mirror-polished 0.5mm-thick n-type Si (100) wafers (*R*a=0.12 nm) were treated in a multistep ultrasonic cleaning procedure before serving as coating substrates. The chamber was pumped down to a base pressure of 3.0×10^{-3} Pa at the temperature of 200 °C. The ion gun system produces ion vapor through a filament cathode which generates electron (e.g., anode current of 0.5 A, filament current of 30 A, reflector voltage of 10 V) to ionize the gas. Ar^+ ion

bombarding was performed for 20 min to assure surface purity of the silicon substrates before deposition. A series of a-C:H:Si films containing different silicon concentration were then deposited in gas mixtures of C_7H_8/TMS through varying the gas flow ratio. The total flow volume was monitored at 5 sccm to keep the working pressure at around 0.22 Pa. The generated ion vapor was accelerated by a 25%duty-1kHz-pulsed bias voltage of 2 kV to arrive at the substrate. The deposition time was kept constant at 3 hour for all samples. The elemental composition of as-deposited a-C:H:Si films is given in Table 4.1.

4.2.2 Characterization

The classical Stoney's equation was employed to calculate the residual stress of the films by measuring the wafer curvature before and after film deposition. The thickness of the films was determined by observing the cross-sectional morphology in a Hitachi S-4800 scanning electron microscope (SEM) system. The hardness and elastic modulus of the films were characterized by nanoindentation (ENT-2100, Elionix). The indentation depth was set to about one-tenth of the film thickness to avoid any effect from substrate. The contact angle was measured by water-droplet shape method as an indicator of wettability for the film.

The friction tests were performed on the CSM standard pin-on-disk tribometer at room temperature. The threshold of the friction force measurement for the sensor is 5 mN when the normal load is within the range of 0-10 N, which indicates an accuracy of about 10^{-3} for the friction coefficient measurement. The coated Si wafer was fixed on a rotary sample platform using a SUJ2 ball of 6 mm in diameter as a counterpart. The rotation radius was 3.5 mm. A humid environment with different levels of humidity or dry inert gas atmosphere was produced by purging water vapor or dry N_2 (RH≤3%) into the tribometer chamber until stability. A Nikon optical microscope was used to observe the wear morphology after friction test.

The elemental composition and chemical bonding state of the asdeposited films

were derived from PHI Quantera II SXM X-ray photoelectron spectroscopy (XPS). XPS measurements were also conducted to analyze the wear debris on the SUJ2 ball and the wear track on the film. Before data collection, Ar^+ sputter was performed for 1 min to remove the contamination adsorbed on the surface. Atomic force microscope (AFM, Digital Instruments NanoScope IIIa) was employed to probe the surface topography and roughness of the films before and after the friction test.

4.3 Results

4.3.1 Overview of Basic Properties of a-C:H:Si Films

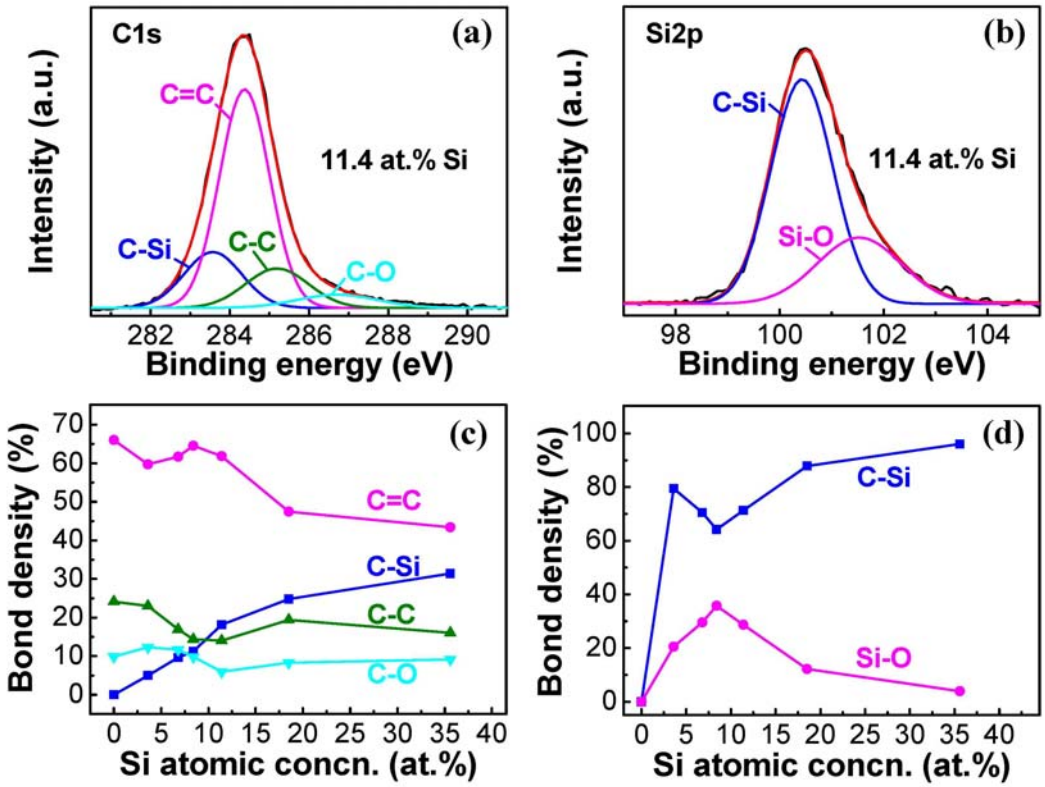

Figure 4.1 C1s (a) and Si2p (b) peak deconvolution for the a-C:H:Si (11.4 at.%) film, and the corresponding carbon-related bond (c) and silicon-related bond (d) density as determined from C1s and Si2p peaks as a function of silicon atomic concentration.

The evolution of elemental constituent of a-C:H:Si films as a function of TMS or C_7H_8 gas flow rate was characterized by XPS after Ar^+ sputter for 1 min, as shown in

Table 4.1. It can be obviously seen that the silicon concentration gradually increases from 0 to 35.6 at.% with raising the TMS flow rate from 0 to 5 sccm, while the carbon concentration decreases conversely. Except for the pure a-C:H (0 at.% Si) or highly-doped a-C:H:Si (35.6 at.% Si) films, a significant amount of oxygen (6.2-8.7 at.%) is incorporated into the films when the silicon concentration is in the range from 3.6 to 18.5 at.%.

Figure 4.1 shows the deconvoluted C1s and Si2p peaks for a-C:H:Si (11.4 at.% Si) film and the corresponding contribution of different bond configurations derived from C1s and Si2p peaks with respect to the silicon concentration. The broad C1s peak is composed of four peaks corresponding to C-Si, C=C (sp^2), C-C (sp^3) and C-O bonds (Figure 4.1(a)), while the Si2p peak is deconvoluted into C-Si and Si-O bonds (Figure 4.1(b)). The effect of Si concentration on the evolution of carbon-related bonds as shown in Figure 4.1(c) indicates that the contribution of C-Si bond increases when more Si atom is incorporated into the network. On the other hand, the amount of C=C (sp^2) bond gradually decreases (except for a temporary small increase when the Si concentration is in the range of 6.8-11.4 at.%) while the C-C (sp^3) bond density first decreases at low Si concentration up to 8.4 at.% and then saturates at the Si concentration above 11.4 at.%. These results indicate that the Si atom preferentially substitutes the sp^2-hybridized C atoms during deposition, which was similar to observations of hydrogen-free a-C:Si films [4.26]. The evolution of chemical bonding state from Si2p (Figure 4.1(d)) implies that the formation of hydrophilic group Si-O is enhanced by increasing the Si concentration up to 8.4 at.%., and then decreases quickly at the Si concentration above 11.4 at.%. It seems that high flow rate of TMS can effectively isolate the Si atom from residual oxygen in the chamber and simultaneously promote the formation of C-Si bond. It should be noted that the bond density of silicon-based surface structure especially the hydrophilic Si-O group plays an important role in determining the frictional performances of a-C:H:Si films (see discussions below).

Table 4.2 Summary of basic properties including film thickness *d*, roughness *R*a, residual stress σ_s, hardness *H*, elastic modulus *E* and contact angle CA of a-C:H:Si films with regard to the silicon concentration.

Sample	Si (at.%)	*d* (μm)	*R*a (nm)	σ_s (GPa)	*H* (GPa)	*E* (GPa)	CA (°)
No.1	0	1.98	0.27	-1.58	19.2	210.3	71.2
No.2	3.6	1.82	0.15	-1.43	20.2	205.1	65.8
No.3	6.8	1.54	0.13	-1.14	17.6	183.2	58.6
No.4	8.4	1.43	0.13	-1.0	17.3	178.6	59.8
No.5	11.4	1.25	0.09	-0.82	17.5	176.5	61.5
No.6	18.5	1.04	0.17	-0.82	17.5	173	68.9
No.7	35.6	0.74	0.11	-0.52	20.3	193.1	68.2

The microstructural, mechanical and surface properties of as-deposited a-C:H:Si films are summarized in Table 4.2. The thickness of the a-C:H:Si films is in the range from 0.74 to 1.98 μm, indicating different deposition rate determined by the ionization character of gas mixture. All the samples exhibit ultrasmooth surfaces with roughness *R*a of approx. 0.1-0.3 nm measured on 8 × 8 μm^2, independent of Si concentration. Being structurally amorphous, the a-C:H:Si films closely mimic the original surface roughness of silicon substrate (*R*a=0.12 nm). As expected, the incorporation of silicon effectively reduces the residual stress in the films. In detail, the residual stress progressively decreases from 1.58 to 0.52 GPa with increasing the Si concentration from 0 (pure a-C:H film) to 35.6 at.%. The hardness maintains a relatively high value (approx. 19-20 GPa) for pure a-C:H or a-C:H:Si films doped with low Si concentration (e.g., 3.6 at.%). Further increasing Si concentration from 3.6 to 18.5 at.% results in a saturation of the hardness at around 17.5 GPa. However, the a-C:H:Si film possesses a relatively high hardness (20.3 GPa) again when the Si concentration is raised to 35.6 at.%, which is attributed to the formation of SiC-rich structure in the films as shown in XPS results. A similar variation trend is also observed for the elastic modulus of the

a-C:H:Si films. The contact angle measurements demonstrate that all the deposited films show hydrophilic characteristic (θ<90°), reflecting the surface constructed by polar functional group (e.g., OH-termination). It is noteworthy that the a-C:H:Si films doped with Si concentration of 6.8-11.4 at% exhibited more hydrophilic (θ~60°) behaviors, compared with other samples, which reveals a close relationship with the surface chemical state (e.g., high bond density of Si-O shown in Figure 4.1) of the films.

4.3.2 Effect of Silicon Concentration on Frictional Performance

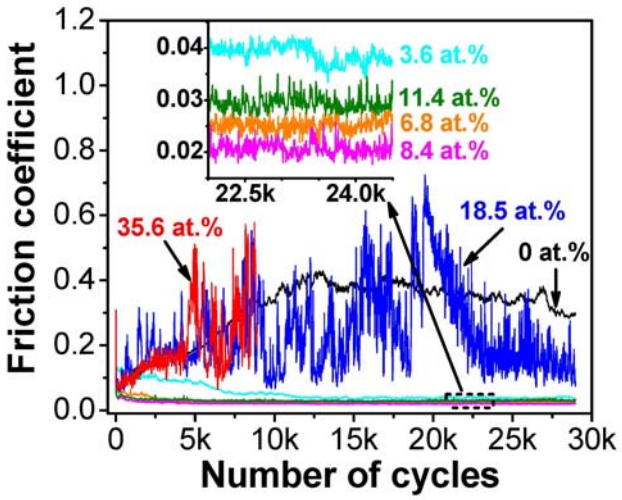

Figure 4.2 Evolution of friction coefficient of a-C:H:Si films with different silicon atomic concentration under testing conditions: SUJ2 counterface ball (diam. 6 mm), load 5 N, sliding velocity 10 cm/s, relative humidity 35%, ambient temperature 25±1 °C.

The evolution of friction coefficient being dependent on Si concentration in humid condition is displayed in Figure 4.2. The observed results clearly show that the amount of Si incorporated in the film microstructure has a remarkable influence on frictional performance of a-C:H:Si films. For pure a-C:H film (0 at.% Si), it exhibits a typical friction coefficient in the range of approx. 0.1-0.4 in humid air, as reported in other previous works [4.8, 27]. However, the steady-state friction coefficients are dramatically reduced to the ultralow level when a small amount of Si is introduced into the film, e.g.,

0.04 (3.6 at.% Si), 0.025 (6.8 at.% Si), 0.02 (8.4 at.% Si) and 0.03 (11.4 at.% Si), respectively. In contrast, the friction coefficients evolve from the ultralow level into a high and unstable state (approx. 0.1-0.7) when further increasing the Si concentration from 18.5 to 35.6 at.%. Especially for the a-C:H:Si film doped with highest Si concentration (35.6 at.%), the friction test was artificially stopped due to the intensive vibration of the CSM tribometer caused by high friction during sliding. The above results demonstrate a close relationship between the silicon-induced bonding structure evolution and the frictional performance of a-C:H:Si films. In the case of low Si concentration (3.6 to 11.4 at.%), the high density of hydrophilic surface bond Si-O (see in Figure 4.1(d)) determines the ultralow friction of a-C:H:Si films in humid air. At Si concentration above 18.5 at.%, the high friction is associated with the transformation from amorphous to SiC-rich structure as shown in Figure 4.1, which was also observed by other researchers [4.28-30]. Compared with amorphous a-C:H:Si films, pure SiC [4.29] or amorphous carbon films with SiC-rich crystallites [4.30] is quite stable and does not undergo surface oxidation by gaseous molecules in the humid environment at normal temperature. Thus, it is of great difficulty in the formation of a hydrated silica layer as well as adsorbing water molecules on the SiC-rich surface [4.29]. Without surface passivation by water molecules, the two slide surfaces get into direct contact which can cause high friction. In addition, hard SiC particles are generated due to brittle fracture during sliding. These particles would adhere on the wear track and act as stress-concentrated third-body abrasives between the contact surfaces, which causes high friction and severe plowing grooves on the worn surfaces (see in Figure 4.3(e) and (f)).

Figure 4.3 shows the surface wear morphologies selected from pure a-C:H (0 at.% Si), moderately-doped a-C:H:Si (8.4 at.% Si) and highly-doped a-C:H:Si (35.6 at.% Si) films, as well as the corresponding wear scars on SUJ2 ball after the friction test. It can be observed from Figure 4.3(a) that a clear wear track was generated on pure a-C:H:Si film. A small amount of wear debris is distributed outside the wear track. The

corresponding SUJ2 ball exhibits an obvious wear scar (~240 μm diam. in Figure 4.3(b)), which is surrounded by a large amount of wear debris. However, the moderately-doped a-C:H:Si (8.4 at.% Si) film reveals much more shallow wear track (Figure 4.3(c)) as well as more effective protection of SUJ2 counterpart (Figure 4.3(d)). The size of wear scar on SUJ2 ball is reduced to ~170 μm in diameter under the same tribotesting condition. An abundance of tribofilm is distributed both inside and outside the wear scar, indicating continuous and durable lubrication effect during sliding. On the contrary, the highly-doped a-C:H:Si (35.6 at.% Si) film suffers severe wear scratch (Figure 4.3(e)) even just after much more shorter friction test (see in Figure 4.2). Correspondingly, the SUJ2 ball is severely worn and no protecting tribofilm is found on the sliding contact area (Figure 4.3(f)).

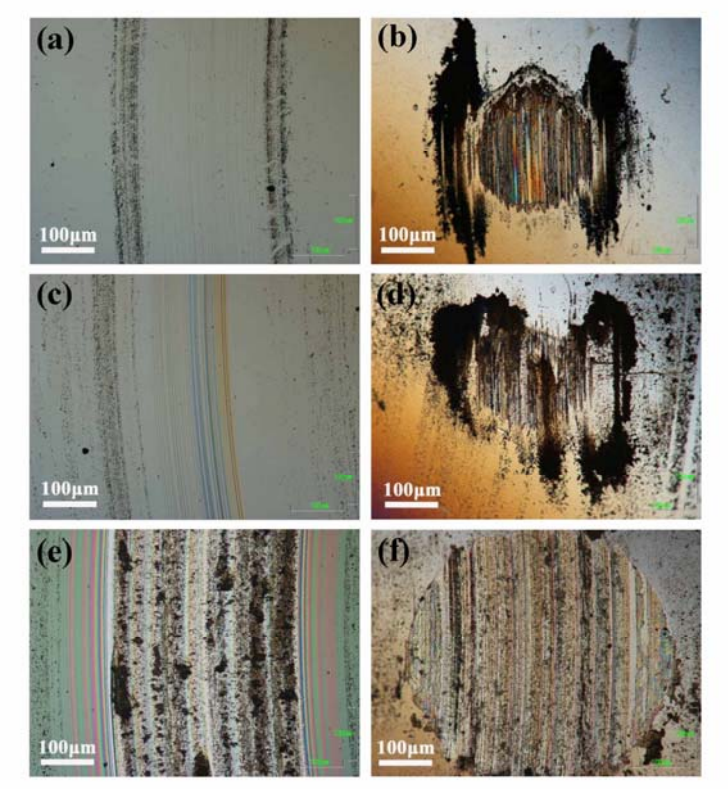

Figure 4.3 Wear tracks of a-C:H:Si films with (a) 0 at.%, (c) 8.4 at.% and (e) 35.6 at.% Si concentration, and the corresponding wear scars on SUJ2 counterparts (b), (d) and (f) after the friction test as shown in Figure 4.2.

4.3.3 Humidity Effect and Contact Pressure Threshold for Superlow Friction in Humid Air

Water adsorption as a result of ambient humidity is a crucial factor to control the tribological properties of sliding contact interface, especially hydrophilic surface. To further elucidate the humidity effect on the frictional behaviour, moderately-doped a-C:H:Si film with 8.4 at.% Si is chosen to be tested under a wide range of humid condition, as displayed in Figure 4.4. For the purpose of clarity, not all the obtained friction data is shown in Figure 4.4. It is obvious that the frictional performance of a-C:H:Si film is strongly dependent on the relative humidity. The average steady-state friction coefficient gradually decreases from about 0.053 at high RH of 95% to 0.012 at RH of 40%, and then reversely increases to 0.02 with further reducing the humid level to RH of 21%.

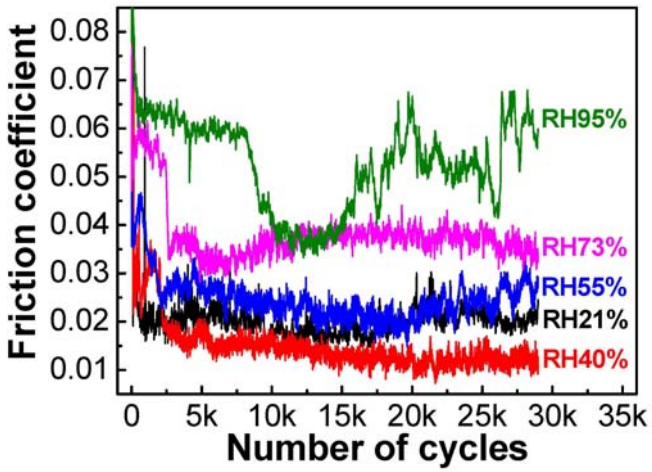

Figure 4.4 Evolution of friction coefficient of a-C:H:Si (8.4 at.%) film as a function of relative humidity (RH) under testing conditions: SUJ2 counterface ball (diam. 6 mm), load 5 N, sliding velocity 10 cm/s, ambient temperature 30±0.5 °C.

On a variety of substrates, adsorbed water layer thickness in the range of 1-20 Å has been reported depending on the surface property of substrate and humid level [4.31, 32]. Using an estimate of 3 Å for the thickness of one monolayer of adsorbed water

molecule, it corresponds to a range of <1 to 6 monolayers of adsorbed water. For a-C:H:Si film, the interaction of water with hydrophilic oxide surface is significantly affected by ambient humid level through hydroxylation of the surfaces due to adsorption and dissociation of water as well as oxygen. The formation of an OH-rich surface can induce a highly oriented growth of the adsorbed water layers through H-bonds with surface OH groups and with other water molecules [4.32].For instance, Asay et al. found that in the RH range of 30-60%, the adsorbed water molecules on hydrophilic silicon oxide surface grow into ~3 molecular underneath layers of ice-like (layer-like) ordered structure and ~1 molecular upper layer of liquid-like structure [4.33]. The friction test results in Figure 4.4 indicate that the humidity-induced oriented structure of confined water between two sliding contact surfaces is highly correlated with the frictional behaviors of a-C:H:Si films in humid environment.

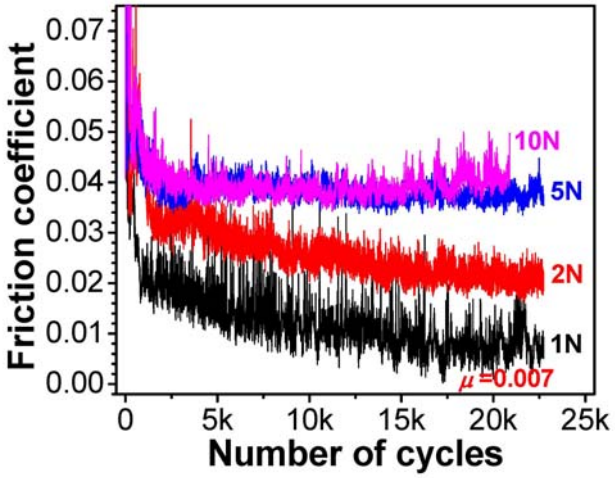

Figure 4.5 Evolution of friction coefficient with respect to applied normal load under testing conditions: SUJ2 counterface ball (diam. 6 mm), sliding velocity 20 cm/s, relative humidity 33±2%, ambient temperature 24±0.4 °C.

The traditional Bowden and Tabor model assumes that the friction coefficient depends on the shear strength S of the interfacial tribofilm, the real contact area A and the normal load W, described as follows [4.34]:

$$\mu = S\frac{A}{W} \tag{4.1}$$

The shear strength of solid lubricant film at high pressure is commonly observed to be pressure dependent, which can be approximately represented as [4.35]:

$$S = S_0 + \alpha P \tag{4.2}$$

Hence, the friction coefficient can be expressed as:

$$\mu = \frac{S_0}{P} + \alpha \tag{4.3}$$

where S_0 is the shear strength of contact interface including a solid lubricant film, P is the real mean contact pressure and α is a constant. Therefore, in a given tribological system, the friction coefficient correlates closely with the contact pressure. However, due to the practical impossibility to calculate the real contact area A, it is a great challenge to obtain the real mean contact pressure P in Equation (4.3). In order to enable the calculation of contact pressure, the classical Hertzian contact model is quoted to simplify this calculation procedure. The Hertzian contact theory assumes that, for smooth balls and flat substrates loaded below the elastic limit, the real contact area corresponds to the Hertzian contact zone. Thus, the initial mean Hertzian contact pressure can be calculated as:

$$P = \pi^{-1}\left(\frac{3R}{4E^*}\right)^{-2/3} W^{1/3} \tag{4.4}$$

where R is the radius of the ball and E^* is the composite elastic modulus of the contact couples. Based on this assumption, the Equation (4.3) can be rewritten as:

$$\mu = S_0\pi\left(\frac{3R}{4E^*}\right)^{2/3} W^{-1/3} + \alpha \tag{4.5}$$

Equation (4.5) indicates that, in general, the friction coefficients tend to decrease with increasing normal load or contact pressure. This Hertzian contact model has been successfully used to predict the decrease in friction coefficient with increasing contact pressure in the case of soft and thin interfacial films such as MoS_2 [4.35] and boric acid

films [4.36]. It should be pointed out that the calculated pressure value in Equation (4.5) corresponds to the initial mean Hertzian contact pressure. However, as the contact interfacial properties such as roughness and rheology are evolving all the time during friction and wear test, the true contact pressure as well as the "apparent" mean Hertzian contact pressure varies correspondingly. In spite of this, the initial mean Hertzian contact pressure is still significant to serve as an index for evaluating the pressure-induced bond breaking and formation during running-in period which remarkably affect the final steady-state frictional performance [4.37].

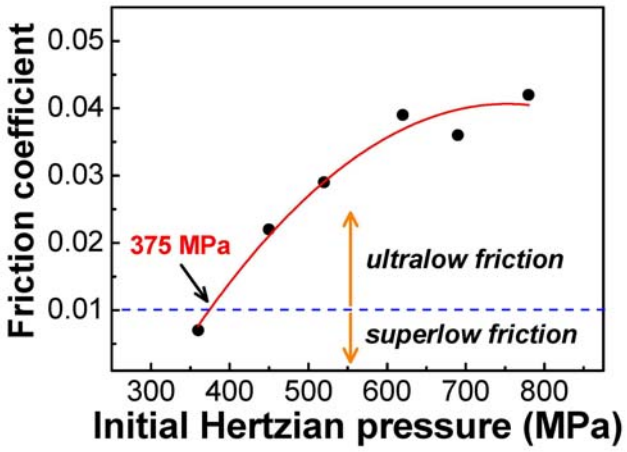

Figure 4.6 Initial mean Hertzian contact pressure dependence of steady-state friction coefficient indicating a contact pressure threshold for the transition from ultralow to superlow friction in the given tribosystem.

For this purpose, the moderately-doped a-C:H:Si film with 8.4 at.% Si was further tribotested under different normal load, as shown in Figure 4.5. It is obviously observed that the friction coefficient increases monotonically with increasing normal load from 1 to 10 N, which shows a reverse trend to the claim mentioned above. Furthermore, for the case of 1 N, the friction coefficient continuously evolves from ultralow into superlow scope and finally stabilizes at ~0.007. In summary, the steady-state friction coefficients obtained from more tribotests are plotted against the initial mean Hertzian contact pressure in Figure 4.6. It indicates that the friction coefficient increases steeply

with increasing the contact pressure up to 550 MPa, and then saturates to a value of ~0.04 at the contact pressure above 600 MPa. By fitting the data, there exists an initial Hertzian contact pressure threshold (~375 MPa) for the transition from ultralow to superlow friction in the given tribosystem. However, it should be pointed out that the pressure threshold is quite sensitive to the change of contact interfacial properties and the tribotesting conditions (e.g., humidity, temperature, sliding velocity). The present results demonstrate that in the case of very thin interface films such as OH-terminated surfaces on hydrophilic carbon materials as well as the confined very thin water layer (such as thickness below 2 nm), the general correlation between contact pressure and friction coefficient for solid lubricant derived from the Hertzian contact model as described in Equation (4.5) is not valid.

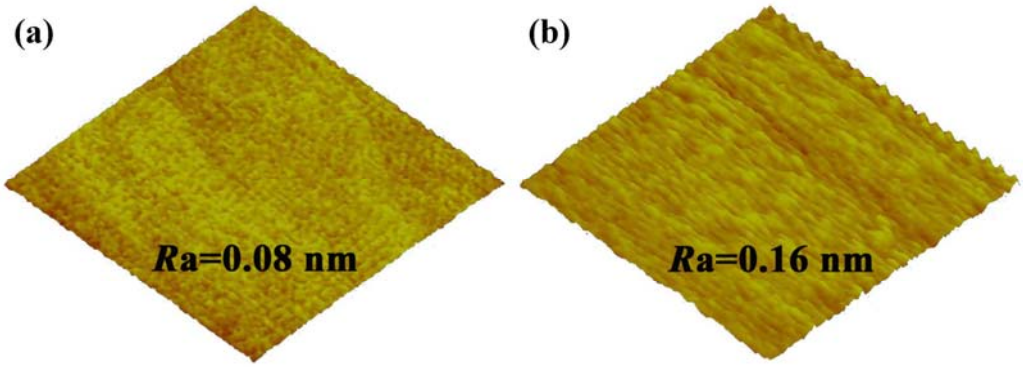

Figure 4.7 AFM micrographs of an area of 0.2×0.2 μm^2 showing the comparison of surface morphology between (a) asdeposited surface of a-C:H:Si (8.4 at.%) film and (b) worn surface located inside the wear track of a-C:H:Si (8.4 at.%) film after the friction test as shown in Figures 4.2 and 4.3(c).

To clarify the possible mechanism of friction and wear behavior, AFM was employed to analyze the wear morphology after sliding test. Figure 4.7 shows the comparison of surface morphology between asdeposited a-C:H:Si (8.4 at.%) film and the corresponding worn surface located inside the wear track as shown in Figure 4.3(c). The wear track is composed of numerous tiny grooves, which are typical morphologies of abrasive wear. The AFM results indicate that the worn surface maintains the

ultrasmooth character as the original asdeposited surface. It implies that the wear behaviour at each local contact junction occurs between atomically smooth surfaces, which enable the low friction due to an apparent lack of interlocking.

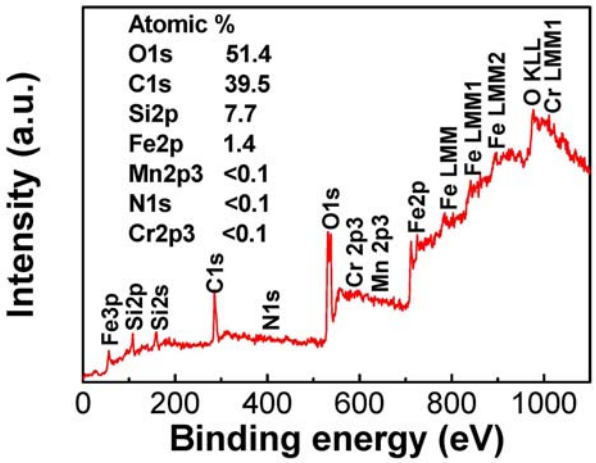

Figure 4.8 XPS full spectrum of the wear scar surface inside the contact area on SUJ2 ball after sliding against a-C:H:Si (8.4 at.%) film-coated silicon wafer as shown in Figures 4.2 and 4.3(d).

To further elucidate the tribochemistry, XPS was hired to characterize the chemical reactions during sliding. Special attention was focused on the formation of a hydrophilic silicon oxide (Si-O) surface, considering the phase separation of the carbon matrix induced by the chemical reaction during contact process. Figure 4.8 shows the full spectrum analysis of wear scar surface inside the contact area on SUJ2 counterpart ball after sliding against a-C:H:Si (8.4 at.%) film-coated silicon wafer as shown in Figures 4.2 and 4.3(d). A highly-oxidized tribofilm (e.g., 51.4 at.% O, 39.5 at.% C, 7.7 at.% Si) was found covering the contact area on SUJ2 ball, while only a small amount of Fe (1.4 at.%) was detected. It indicates that the tribofilm produced by sliding contact was transferred and tightly bonded to the SUJ2 surface, resulting in a tribofilm/tribofilm counterface sliding system. The chemical bonding change of C1s and Si2p between asdeposited a-C:H:Si film (8.4 at.%) and tribofilm inside the wear scar on SUJ2 ball is shown in Figure 4.9. For carbon-based bonds (see C1s peaks in Figure 4.9(a) and (b)),

the bond density of C-Si decreased during sliding process while the carbon matrix (such as sp^2(C=C) and sp^3(C-C) bonds) was in a large extent oxidized into carbon oxides (e.g., C-O, C=O, O-C=O). The evolution of Si2p peaks (Figure 4.9(c) and (d)) conforms the phase separation of surface Si-C bond during sliding into a main component of SiO_2 and some silicon suboxide species (Si^{2+}-Si^{3+}) [4.38].

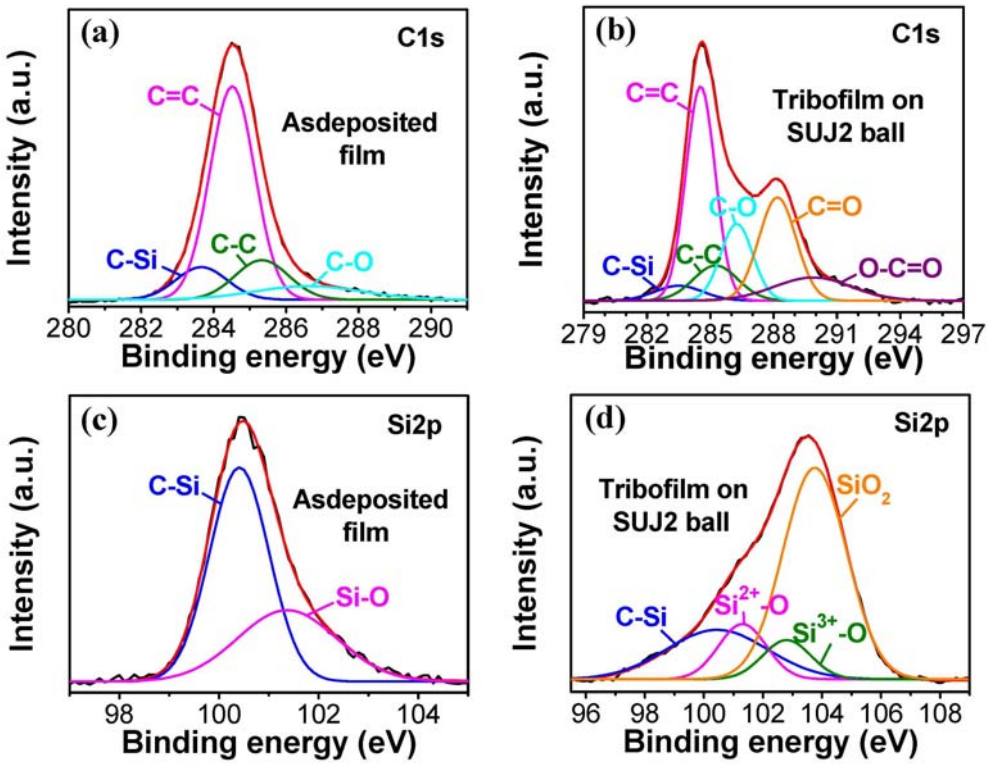

Figure 4.9 Comparison in chemical bonding change of C1s peaks between (a) asdeposited a-C:H:Si film (8.4 at.%) and (b) transferred tribofilm inside the wear scar on SUJ2 ball after the friction test as shown in Figures 4.2 and 4.3(d), as well as the case of Si2p peaks (c) and (d).

The surface chemical bonding information inside the wear track of a-C:H:Si film (8.4 at.%) after the friction test as shown in Figures 4.2 and 4.3(c) was collected by XPS depth profile as a function of Ar^+ sputter time, as displayed in Figure 4.10. During sputter depth profiling, accelerating Ar^+ ions of 4 keV at a scan size of 2×2 mm^2 and a 0.5 min sputter interval were used. The total sputter time was 3 min. These conditions

result in a typical sputter rate of ~30 nm/min for standard SiO_2. For the top-most surface of the wear track (Ar^+ sputter time: 0 min), the C1s spectrum (Figure 4.10(a)) verifies the evolution of carbon matrix into a highly-oxidized state (e.g., C1s peak shifts to a higher position of C-O) during sliding process in ambient gaseous environment, while the Si2p spectrum (Figure 4.10(b)) indicates the existence of a silicon oxide layer on the near surface (e.g., Si2p peak shifts to a higher position of Si-O). In addition, the O1s spectrum (Figure 4.10(c)) appears to show a strong intensity, confirming the main oxidized states of carbon and silicon in the form of C-O and Si-O, respectively.

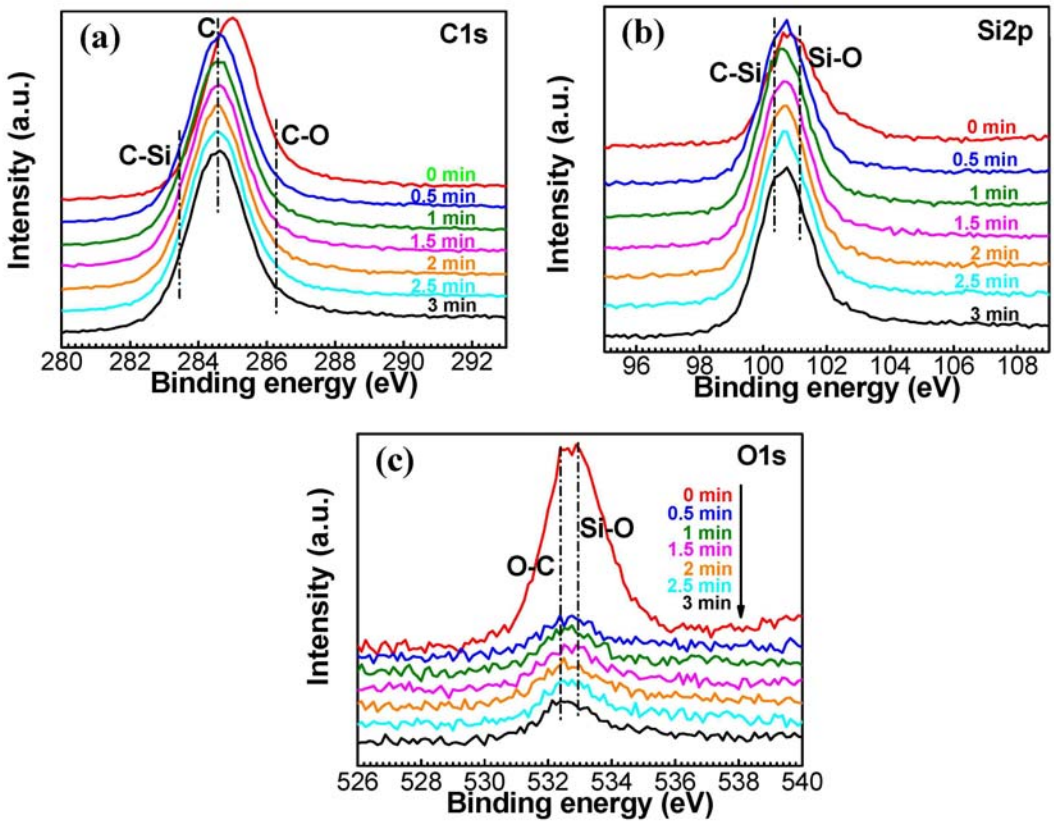

Figure 4.10 XPS depth profile of (a) C1s, (b) Si2p and (c) O1s as a function of Ar^+ sputter time measured inside the wear track of a-C:H:Si (8.4 at.%) film after the friction test as shown in Figures 4.2 and 4.3(c). Ar^+ sputter rate for SiO_2: 30 nm/min.

However, after 0.5 min sputter by Ar^+ ions, the highly-oxidized characters in the C1s and Si2p peaks disappear, which show similar spectrum shape to the asdeposited

a-C:H:Si film as shown in Figure 4.9(a) and (c). The peak shape and intensity of C1s and Si2p sustain almost the same with further increase in the sputter time, indicating that Ar^+ ion etching reaches the bulk film. Thus, it is inferred that 0.5 min Ar^+ ion sputter removes the whole highly-oxidized layer composed of carbon and silicon oxide on the tribofilm surface. Considering the sputter rate for standard SiO_2, it corresponds to ~15 nm sputter depth. It should be pointed out that the sputter rate is determined by the chemical bonding characteristics and composition of the film. Due to the composition discrepancy between the tribofilm (mainly silicon and carbon oxide) and the standard SiO_2, the actual sputter rate for the tribofilm is unknown in the given condition if without reference calibration such as mesh-replica method. In spite of this, the present XPS depth profiling results clearly confirm the existence of a few or a dozen nm thick silicon oxide layer on the near-surface tribofilm.

4.3.4 Tribofilm Build-Up and Durable Superlubricity in Dry Nitrogen

As compared with humid environment, friction test was also performed in dry N_2 atmosphere (RH≤3%). Figure 4.11 shows the comparison of superlow friction behaviours in dry N_2 conditions between bare SUJ2 ball/a-C:H:Si (8.4 at.%) film counterfaces and self-mated a-C:H:Si (both the Si wafer and the SUJ2 ball were coated with a-C:H:Si (8.4 at.%) film) sliding interfaces. It is observed from Figure 4.11(a) that after a short running-in period (μ~0.7), the friction coefficient sharply decreased to an extremely low value (μ~0.005). After several hundreds of sliding cycles, the superlow friction disappeared and the friction coefficient quickly rose to a high level (e.g., μ>0.2). However, the friction coefficient evolved into the superlow scope again with increasing the sliding cycles. This phenomenon of oscillating switch between superlow and high friction recurred continuously throughout the whole friction test. Severe worn surfaces were produced both on the film and SUJ2 ball as shown in Figure 4.11(b) and (c). It seems that no tribofilm was built up on the SUJ2 steel surface in dry N_2 atmosphere, resulting in a poor protection of the sliding interfaces. As a consequence, it also

deteriorated the wear resistance of the a-C:H:Si film.

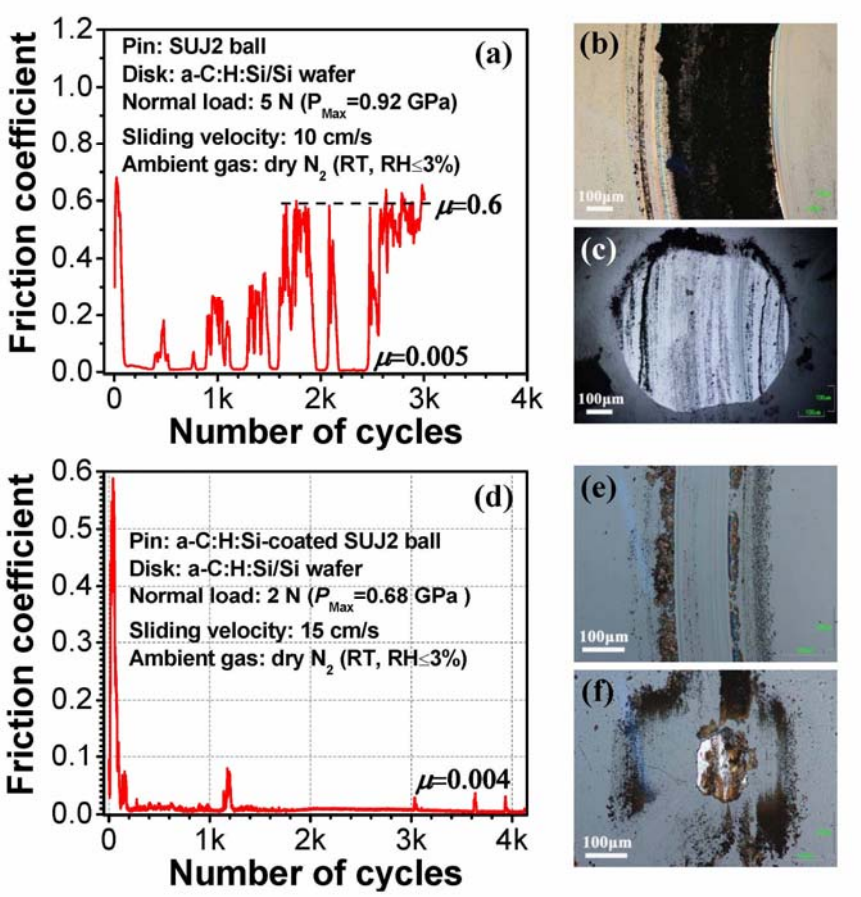

Figure 4.11 Friction coefficient in dry N_2 atmosphere at room temperature (RH≤3%), versus the number of sliding cycles, of (a) SUJ2 ball/a-C:H:Si (8.4 at.%) film counterfaces and the corresponding (b) wear track on film and (c) wear scar on ball, and of (d) self-mated a-C:H:Si (8.4 at.%) film counterfaces as well as the resulted (e) wear track on disk and (f) wear scar on pin.

To the contrary, Figure 4.11(d) displays a stable and durable superlow frictional performance with a steady-state friction coefficient of ~0.004 (except for several temporary vibration in the friction coefficient, which indicates a short period of failure in building-up of tribofilm) in the case of self-mated a-C:H:Si (8.4 at.%) film counterfaces. The resulting wear track on disk and wear scar on pin are shown in Figure 4.11(e) and (f), respectively. The track on a-C:H:Si coated Si wafer is quite smooth and mild, and some dark brown fragments can be observed to distribute along the wear track.

For the wear scar on a-C:H:Si coated SUJ2 ball, a dark brown to black tribofilm is accumulated in the central contact area and also spread around the contact area. These observations suggest that the continuous formation of cohering and stable tribofilm between self-mated a-C:H:Si counterfaces is the crucial requirement for obtaining superlow friction as well as improving the durability of sliding surfaces in dry N_2 environment.

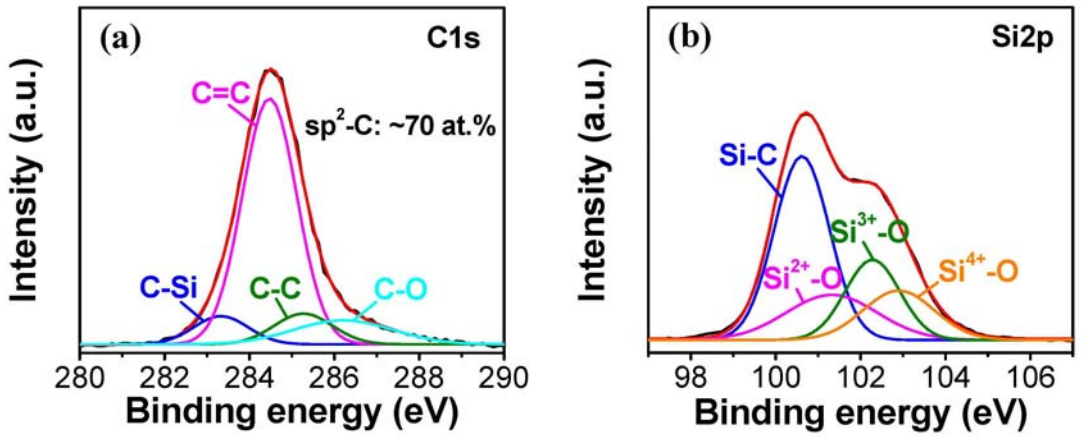

Figure 4.12 Chemical bonding states of (a) C1s and (b) Si2p peaks of the tribofilm formed inside the wear scar on SUJ2 ball after the friction test in dry N_2 atmosphere as shown in Figure 4.11(f).

Further analysis by XPS reveals that the tribofilm produced on SUJ2 ball worn surface is composed of 75.5 at.% C, 13.4 at.% O, 9.7 at.% Si, 1.3 at.% N and 0.1 at.% other trace elements, which is very close to the composition of the counterface film (see in Table 4.1). The chemical bonding states of C1s and Si2p of the tribofilm inside the wear scar on SUJ2 ball as shown in Figure 4.11(f) are indicated in Figure 4.12(a) and (b), respectively. The C1s peak indicates that the sp^2-bonded carbon (up to 70 at.%) is dominant in the carbon-based tribofilm, while the Si2p peak demonstrates that the Si atom is mainly in the chemical bonding state of Si-O and C-Si. These results suggest that wear-induced graphitization of carbon matrix and phase separation of silicon-related bonds occurred during the sliding process. The observed superlow

friction can be attributed to the development of a low shear strength tribolayer containing graphitized carbon and silicon oxide, whereas the temporary vibration in friction coefficient might be originated from the formation of some C-Si fragments during sliding. Under these conditions, the wear process can be regarded as a low-rate continuous consumption of counterface material and generation of the friction-reducing tribofilm.

4.4 Discussion

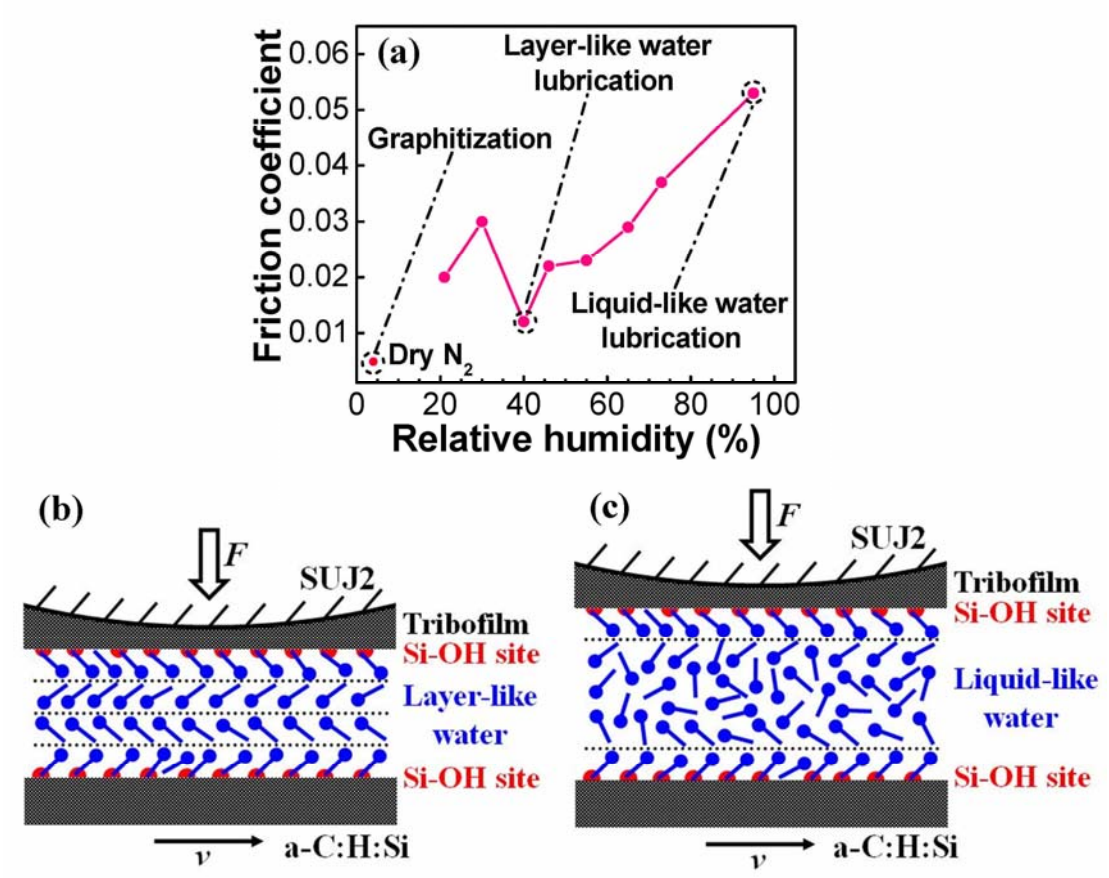

Figure 4.13 Lubrication mechanism of a-C:H:Si (8.4 at.%) film indicating (a) the evolution of friction coefficient as a function of relative humidity, and schematic diagrams of water-involved lubrication effect on hydrophilic Si-OH surface: (b) layer-like water lubrication under an intermediate relative humidity and (c) liquid-like water lubrication under a high relative humidity.

Reactive gas molecules in the surrounding environment are involved in governing the tribological behaviours of a-C:H films. In ambient humid condition, adsorbed water and oxygen molecules interact with the carbonaceous surface, which acts as a hindrance to the low friction of carbon film [4.8]. The incorporation of Si into a-C:H film is feasible to lower the friction by utilizing these gaseous molecules to form hydrophilic surface and the following water-mediated aqueous lubrication. Generally water has a low viscosity so it is difficult to directly form an EHL lubrication layer in a sphere-on-plane contact configuration at high contact pressure, even at high sliding velocity [4.39]. Therefore water is not so effective in lubricating hard steel contact interfaces, except in the case of hydrodynamic lubrication regime when a continuous fluid water layer is formed [4.40]. However, when water molecules are confined to micro- or nano-scale contact space, especially on hydrophilic interface, the dissociative species (H- or OH-) and orientation of molecular structure of adsorbed water are found to produce ultralow friction [4.24, 41]. Recently, Konicek has evidenced that the passivation of dangling bonds on ultrananocrystalline diamond surface by OH-termination instead of sliding-induced graphitization is the intrinsic origin of ultralow friction (0.015-0.03) in presence of water adsorption [4.25, 37]. As noted in section 4.3.3, one important issue is the extent of hydroxylation of carbon surface due to silicon oxidation (controlled by the concentration of doped silicon atom) and water adsorption together with water dissociation (determined by the humidity level). The formation of an OH-rich surface can induce a highly oriented growth of the adsorbed water layers through hydrogen bonds with surface OH groups and with other water molecules. This has been verified from ATR-IR analysis of the evolution of adsorbed water layer structure on silicon oxide as a function of relative humidity (RH) [4.33]. A completely hydrogen-bonded icelike (layer-like) network of water molecules grows up to three monolayers (equivalent to about 0.85 nm) on Si-OH surface when the RH increases from 0 to 30%, and then the liquid-like water molecular structure appears while the layer-like structure continues growing to saturation in the RH range of

30-60%. Above 60% RH, the liquid water configuration grows on top of the icelike layer. The total thickness of adsorbed water layer is ~3 nm when the RH reaches 99.4% [4.33]. It is worth emphasizing that the first Si-OH layer plays a significant role in determining the interfacial behaviour and can be strongly influenced by the surface chemistry of the film, and this influence can propagate into the subsequently adsorbed multilayers of water, until the water film reverts to its bulk structure (liquid-like) [4.32]. However, it should be pointed out that the ATR-IR confirmation of water layer on Si-OH surface was measured under static and unconfined conditions, which is different from the confined geometry and shear deformation during sliding contact. Recently, molecular dynamics simulations on OH-terminated Si substrates under a sliding condition reveal that the water molecules can still be formed in a layered structure under high pressure and steady shear, which acts as a boundary lubrication film to lower the friction [4.42].

Considering both these reports and the present work, the specific role of adsorbed water on hydrophilic surface in humid environment and its tribochemical influence on lubricating mechanism of a-C:H:Si films can be highlighted, as schematically summarized in Figure 4.13. At an appropriate RH of ~40%, the a-C:H:Si film exhibits the lowest friction coefficient (~0.012, Figure 4.13(a)) due to the development of low shear strength layer-like water boundary lubrication (Figure 4.13(b)). Increase in the RH above 40% causes water to adsorb as in the liquid-like configuration (Figure 4.13(c)), which results in a gradual increase in the friction coefficient. Special attention should be paid to the superior friction-reduction effect of the layer-like water to the liquid-like water. As shown in Figure 4.13(b), one monolayer of water molecules are strongly bound to the Si-OH surface, and the subsequently adsorbed water molecules are bound to the neighboring ones through hydrogen bonds. Finally, a layer-like structure linked by hydrogen bond networks develops on top of the Si-OH surface. When two such boundary layers slide past each other, the slip plane shifts from the original carbon-film/tribofilm interface to the mid-plane between the boundary layers. Due to

the relatively week shear strength of the repulsive interaction between them exerted by the same polarity end-group (such as H-/H- or OH-/OH- Van der Waals interaction, 0.08 eV/bond [4.27]), the two boundary layers can now slide easily past each other. A similar friction-reduction owing to the slide plane shifts has also been reported in hydration boundary lubrication under water [4.43, 44]. In contrast, the water molecules in liquid-like configuration as shown in Figure 4.13(c) distribute randomly along the entire boundary water layer. The strong hydrogen bonds (0.2 eV/bond [4.27]) between the neighboring water molecules increase the adhesive resistance to shear during sliding, which cause a higher friction in comparison to layer-like water structure. However, we should point out a remarkably different lubricating behaviour of layer-like water under atomic-scale friction observed by Jinesh and Frenken [4.45, 46]. They employed a friction force microscopy to scan a sharp tungsten tip over a graphite surface under humid condition. The results demonstrate that the capillary condensation of water between the tungsten tip and the graphite surface leads to the formation of ice-lie water at room temperature, which increases the friction force [4.45, 46]. The major reason for friction increase in such atomic single-asperity contact, as opposed to the present pin-on-disk multiple-asperity contact, is the pressure-induced high viscosity of the capillary meniscus between the sharp tip and the smooth surface [4.47]. This high capillary force and the repeating occurrence of stick-slip motions make the ice-structure water condensate behave like glue rather than a lubricant [4.45].

On the other hand, decrease of the RH from 40 to 30% leads to a temporary rebound of friction coefficient up to 0.03 due to the attenuation of adsorbed water layer. Further decrease in the RH below 30% quickly diminishes the coverage of adsorbed water, which exposes the sliding surfaces to direct contact and enhances the graphitization process for friction reduction. Finally, the graphitization dominates the friction-induced structural transformation for superlubiricity in dry N_2 atmosphere. In addition, it is noteworthy that the ultralow friction coefficient of Si-OH surface saturates at around 0.04 when further increasing the initial mean Herztian contact pressure to a

high value (see in Figure 4.6). This phenomenon can be explained by the atomic interaction characteristics of OH-terminated surfaces. The high contact pressure promotes breaking the hydrogen bonds between adjacent water molecules and squeezing the adsorbed water out of the contact space layer by layer when the contact pressure is increased. Finally, sliding contact occurs primarily between two Si-OH surfaces. These OH-terminated surfaces can provide strong repulsive interaction against each other to lower the shear strength during sliding, which sustains the ultralow friction between two Si-OH surfaces even under high contact pressure. This proposal is also confirmed by MD simulations on OH-terminated diamond or DLC surfaces [4.48, 49]. For instance, atomic friction between OH-terminated DLCs simulated by tight-binding quantum chemical molecular dynamics indicates that OH-termination can effectively suppresses the formation of C–C covalent bonds at the friction interface and it leads to a ultralow friction coefficient even at a high contact pressure of 7 GPa [4.49]. This saturation of friction coefficient to the applied contact pressure has also been observed in an atomic-scale friction experiment in humid environment [4.46].

4.5 Summary

Tribochemistry between gaseous molecules and the hydrophilic surface has been shown to be responsible for the control of ultralow friction in humid environment observed with a-C:H:Si films by accurately controlling the film composition and the tribotesting conditions. Both surface density of silicon hydroxyl group (Si-OH) and humidity level determine the frictional performance of a-C:H:Si films. Ultralow friction is feasible in a wide range of relative humidity for a-C:H:Si film with low concentration of Si (e.g., below 11.4 at.%), while this kind of low friction disappears due to the formation of SiC-rich structure for highly-doped a-C:H:Si film (e.g., Si concentration above 18.5 at.%). An extremely low friction of ~0.01 can be realized by a suitable control of the silicon concentration (e.g., 8.4 at.%) and the humid level (e.g., RH of 40%). The load-capacity tribotest reveals that the correlation between contact pressure

and friction coefficient derived from Hertzian contact model for solid lubricant is not valid in the case of very thin interface films such as OH-terminated surface together with the confined water layer. Furthermore, there exists an initial mean contact pressure threshold for the transition from ultralow to superlow friction (~0.007) in the given tribosystem. The dissociative formation of OH-terminated surface and the orientation of molecular structure of adsorbed water is the origin of ultralow friction of Si-OH surface in humid condition. At an appropriate RH level, the formation of low shear strength layer-like water film provides effective boundary lubrication, while the development of liquid-like water configuration in high humidity deteriorates the friction property. In contrast, the superlow friction (~0.004) in dry N_2 atmosphere is attributed to the wear-induced graphitization and the resulting formation of a low shear strength tribolayer containing graphitized carbon and silicon oxide.

References

[4.1] J. Fontaine, T. Le Mogne, J. L. Loubet, M. Belin. Achieving superlow friction with hydrogenated amorphous carbon: some key requirements. *Thin Solid Films* **2005**, 482, 99-108.

[4.2] A. Erdemir. Design criteria for superlubricity in carbon films and related microstructures. *Tribol. Int.* **2004**, 37, 577-583.

[4.3] C. Donnet, J. Fontaine, A. Grill, T. Le Mogne. The role of hydrogen on the friction mechanism of diamond-like carbon films. *Tribol. Lett.* **2000**, 9, 137-142.

[4.4] C. Matta, O. L. Eryilmaz, M.-I. De Barros Bouchet, A. Erdemir, J.-M. Martin, K. Nakayama. On the possible role of triboplasma in friction and wear of diamond-like carbon films in hydrogen-containing environments. *J. Phys. D: Appl. Phys.* **2009**, 42, 075307.

[4.5] J. A. Heimberg, K. J. Wahl, I. L. Singer, A. Erdemir. Superlow friction behavior of diamond-like carbon coatings: time and speed effects. *Appl. Phys. Lett.* **2001**, 78, 2449-2451.

[4.6] L .Ji, H. Li, F. Zhao, W. Quan, J. Chen, H. Zhou. Effects of environmental molecular characteristics and gas–surface interaction on friction behaviour of diamond-like carbon films. *J. Phys. D Appl. Phys.* **2009**, 42, 135301.

[4.7] J. A. Johnson, J. B. Woodford, X. Chen, J. Andersson, A. Erdemir, G. R. Fenske. Insights into ‘‘near-frictionless carbon films’’. *J. Appl. Phys.* **2004**, 95, 7765-7771.

[4.8] C. Donnet, T. Le Mogne, L. Ponsonnet, M. Belin, A. Grill, V. Patel, C. Jahnes. The respective role of oxygen and water vapor on the tribology of hydrogenated diamond-like carbon coatings. *Tribol. Lett.* **1998**, 4, 259-265.

[4.9] H. Li, T. Xu, C. Wang, J. Chen, H. Zhou, H. Liu. Effect of relative humidity on the tribological properties of hydrogenated diamond-like carbon films in a nitrogen environment. *J. Phys. D: Appl. Phys.* **2005**, 38, 62-69.

[4.10] J. Andersson, R. A. Erck, A. Erdemir. Friction of diamond-like carbon films in different atmospheres. *Wear* **2003**, 254, 1070-1075.

[4.11] Y. T. Pei, P. Huizenga, D. Galvan, J. Th. M. De Hosson. Breakdown of the Coulomb friction law in TiC/aC:H nanocomposite coatings. *J. Appl. Phys.* **2006**, 100, 114309.

[4.12] C. Corbella, E. Bertran, M. C. Polo, E. Pascual, J. L. Andújar. Structural effects of nanocomposite films of amorphous carbon and metal deposited by pulsed-DC reactive magnetron sputtering. *Diamond Relat. Mater.* **2007**, 16, 1828-1834.

[4.13] R. Gilmore, R. Hauert. Control of the tribological moisture sensitivity of diamond-like carbon films by alloying with F, Ti or Si. *Thin Solid Films* **2001**, 398-399, 199-204.

[4.14] J. Jiang, J. Hao, P. Wang, W. Liu. Superlow friction of titanium/silicon codoped hydrogenated amorphous carbon film in the ambient air. *J. Appl. Phys.* **2010**, 108, 033510.

[4.15] B. Racine, A. C. Ferrari, N. A. Morrison, I. Hutchings, W. I. Milne, J. Robertson. Properties of amorphous carbon–silicon alloys deposited by a high plasma density source. *J. Appl. Phys.* **2001**, 90, 5002-5012.

[4.16] H. Mori, H. Tachikawa. Increased adhesion of diamond-like carbon–Si coatings and its tribological properties. *Surf. Coat. Technol.* **2002**, 149, 224-229.

[4.17] S. G. Kim, S. W. Kim, N. Saito, O. Takai. Effect of increasing hardness on Si-containing diamond-like carbon film during tribo-test. *Diamond Relat. Mater.* **2010**, 19, 1017-1020.

[4.18] R. Hatada, S. Flege, K. Baba, W. Ensinger, H.-J. Kleebe, I. Sethmann, S. Lauterbach. Temperature dependent properties of silicon containing diamondlike carbon films prepared by

plasma source ion implantation. *J. Appl. Phys.* **2010**, 107, 083307.

[4.19] K. Oguri, T. Arai. Tribological properties and characterization of diamond-like carbon coatings with silicon prepared by plasma-assisted chemical vapour deposition. *Surf. Coat. Technol.* **1991**, 47, 710-721.

[4.20] R. Gilmore, R. Hauert. Comparative study of the tribological moisture sensitivity of Si-free and Si-containing diamond-like carbon films. *Surf. Coat. Technol.* **2000**, 133-134, 437-442.

[4.21] F. Zhao, H. X. Li, L. Ji, Y. F. Mo, W. L. Quan, H. D. Zhou, J. M. Chen. Structural, mechanical and tribological characterizations of a-C:H:Si films prepared by a hybrid PECVD and sputtering technique. *J. Phys. D: Appl. Phys.* **2009**, 42, 165407.

[4.22] F. Zhao, H. X. Li, L. Ji, Y. F. Mo, W. L. Quan, W. Du, H. D. Zhou, J. M. Chen. Superlow friction behavior of Si-doped hydrogenated amorphous carbon film in water environment. *Surf. Coat. Technol.* **2009**, 203, 981-985.

[4.23] J. Choi, S. Nakao, M. Ikeyama, T. Kato. Effect of oxygen plasma treatment on the tribological properties of Si-DLC coatings. *Phys. Stat. Sol. (c)* **2008**, 5, 956-959.

[4.24] J.-M. Martin, M.-I. De Barros Bouchet, C. Matta, Q. Zhang, W. A. Goddard III, S. Okuda, T. Sagawa. Gas-phase lubrication of ta-C by glycerol and hydrogen peroxide. Experimental and computer modeling. *J. Phys. Chem. C* **2010**, 114, 5003-5011.

[4.25] A. R. Konicek, D. S. Grierson, P. U. P. A. Gilbert, W. G. Sawyer, A. V. Sumant, R. W. Carpick. Origin of ultralow friction and wear in ultrananocrystalline diamond. *Phys. Rev. Lett.* **2008**, 100 235502.

[4.26] S.-E. Ong, S. Zhang, H. Du, D. Sun. Relationship between bonding structure and mechanical properties of amorphous carbon containing silicon. *Diamond Relat. Mater.* **2007**, 16, 1628-1635.

[4.27] A. Erdemir, C. Donnet. Tribology of diamond-like carbon films: recent progress and future prospects. *J. Phys. D: Appl. Phys.* **2006**, 39, R311-R327.

[4.28] J. Choi, S. Nakao, S. Miyagawa, M. Ikeyama, M. Miyagawa. The effects of Si incorporation on the thermal and tribological properties of DLC films deposited by PBII&D with bipolar pulses. *Surf. Coat. Technol.* **2007**, 201, 8357-8361.

[4.29] V. S. R. Murthy, H. Kobayashi, N. Tamari, S. Tsurekawa, T. Watanabe, K. Kato. Effect of

doping elements on the friction and wear properties of SiC in unlubricated sliding condition. *Wear* **2004**, 257, 89-96.

[4.30] V. Kulikovsky, V. Vorlicek, R. Ctvrtlik, P. Bohac, J. Suchanek, O. Blahova, L. Jastrabik. Mechanical and tribological properties of coatings sputtered from SiC target in the presence of CH_4 gas. *Surf. Coat. Technol.* **2011**, 205, 3372-3377.

[4.31] D. B. Asay, A. L. Barnette, S. H. Kim. Effects of Surface Chemistry on Structure and Thermodynamics of Water Layers at Solid-Vapor Interfaces. *J. Phys. Chem. C* **2009**, 113, 2128-2133.

[4.32] A. Verdaguer, G. M. Sacha, H. Bluhm, M. Salmeron. Molecular structure of water at interfaces: wetting at the nanometer scale. *Chem. Rev.* **2006**, 106, 1478-1510.

[4.33] D. B. Asay, S. H. Kim. Evolution of the adsorbed water layer structure on silicon oxide at room temperature. *J. Phys. Chem. B* **2005**, 109, 16760-16763.

[4.34] F. P. Bowden, D. Tabor. *The Friction and Lubrication of Solids*, Clarendon Press, Oxford, 1964.

[4.35] I. L. Singer, R. N. Bolster, J. Wegand, S. Fayeulle, B. C. Stupp. Hertzian stress contribution to low friction behavior of thin MoS_2 coatings. *Appl. Phys. Lett.* **1999**, 57, 995-997.

[4.36] A. Erdemir, R. A. Erck, J. Robles. Relationship of hertzian contact pressure to friction behavior of self-lubricating boric acid films. *Surf. Coat. Technol.* **1991**, 49, 435-438.

[4.37] A. R. Konicek, D. S. Grierson, A. V. Sumant, T. A. Friedmann, J. P. Sullivan, P. U. P. A. Gilbert, W. G. Sawyer, R. W. Carpick. Influence of surface passivation on the friction and wear behavior of ultrananocrystalline diamond and tetrahedral amorphous carbon thin films. *Phys. Rev. B* **2012**, 85 155448.

[4.38] K. J. Kim, J. W. Kim, M.-S. Yang, J. H. Shin. Oxidation of Si during the growth of SiO_x by ion-beam sputter deposition: *In situ* x-ray photoelectron spectroscopy as a function of oxygen partial pressure and deposition temperature. *Phys. Rev. B* **2006**, 74, 153305.

[4.39] E. Höglund. Influence of lubricant properties on elastohydrodynamic lubrication. *Wear* **1999**, 232, 176-184.

[4.40] M. Ratoi, H. A. Spikes. Lubricating Properties of Aqueous Surfactant Solutions. *Tribol. Trans.*

1999, 42, 479-486.

[4.41] M.-I. De Barros Bouchet, G. Zilibotti, C. Matta, M. C. Righi, L. Vandenbulcke, B. Vacher, J.-M. Martin. Friction of diamond in the presence of water vapor and hydrogen gas. Coupling gas-phase lubrication and first-principles studies. *J. Phys. Chem. C* **2012**, 116, 6966-6972.

[4.42] H. Washizu, S. Sanda, S.-A. Hyodo, T. Ohmori, N. Nishino, A. Suzuki. Molecular dynamics simulations of elasto-hydrodynamic lubrication and boundary lubrication for automotive tribology. *J. Phys.: Conf. Ser.* **2007**, 89, 012009.

[4.43] W. H. Briscoe, S. Titmuss, F. Tiberg, R. K. Thomas, D. J. McGillivray, J. Klein. Boundary lubrication under water. *Nature* **2006**, 444, 191-194.

[4.44] J. Klein. Hydration lubrication. *Friction* **2013**, 1, 1-23.

[4.45] K. B. Jinesh, J. W. M. Frenken. Capillary Condensation in Atomic Scale Friction: How Water Acts like a Glue. *Phys. Rev. Lett.* **2006**, 96, 166103.

[4.46] K. B. Jinesh, J. W. M. Frenken. Experimental evidence for ice formation at room temperature. *Phys. Rev. Lett.* **2008**, 101, 036101.

[4.47] I. Szlufarska, M. Chandross, R. W. Carpick. Recent advances in single-asperity nanotribology. *J. Phys. D: Appl. Phys.* **2008**, 41, 123001.

[4.48] Y. Morita et al. Structural and environmental dependence of superlow friction in ion vapour-deposited a-C:H:Si films for solid lubrication application. *Jpn. J. Appl. Phys.* **2008**, 47, 3032-3035.

[4.49] K. Hayashi, S. Sato, S. Bai, Y. Higuchi, N. Ozawa, T. Shimazaki, K. Adachi, J.-M. Martin, M. Kubo. Fate of methanol molecule sandwiched between hydrogen-terminated diamond-like carbon films by tribochemical reactions: tight-binding quantum chemical molecular dynamics study. *Faraday Discuss.* **2012**, 156, 137-146.

Chapter 5

Hydrogen Dependence of Superlubricity of a-C:H:Si Films in Various Gaseous Atmospheres

In this chapter, the influence of hydrogen on the fictional behaviors of a-C:H:Si films in different gaseous atmospheres is presented. Different hydrogen contents in the films were achieved by varying the bias voltage (refer to Chapter 2), while the silicon content was kept almost constant at ~10 at.% by fixing the gas flow ratio of TMS/C_7H_8 (refer to Chapter 4). The correlation between hydrogen-induced structural diversity, environmental medium and tribological properties of a-C:H:Si films is highlighted..

5.1 Background

In Chapter 4, it is shown that ultralow or even superlow friction is feasible in ambient environment by controlling the Si content in a-C:H:Si films, i.e, 8.4 at.% Si. Moreover, it is also indicated that superlow friction is possible for this film in dry N_2 even though some vibrations were observed in the steady state during sliding (Figure 4.11(d), Chapter 4). The occurrence of this superlubric state should be in some extent correlated with hydrogen inherent in the film since numerous studies have emphasized that hydrogen is a key factor in achieving low or superlow friction in a-C:H films [5.1-14]. However, the exact role of hydrogen involved in this friction-reduction process is not well understood in Chapter 4.

In order to effectively exploit the anti-friction capacity of a-C:H:Si film, a ternary phase diagram of carbon-silicon-hydrogen is proposed for synthesizing new a-C:H:Si

lubricants, as shown in Figure 5.1. The silicon content is kept almost constant at ~10 at.% by fixing the gas flow ratio of TMS/C_7H_8 at 1 (see Chapter 4), with the aim of maintaining the effective hydrophilic boundary water lubrication by forming Si-OH sites in humid environment. Different hydrogen contents ranging from 15 to 40 at.% in the films are obtained by changing the applied bias voltage from 0.25 to 3.5 kV (see Chapter 2), in order to achieve more durable superlubricity in inert gas atmosphere, UHV or H_2. Therefore, it is of high interest to further investigate the structural dependence of frictional behaviors of these a-C:H:Si films in different gaseous environments.

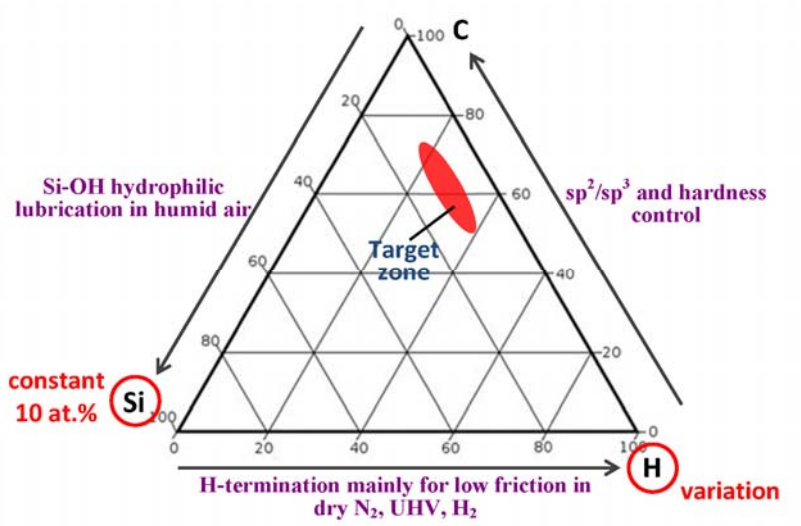

Figure 5.1 Ternary phase diagram of C-Si-H showing the structural control of a-C:H:Si film and the corresponding environmental adaptation of each phase component .

In this Chapter, a systematic study on the frictional behaviors of a-C:H:Si films depending on the film bonding structure (i.e., hydrogen-induced structural diversity such as H-rich polymer-like, cross-linked diamond-like and hydrogen-deficient sp^2-bonded a-C) and the environmental atmospheres including dry inert N_2, reactive H_2 and humid air is presented. Hydrogen is highlighted for their crucial roles in providing lubrication units.

5.2 Experimental Methods

The a-C:H:Si films with different hydrogen contents were prepared at a fixed gas flow ratio of TMS/C_7H_8 by varying the applied bias voltage from 0.25 to 3.5 kV in the IVD system. Relevant details on the growth conditions and structural investigations are described in Chapter 2. The friction tests were performed on the CSM pin-on-disc tribometer at room temperature. The normal load was set at 2 N. The film-coated Si wafer was fixed on a rotary sample platform using a bare (for test in humid air) or same-film-coated (for test in dry N_2 and H_2) SUJ2 ball of 6 mm in diameter as a counterpart. The rotation radius was 3.5 mm, and the linear sliding speed was 15 cm/s (for test in humid air) or 20 cm/s (for test in dry N_2 and H_2). Different gaseous environments including humid air (22 ± 2 % RH), dry inert N_2 and diluent reactive H_2 (40 vol.% H_2 + 60 vol.% He) were produced by purging water vapor or distinct gas source into the tribometer chamber until stability before friction test. A Nikon optical microscope and a 3D white-light interferometer (Zygo NewView 6300) were used to measure the wear morphology and topography.

Table 5.1 Overview of properties of a-C:H:Si films as discussed in Chapter 2, including composition, roughness *R*a, hardness *H*, elastic modulus *E*, residual stress σ and viscoplastic exponent *x*, as a function of bias voltage.

Bias (kV)	Composition (at.%)					*R*a (nm)	*H* (GPa)	*E* (GPa)	σ (GPa)	*x*
	H	C	Si	O	N					
0.25	36.7	52.5	9.3	1.2	0.3	0.08	13.8	123.9	0.78	0.059
0.5	31.9	57.2	9.3	1.2	0.4	0.13	16.2	155.7	1.04	0.031
1.0	25.8	61.2	9.2	2.7	1.1	0.17	17.9	175.7	1.41	0.017
1.5	23.2	64.8	9.1	2.1	0.8	0.09	17	176.1	1.12	0.021
2.0	20.8	68.1	8.9	1.7	0.5	0.11	17.3	178.6	1.0	0.015
2.5	20.5	66.6	9.6	3.0	0.3	0.1	15.8	166	0.77	0.007
3.0	18.2	68.8	9.7	2.7	0.6	0.09	15.2	164.3	0.86	0.022
3.5	17.3	70.1	9.9	2.0	0.7	0.09	14.9	150.2	0.84	0.006

5.3 Results

5.3.1 Overview of Basic Properties of a-C:H:Si Films upon Bias Voltage

As discussed in detail in Chapter 2, depending on the applied bias voltage, the bonding structure of a-C:H:Si films grown in different ion energy regions evolves from hydrogen-rich chain-developed polymer-like (0.25-0.5 kV) to cross-linked diamond-like (1.0-2.5 kV) to hydrogen-deficient sp^2-bonded a-C (3.0-3.5 kV), as revealed by XPS, Raman and FTIR analysis. Here, a brief summary about the basic properties of these films is given in Table 5.1 to facilitate understanding of the frictional behaviors studied in this Chapter. With increasing the bias voltage from 0.25 to 3.5 kV, the hydrogen content determined by ERDA in the films decreases gradually from 36.7 to 17.3 at.%, while the carbon content increases correspondingly from 52.5 to 70.1 at.%. Meanwhile, the Si content is kept almost constant at ~9-10 at.% for the fixed gas flow ratio of TMS/C_7H_8 during deposition, irrespective of the bias voltage. In addition, a small amount of oxygen (i.e., 1-3 at.%) was present in all the as-grown a-C:H:Si films, as well as some traces of nitrogen remaining in the films. A dynamic smoothening behavior was universally observed for these films grown from energetic ions in a wide range of ion energy, and an atomically smooth surface with RMS roughness of ~0.1 nm was recorded for all these films. The mechanical properties have a close relationship with the film bonding structure. A relatively low hardness (~13-15 GPa) was measured for both polymeric and sp^2-bonded amorphous structures, while a higher value (~17-18 GPa) was achieved for diamond-like film. A similar variation trend depending on the bias voltage is also observed for the measured elastic modulus. The stress state confirms the above argument, that is, the as-grown a-C:H:Si films display significantly low residual stresses (~0.8 GPa) in both polymeric and sp^2-bonded a-C films while possessing a relatively high compressive stress (~1.4 GPa) inherent in the hard

diamond-like network. The viscoplastic exponent x, an evaluation index for the rheological properties of materials, indicates an enhanced viscous property (i.e., interfacial flexibility) for hydrogen-rich a-C:H:Si films, and obtains a value of ~0.06 for the polymeric sample with H content of 36.7 at.%.

5.3.2 Hydrogen Dependence of Friction in Dry N_2

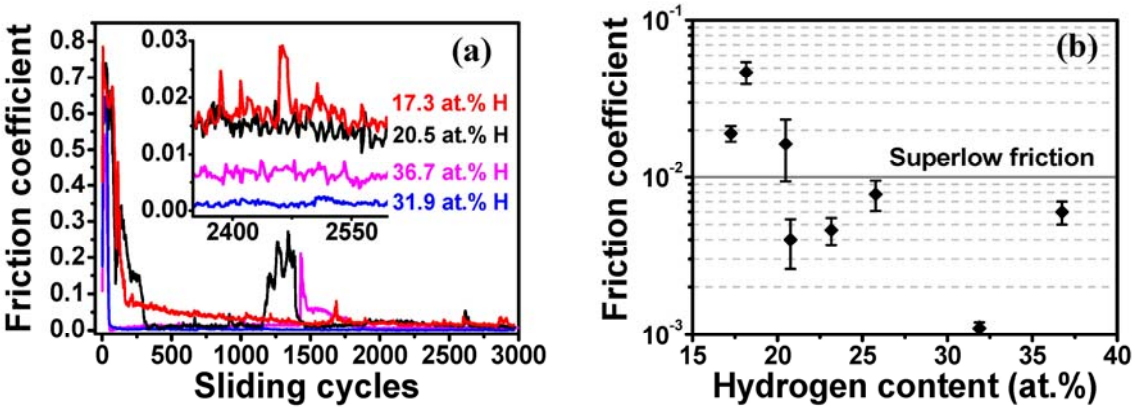

Figure 5.2 Frictional behaviors of a-C:H:Si films tribotested in dry N_2: (a) representative friction coefficient curves of samples with different hydrogen contents. The inset figure shows the magnified friction curves in the steady state. (b) Hydrogen dependence of average steady-state friction coefficient, indicating the existence of a superlow friction region when H>20 at.%.

The frictional behaviors of a-C:H:Si films tribotested in dry N_2 are shown in Figure 5.2, which were previously shown in Chapter 2. Figure 5.2(a) indicates the friction coefficient curves from four representative samples containing different hydrogen contents. It can be observed that for all the tested samples the friction coefficient evolves from an intensive running-in period (i.e., initial friction coefficient μ_{in} around 0.5-0.8) into a low-friction steady state. The running-in period differs significantly in the rubbing cycles with regard to the hydrogen content in the films: ~1500 cycles (17.3 at.% H), ~300 cycles (20.5 at.% H), ~75 cycles (31.9 at.% H) and ~55 cycles (36.7 at.% H), respectively. In addition to the prolonged running-in period, a noticeable number of fluctuations in the steady-state friction coefficients (μ_{ss}) are observed for the

hydrogen-deficient a-C:H:Si samples, i.e., 17.3 and 20.5 at.% H-containing films. The inset figure shows the magnified friction coefficient curves in the steady state. An extremely low and stable friction coefficient (μ_{ss}~0.001) is recorded for the sample with hydrogen content of 31.9 at.%, implying nearly vanishing of friction upon sliding. The amplitude of variation in the steady-state friction coefficient is ±0.0005, indicating an ultrasmooth rubbing process in the superlubric state for the self-mated a-C:H:Si films. This extremely stable near-frictionless state continued until the end of the test. In comparison, the friction coefficient of an uncoated SUJ2 ball against an uncoated Si wafer was quite unstable and reached a high value in the range of 0.3-0.6 when tested under the same conditions. A slightly increased but still superlow friction coefficient (μ_{ss}~0.006) is also detected for the sample hydrogenated to 36.7 at.%. It seems that the relatively low hardness (~13.8 GPa) of this sample deteriorates the anti-friction performance to some extent when considering the presence of plentiful tribodebris produced in the contact area, as shown in Figure 5.3(a4) below. In contrast, the friction coefficients obtained from the hydrogen-deficient samples just approach a quasi-superlubric state: 0.019 for 17.3 at.% H and 0.016 for 20.5 at.% H, respectively. Moreover, the amplitude of fluctuations in the friction curves is strengthened with decreasing the hydrogen content in the films, indicating a worsening stability of lubricating state. Figure 5.2(b) summarizes the evolution of average μ_{ss} as a function of hydrogen content in the films. There seems to be a hydrogen content threshold (i.e., ~20 at.%) existed for the a-C:H:Si films to achieve superlow friction in dry N_2.

Figure 5.3 shows the optical wear morphologies of the sliding pairs in the contact area after the friction tests in dry N_2 as shown in Figure 5.2. It is obviously seen that white wear scars, barely (a1) or partially (a2-a4) covered by tribolayers, are formed on the film-coated SUJ2 balls. In addition, a large amount of tribodebris is distributed outside the wear scar. Correspondingly, a large number of tribolayers are formed in the wear track (b1-b4) on the film-coated Si substrates. It seems that these tribolayers were mainly transferred from the film materials coated on SUJ2 balls, as will be discussed

below. Note that the white color of wear scars on film-coated SUJ2 balls implies that the wear depth has approached the Fe basement since the ferrite iron usually appears in white color under an optical microscope when considering the sliding-induced surface polishing effect. This argument is based on the SEM-EDS analysis below.

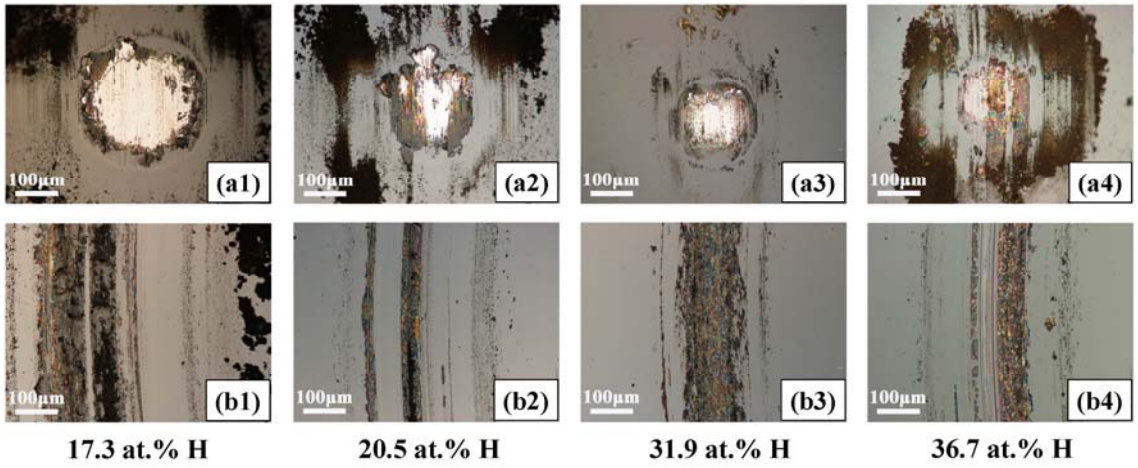

Figure 5.3 Wear morphologies of the sliding pairs after the friction tests in dry N_2 as shown in Figure 5.2: (a1-a4) wear scars on the film-coated SUJ2 balls and (b1-b4) the corresponding wear tracks on the film-coated Si substrates with H contents of 17.3, 20.5, 31.9 and 36.7 at.% in the films, respectively.

The above results clearly indicate that the frictional performances of a-C:H:Si films in dry N_2 are highly dependent on the hydrogen content in the films, which are similar to what have been found in near-frictionless carbon (NFC) films by Erdemir [5.5-7]. In Erdemir's work, the hydrogen content in a-C:H films could be controlled by varying the source gas composition of H_2 + CH_4 in the plasma during the PECVD process. The lowest friction coefficient (μ_{ss}~0.001) in dry N_2 was achieved for the highly-hydrogenated (39 at.% H) a-C:H films grown from a 75% H_2 + 25% CH_4 gas precursor. Further increase of hydrogen content in the film to 45 at.% (grown from 100% CH_4) weakened the anti-friction properties of a-C:H film to some extent, and the friction coefficient increased to ~0.014 [5.5-7]. Similarly, in the present work, the most stable and lowest friction coefficient (μ_{ss}~0.001) in dry N_2 was recorded for the 31.9

at.% H-containing a-C:H:Si film, while an increased friction coefficient (μ_{ss}~0.006) was observed for the sample with maximum hydrogen content of 36.7 at.%. For both a-C:H and a-C:H:Si films, the superlubric state is more likely to appear when the film structure evolves into hydrogen-rich polymer-like. However, the most noticeable difference between these two cases is that almost no visible tribolayer could be found in the sliding areas for NFC self-mated contacts even though this tribopair also suffered an initial high friction in the running-in period. It seems that the hydrocarbon network in the pure a-C:H film is stiff enough to bear the initial high contact pressure (i.e., a peak Hertz pressure of ~1 GPa under 10 N in Erdemir's work), and thus to avoid huge material loss in this harsh stage. In comparison, a noticeable tribolayer was formed in the wear track during the initial running-in process for a-C:H:Si self-mated contacts. On one hand, superlow friction is maintained when a high hydrogen content (i.e., 31.9 at.% in this work) is hold in a-C:H:Si film. On the other hand, the incorporation of Si into a-C:H matrix seems to weaken the load capacity of the hydrocarbon network. Under the initial high contact pressure (a peak Hertz pressure of 0.68 GPa under 2 N), film material is mainly transferred from the ball side to the Si substrate side, producing a newly restructured tribolayer (Figure 5.3(b3)). The possible forming process of this friction-reducing tribolayer is discussed in Section 5.3.5.

It should be mentioned that the occurrence of such an extremely low friction coefficient in this polymeric a-C:H:Si film relies on some key factors. One is contact pressure. In Chapter 3, it has been shown that a highly-hydrogenated a-C:H film was synthesized from 100% C_7H_8 gas under 0.25 kV in the same ionization system. The hydrogen content in this polymer-like a-C:H film is around 40%. It was found that higher contact pressure is favorable for achieving lower friction coefficient. An extremely low and stable value of ~0.001 was obtained when the applied load was 10 N. After the friction test, wear tracks on the disc side were barely visible (i.e., unmeasurable wear rate, Figure 3.13), and very mild wear scars were produced on the pin surface. This result is quite consistent with Erdemir's NFC findings for a-C:H films

[5.5-7] in view of the extremely low friction coefficient and wear rate under the same gaseous atmosphere (dry N_2) and comparable contact pressure (a peak Hertz pressure of ~1.15 GPa under 10 N in our case). Note that measuring friction coefficient in the range of 10^{-3} or lower is intractable for most tribometers. Any system error would result in inaccurate outcomes. Therefore, lateral force calibration should be carried out before each friction test. For the sake of reliability, we further conducted free-contact rotations before and after each friction test to ensure that no zero shift occur for the load cell. The friction coefficient should be zero in this mode since no friction force was produced. Due to the minimum sensitivity of lateral force sensor being a few mN in most macroscopic pin-on disc tribometers (5 mN in our CSM tribometer), measuring a friction coefficient down to 0.001 under a relatively low load such as 1 or 2 N means approaching the detect limit of the sensor sensitivity. Therefore, sliding contact under higher load such as 10 N would improve the stability of frictional force measurement. However, the anti-friction behaviors of this polymeric a-C:H:Si film are pressure-dependent. Superlow friction could not be preserved when the normal load was higher than 2 N, due to the pressure-induced crack failure of the film. This is understandable when considering the relatively low hardness and nanoporous microstructure, as will be confirmed by HRTEM in Chapter 6, of this hydrogen-rich a-C:H:Si sample. Another important factor affecting anti-friction behavior of a-C:H:Si films is the sliding speed. Our preliminary experiments indicate that a sliding peed in the range of 15-20 cm/s is more favorable for achieving the extraordinarily stable and lowest friction coefficient, while a rather low speed (i.e., below 5 cm/s) weakens or even completely disables the superlubric performances. The underlying mechanism, i.e., dynamic gas adsorption and removal, needs further investigation.

5.3.3 Hydrogen Dependence of Friction in Diluent Reactive H_2

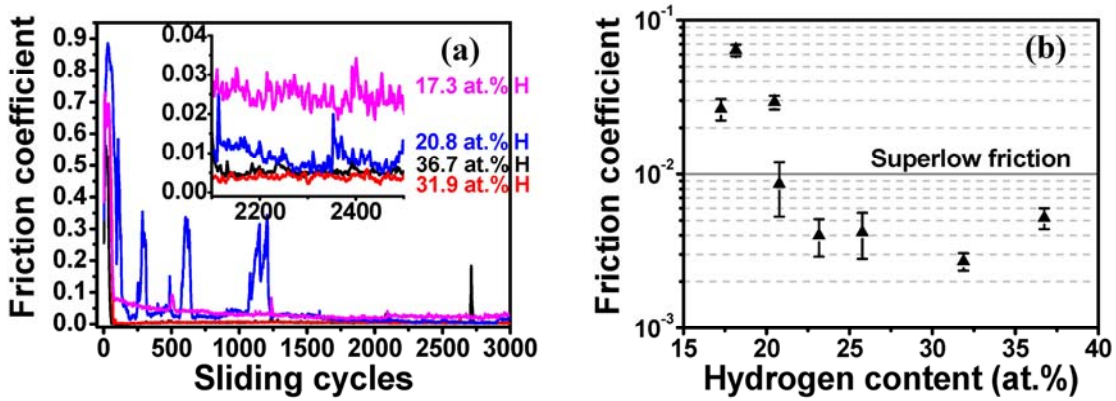

Figure 5.4 Frictional behaviors of a-C:H:Si films tribotested in diluent reactive H_2: (a) representative friction coefficient curves of samples with different hydrogen contents. The inset figure shows the magnified friction curves in the steady state. (b) Hydrogen dependence of average steady-state friction coefficient, indicating the existence of a superlubric region when H>20 at.%.

Figure 5.4 shows the frictional performances of a-C:H:Si films tribotested in diluent H_2 gas in consideration of the lubrication effect of hydrogen. Note that, due to the low density of H_2 gas, the outlet of gas pipe was placed near the contact area to ensure the presence of sufficient hydrogen on the contact surfaces before it floats upward. The friction coefficient curves from four representative samples with different hydrogen contents are indicated in Figure 5.4(a). Being similar to the case of dry N_2, the friction coefficient evolves into a steady state after an intensive running-in process. Prolonged running-in period and intensified fluctuations in the friction curves are observed for the H-deficient samples, i.e., 17.3 and 20.8 at.% H-containing films. As shown in the inset figure, extremely low and stable friction coefficients, i.e, 0.003 and 0.005, are detected for 31.9 and 36.7 at.% H-containing a-C:H:Si films, respectively. As the hydrogen content decreases, the friction coefficient increases close to or exceeding the value of 0.01, i.e., 0.009 for 20.8 at.% H and 0.027 for 17.3 at.% H. Noticeable fluctuations and instability still exist in the friction curves for these H-deficient samples.

The above results imply that superlubricity is not likely to occur even under the lubrication by hydrogen-providing source such as H_2 if the as-grown film structure is unable to meet some requirements, for instance, the H content inherent in the film or the H-passivating degree on the pristine film surface. Figure 5.4(b) summarizes the hydrogen dependence of average μ_{ss} for the as-grown a-C:H:Si films. Superlow friction is feasible in lubricating H_2 for the samples with H content larger than ~20 at.%.

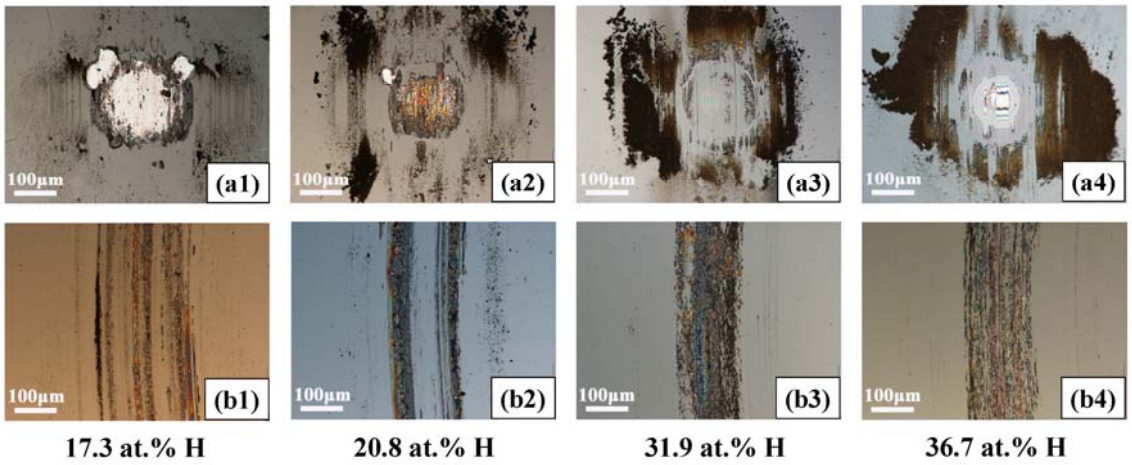

Figure 5.5 Wear morphologies of the sliding pairs after the friction tests in diluent reactive H_2 as shown in Figure 5.4: (a1-a4) wear scars on the film-coated SUJ2 balls and (b1-b4) the corresponding wear tracks on the film-coated Si substrates with H contents of 17.3, 20.8, 31.9 and 36.7 at.% in the films, respectively.

The corresponding wear morphologies of sliding pairs after the friction tests in diluent H_2 are shown in Figure 5.5. It is observed that white wear scar without covering by any tribolayers is only found on the SUJ2 ball coated by the most H-deficient film (17.3 at.% H, a1), while the other three ones are totally covered by brown tribolayers (a2) or possess smooth contact surface with the color close to the film (a3, a4). This result suggests that the presence of gaseous H_2 can effectively facilitate the formation of tribolayers and protect the contact surfaces upon sliding especially for the films with hydrogen content exceeding a value, i.e., ~20 at.%. As for the film-coated Si substrates,

the wear tracks (b1-b4) are covered by continuous tribolayers, which is similar to the case in dry N_2 atmosphere.

5.3.4 Hydrogen Dependence of Friction in Humid Air

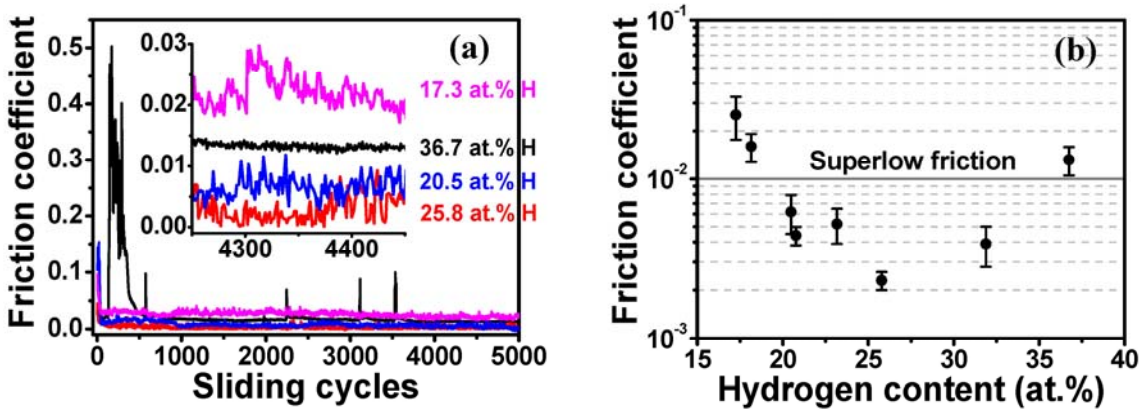

Figure 5.6 Frictional behaviors of a-C:H:Si films tribotested in humid air (22 ± 2 % RH): (a) representative friction coefficient curves of samples with different hydrogen contents. The inset figure shows the magnified friction curves in the steady state, and (b) hydrogen dependence of average steady-state friction coefficient.

To further evaluate the frictional response to the presence of water molecules, we tested these films in humid environment with RH of 22 ± 2 %. To be comparable with the results in Chapter 4, we chose bare SUJ2 balls instead of film-coated ones as counterparts for sliding tests, as shown in Figure 5.6. The frictional behaviors from four representative samples with different hydrogen contents are compared in Figure 5.6(a). As noticed, the initial friction coefficients in humid air are significantly reduced for most samples (i.e., μ_{in}~0.05-0.15) except for the film with maximum hydrogen content (i.e., μ_{in}~0.5). In addition, the running-in period is shortened, and no sharp fluctuations as found for the hydrogen-deficient samples in dry N_2 or H_2 are observed in the whole sliding process. It is obviously seen from the inset figure that superlow friction is feasible for the samples hydrogenated to some extent, i.e, 25.8 and 20.5 at.%, while the most polymeric (36.7 at.% H) and H-deficient (17.3 at.% H) samples just achieve a

quasi-superlubric state (μ_{ss}~0.013) and a ultralow friction (μ_{ss}~0.025), respectively. It indicates that, in addition to the Si-OH passivating group, H-termination is also involved in achieving superlubricity in humid air. The steady-state friction curve of the polymeric sample (36.7 at.% H) is very smooth, which is an indirect hint for the passivation effect of H on the contact surface. Note that the superlow friction curves obtained in humid air for a-C:H:Si films (i.e, 25.8 and 20.5 at.% H) display a lot of remarkable fluctuations, which is indicative of a more complex surface-gas interaction process in this condition. Figure 5.6(b) indicates the hydrogen dependence of μ_{ss} for all the as-grown a-C:H:Si films. It is seen that superlow friction is more feasible for the films with an appropriate hydrogen content, i.e., 20-35 at.%.

The wear morphologies of the sliding pairs corresponding to the tests in Figure 5.6 are shown in Figure 5.7. Overall, the wear morphologies in humid air are totally different from those obtained in dry N_2 or diluent H_2. As shown in Figure 5.7(a1-a4), white wear scars are not found in the contact areas for the bare SUJ2 balls. Instead, a large number of tribolayers are distributed in the center of wear scars or around the contact areas. It seems that these tribolayers were mainly transferred from the film materials coated on Si substrates to the bare SUJ2 ball surfaces, which is contrary to the case in dry N_2 or H_2. Correspondingly, worn tracks (b1-b4) are produced on the film-coated Si substrates. As indicated in Chapter 4, the dissociative formation of hydrophilic silicon oxide layers (Si-OH) between the contact surfaces along with the adsorbed boundary water layer is the origin of ultralow friction for a-C:H:Si films in humid air. The present results demonstrate that hydrogen also participates in either shielding the film surfaces from or reacting with the surrounding gaseous medium such as H_2O molecules. The combined function of all these factors finally determines the frictional behaviors of a-C:H:Si films in humid air. However, at present, we don't have direct evidence for the argument of shielding effect of hydrogen on hydrophilic contact surfaces in humid air. Further work such as molecular dynamics simulations is necessary to uncover this query.

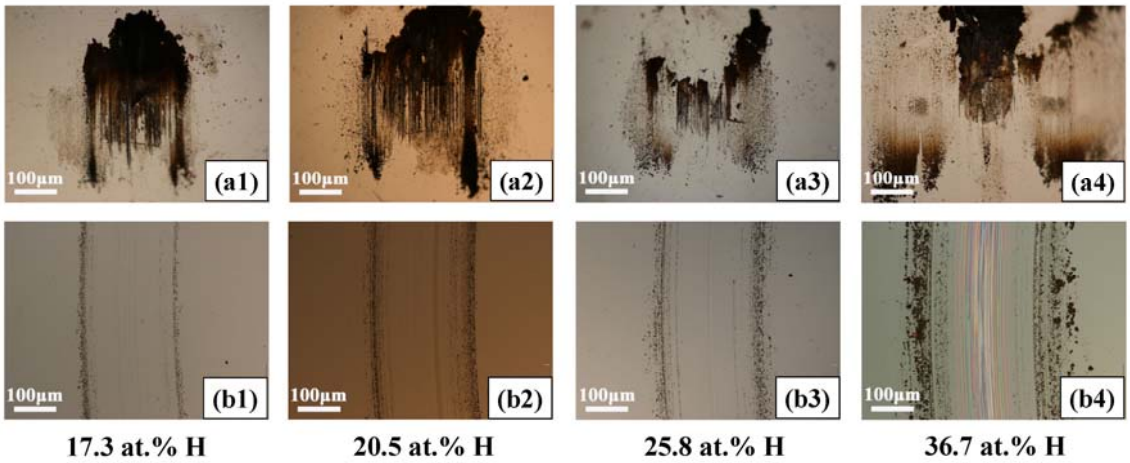

Figure 5.7 Wear morphologies of the sliding pairs after the friction tests in humid air as shown in Figure 5.6: (a1-a4) wear scars on bare SUJ2 balls and (b1-b4) the corresponding wear tracks on the film-coated Si wafers with H contents of 17.3, 20.5, 25.8 and 36.7 at.% in the films, respectively.

5.3.5 Tribolayer Formation on Contact Surface

To gain further insight into the relationship between tribolayer formation and frictional behaviors of a-C:H:Si films, white-light interferometer was utilized to characterize the topographical features of the contact surfaces. Figure 5.8 shows the three-dimensional morphologies and cross sections of wear tracks from the a-C:H:Si (31.9 at.%) sample after the friction tests in the three gaseous atmospheres. Two distinct types of wear morphologies can be distinguished with respect to the tribotesting condition. In both dry N_2 (Figure 5.8(a)) and diluent H_2 (Figure 5.8(b)), a tribolayer with an average thickness of ~100-200 nm is found to uniformly cover the wear track, indicating the film material transfer from film-coated ball surface to film-coated Si substrate. This tribolayer is exactly located in the center of the contact areas rather than squeezed out from the wear track. Very little tribodebris can be found on the edge of the wear track. Therefore, this newly-formed tribolayer is directly involved in the rubbing process throughout the experiment to eliminate friction between the two contact surfaces. The present observed formation and distribution of tribolayer during sliding is quite consistent with recent large-scale molecular dynamics simulations of wear in DLC

films by Sha et al [5.15]. A tribolayer covering the wear track is also found to be formed for DLC self-mated contacts in the running-in period through the material loss from the ball side by a cluster detachment process. Due to the high stress localization at contact point on the ball side, lateral mass transport evolves along the interface towards the trailing edge of the sliding asperity. Consequently, material detachment occurs due to strong chemical bonding across the interface, and a newly-restructured tribolayer is formed on the opposing flat surface [5.15]. At present, we cannot completely understand how this tribolayer is working to eliminate friction for the polymeric a-C:H:Si film during the rubbing process, especially when considering the roughness of these tribolayer-covering contact surfaces increased to a noticeable extent (Figure 5.8(a) and (b)) as compared with the original as-grown ultrasmooth surface. This is totally different from the near-wearless and smooth contact surfaces after the friction test in Erdemir's NFC a-C:H films [5.5-7] or in our C_7H_8-grown superlubric a-C:H film (Figure 3.13). The most likely scenario we speculate is that these tribolayers are acting as lubricating "tribo-polymers", which are soft and flexible byproducts due to tribochemical polymerization during sliding contact. The presence of tribo-polymers for friction reduction was also reported by other researchers [5.16-18]. This is reasonable when considering the hydrogen-rich polymeric and nanoporous characteristic (TEM results in Figure 6.1) of the original a-C:H:Si film, the enhanced photoluminescence background (Raman results in Figure 6.6(a) and (b)) and the hydrocarbon-rich fragmentation (ToF-SIMS results in Figure 6.7) of these tribolayers after the friction test. During sliding, these tribolayers are flexible and conformal at each contact asperity (i.e., local smoothening effect) to accommodate the lateral movements of the interface and to lower the friction, rather than to increase friction by acting as hard third bodies. In comparison, a typical abrasive groove (Figure 5.8(c)) is found on the wear track after the friction test in humid air, implying that the film material was mainly transferred to the bare SUJ2 ball surface for tribolayer build-up as observed in Figure 5.7.

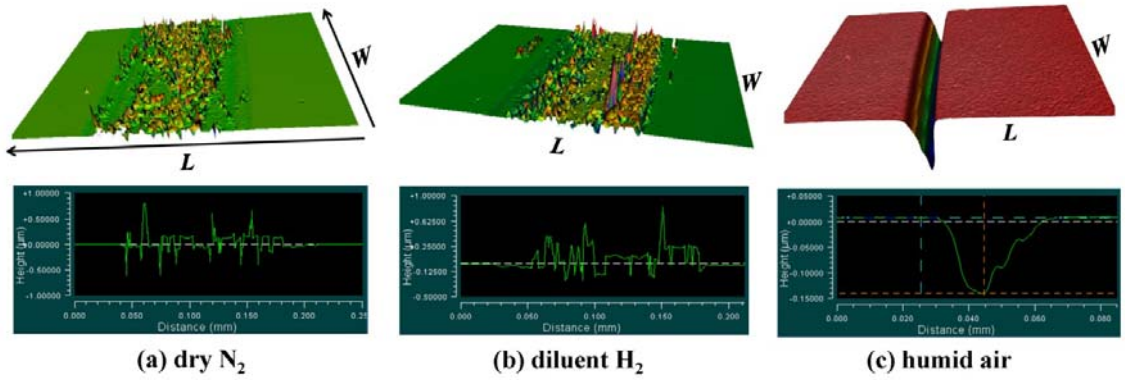

Figure 5.8 Three-dimensional morphologies (upper portion) and cross sections (lower portion) of wear tracks formed on the polymeric-film-coated Si substrates with hydrogen content of 31.9 at.% in the film after the friction tests in (a) dry N_2, (b) diluent H_2 and (c) humid air, respectively. Scan size: L=350 μm, W=260 μm. Scale bars in each cross-sectional image are as follows: (a) 0.5, (b) 0.375 and (c) 0.05 μm per major tick in the vertical height axis, and (a) 0.05, (b) 0.05 and (c) 0.02 mm per major tick in the horizontal distance axis. The white dashed lines in the cross-sectional images indicate the horizontal planes of the original as-grown film. The thickness of the tribolayer or the depth of the wear track can thus be roughly deduced from these morphological profiles.

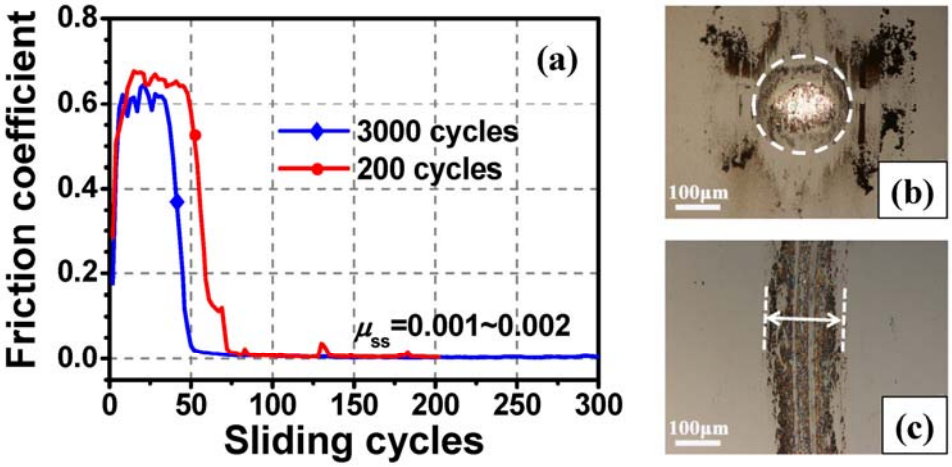

Figure 5.9 (a) Friction curve of a-C:H:Si (31.9 at.% H) self-mates run for 200 cycles in dry N_2, along with the first 300 cycles re-plotted from the case run for 3000 cycles as already shown in Figures 5.2(a), 5.3(a3) and 5.3(b3), and the corresponding (b) wear scar on film-coated SUJ2 ball and (c) wear track on film-coated Si substrate.

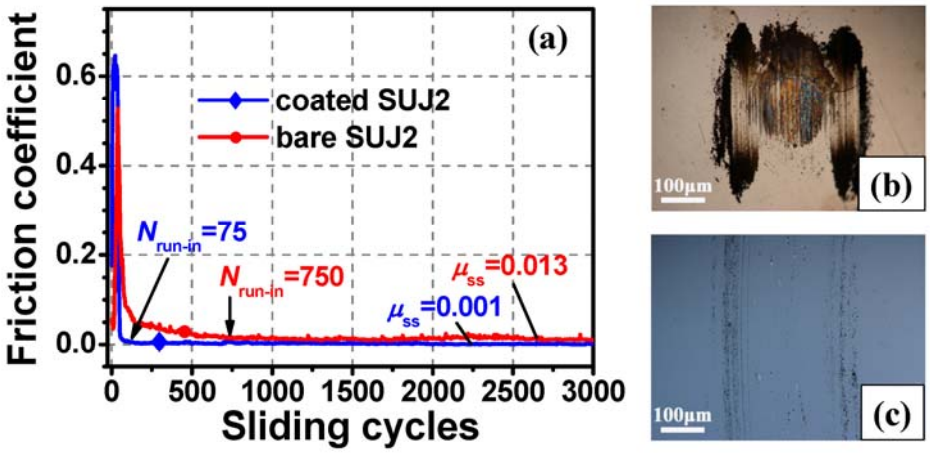

Figure 5.10 (a) Frictional behavior of polymer-like a-C:H:Si (31.9 at.% H) film coated on Si substrate run against bare SUJ2 ball in dry N_2, compared with the self-mated case as shown in Figures 5.2(a), 5.3(a3) and 5.3(b3), and the corresponding (b) wear scar on bare SUJ2 ball and (c) wear track on film-coated Si substrate.

As shown in Figure 5.2(a), the establishment of an extremely low friction state (μ_{ss}~0.001) after the running-in period in dry N_2 for the a-C:H:Si (31.9 at.% H) self-mates signifies a subsequent stable rubbing process and minimal material transformation between contact surfaces. Thus, it is highly necessary to determine the role of running-in process in tribolayer formation. For this purpose, we substantially shortened the total sliding cycles to 200 and re-tested this polymer-like a-C:H:Si film in dry N_2. Figure 5.9 shows the friction curve of 200 cycles along with the first 300 cycles of the case run for 3000 cycles as already shown in Figure 5.2(a), and the corresponding wear morphologies of the sliding pair. It is seen that good reproducibility of suplerlow friction (Figure 5.9(a)) can be obtained in dry N_2, and both the friction coefficients evolve quickly into a superlow region (μ_{ss}~0.001-0.002) after a high-friction running-in period with sliding cycles of ~75. The wear morphologies of the contact pair after 200-cycle sliding (Figure 5.9(b) and (c)) are similar to the case of 3000 cycles as shown in Figure 5.3(a3) and (b3). The measured diameter of wear scar on film-coated SUJ2 ball and width of tribolayer track on film-coated Si substrate in the case of 200-cycle sliding are quite close to that of 3000 cycles: 216.9 μm (200 cycles) vs 226.3 μm (3000

cycles) and 197.8 μm (200 cycles) vs 206.5 μm (3000 cycles), respectively. These results demonstrate that the friction-reduction tribolayer or tribodebris on contact surfaces is mainly formed during the running-in period rather than in the steady state.

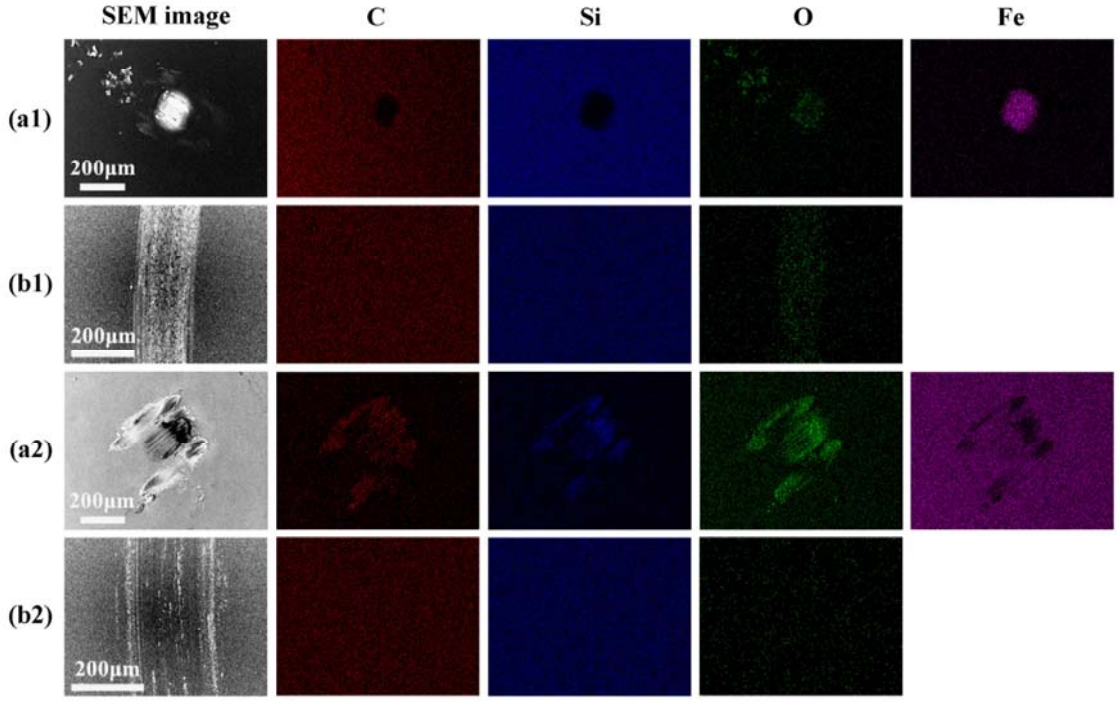

Figure 5.11 SEM-EDS mapping of the contact surfaces after sliding in self-mates or against bare SUJ2 ball for polymer-like a-C:H:Si film (31.9 at.%) in dry N_2: (a1) wear scar as shown in Figure 5.3(a3), (b1) wear track as shown in Figure 5.3(b3), (a2) wear scar as shown in Figure 5.10(b) and (b2) wear track as shown in Figure 5.10(c).

Counterface material is acting as another important factor controlling tribolayer formation and tribochemical state between sliding interfaces. Figure 5.10 compares the frictional behavior of the polymeric a-C:H:Si (31.9 at.% H) film run in self-mate with that slid against bare SUJ2 ball in dry N_2. It is obviously seen from Figure 5.10(a) that running against bare SUJ2 significantly prolongs the running-in period to ~750 cycles as compared to ~75 cycles in self-mate. Furthermore, the μ_{ss} finally stabilizes at a quasi-superlubic value of ~0.013 instead of a superlow one such as ~0.001 in the case of self-mate. A large amount of black-brown tribodebris is accumulated around the wear

scar on bare SUJ2 ball surface as shown in Figure 5.10(b), indicating the continuous lubrication effect through material transfer from a-C:H:Si film on Si substrate. In comparison, a uniform black-brown tribolayer as observed in the case of self-mate (Figures 5.3(b3) and 5.8(a)) is no longer found on the wear track surface in the present case (Figure 5.10(c)).

The counterpart, SUJ2 bearing steel, is a high-carbon chromium alloy steel and the main chemical composition is as follows: C (0.95-1.05%), Cr (1.3-1.6%), Si (0.15-0.35%), Mn (0.25-0.45%) and other trace elements (P, S, Mo, Ti, Cu). To further elucidate the chemical state on contact surfaces, we performed SEM-EDS mapping analysis on the polymeric a-C:H:Si film (31.9 at.%) after sliding in self-mate or against bare SUJ2 ball in dry N_2. Four elements including C, Si, Fe and O were chosen as detecting objects, and the results are shown in Figure 5.11. For self-mate, the wear scar surface is lack in C and Si and rich in Fe (Figure 5.11(a1)), implying deep removal of film material coated on SUJ2 ball surface during sliding. This is consistent with the optical observation results as shown in Figure 5.3(a3). However, it should be pointed out that the weak signals of C and Si are not representative of complete absence of a friction-reducing tribolayer on the wear scar surface, especially when in view of the superlow friction (μ_{ss}~0.001) obtained in this condition. The thickness of this tribolayer is expected to be quite small such as at the nanoscale, since recent experiment has found that the HRTEM confirmation of a very thin (~10 nm) carbon tribolayer formed on the wear scar of ball surface is enough for achieving stable and low friction for CN_x coatings in dry inert gas [5.19]. In addition, the considerable signal reinforcement of O is expected to come from the water adsorption on the porous polymer-like tribolayer when exposing to the air during sample transfer after the friction test in dry N_2. The tribolayer formed on the wear track surface almost maintains the elemental composition of the as-grown film in view of the uniform signal distribution of C and Si as shown in Figure 5.11(b1). The distinguishable signal reinforcement of O is derived from the same reason as discussed above. For the case of sliding against bare SUJ2 ball, the

significantly intensified signals of C, Si and O in the contact area in Figure 5.11(a2) demonstrate the covering of wear scar on iron surface by carbon-rich tribolayers. The uniform weak signal of O on the wear track surface (Figure 5.11(b2)) confirms the very thin thickness of the black-brown tribolayer as observed in Figure 5.10(c). The above results indicate that self-mated sliding is more effective in achieving superlow friction due to quick tribolayer build-up, i.e., running-period just lasting for ~75 cycles. In comparison, the pristine SUJ2 ball surface is generally covered by adventitious carbon and iron oxide layers. The existence of such oxide layers seems to slow the tribolayer growth and thus affect the final rubbing state, as also observed by other researchers [5.20].

5.4 Discussion

Superlubricity is a quite complex subject in tribology, since its interpretation requires knowledge of various disciplines including materials science, physics, chemistry, solid mechanics, thermodynamics, heat transfer, rheology and so on [5.21]. This chapter has provided some understanding of basic features of superlubricity in a-C:H:Si films. Film bonding structure and environmental medium are the two most influential factors controlling frictional behaviors in amorphous carbon material. Structurally, inclusion of an appropriate amount of silicon into carbon matrix is effective in suppressing moisture sensitivity of friction in humid atmosphere, while a relatively high content of hydrogen in the films favors friction reduction in dry inert gas. In addition, ultrasmoothness of film surface guarantees a minimum mechanical interaction between contact surfaces. Environmentally, the molecular characteristic of surrounding gases determines the tribochemistry at sliding interface, finally altering the frictional response of films.

5.4.1 Effect of Film Structure on Superlubricity

The frictional behaviors of a-C:H:Si films depending on the film bonding structure (i.e., hydrogen content, viscoplastic exponent x) are summarized in Figure 5.12. As discussed in Chapter 2, the film structure of a-C:H:Si films grown under different bias voltage evolves from chain-developed polymer-like to cross-linked diamond-like to sp^2-bonded a-C as the hydrogen content gradually decreases from 36.7 to 17.3 at.%. For mainly sp^3-hybridized polymeric film, the capability to deform and the mobility of such a hydrocarbon chain with their structural arrangements under contact pressure provide a flexible shear deformation at sliding interface [5.22, 23]. Sufficient hydrogen (i.e., 31.9 at.%) inherent in the as-grown film produces a chemically inert rubbing surface when brought into contact. The most stable and lowest friction coefficient (μ_{ss}~0.001) in dry N_2 is realized in this film (Figure 5.12(a)). However, excessive hydrogen incorporated in the film (i.e., 36.7 at.%) causes a softening of the film structure (Figure 5.12(a)). This renders the film fragile by undergoing larger strain and severe bond breaking under a applied load in view of the plentiful tribodebris around the contact area (Figures 5.3(a4) and 5.5(a4)), which deteriorates the superlubric state. For diamond-like films, superlow friction is still achievable for some of them in dry N_2 (i.e., 20.8-25.8 at.% hydrogenated samples, Figure 5.12(a)). Nonetheless, the relatively low hydrogen coverage [5.24] on the pristine film surface leads to obvious instabilities and fluctuations in the superlubric state even when these covalently cross-linked films are tribotested in diluent H_2 (i.e., 20.8 at.% hydrogenated sample, Figure 5.4). However, these films exhibit improved wear resistance under lubrication of Si-OH by water molecules in humid air (i.e., 25.8 at.% hydrogenated sample, Figures 5.6 and 5.7) due to their high hardness and elastic constants. Special attention should be given to the mainly sp^2-bonded a-C films even though these samples cannot achieve superlow friction in all the gaseous atmospheres (Figure 5.12(a)). But high friction and catastrophic film failure in dry N_2, generally observed for other sp^2-rich materials such as graphite [5.25], are not recorded for these

films. In contrast, quite stable and ultralow friction is maintained for these hydrogen-deficient films, i.e., μ_{ss}~0.02 for 17.3 at.% hydrogenated sample in dry N_2 as shown in Figure 5.2. By plotting the steady-state friction coefficient as a function of viscoplastic exponent (Figure 5.12(b)), it can be found that superlow friction is only feasible for films with significant viscoplastic exponent, namely diamond-like or polymer-like a-C:H:Si samples. The best anti-friction performances in all the three gaseous atmospheres are achieved for the polymeric sample with viscoplastic exponent of ~0.03.

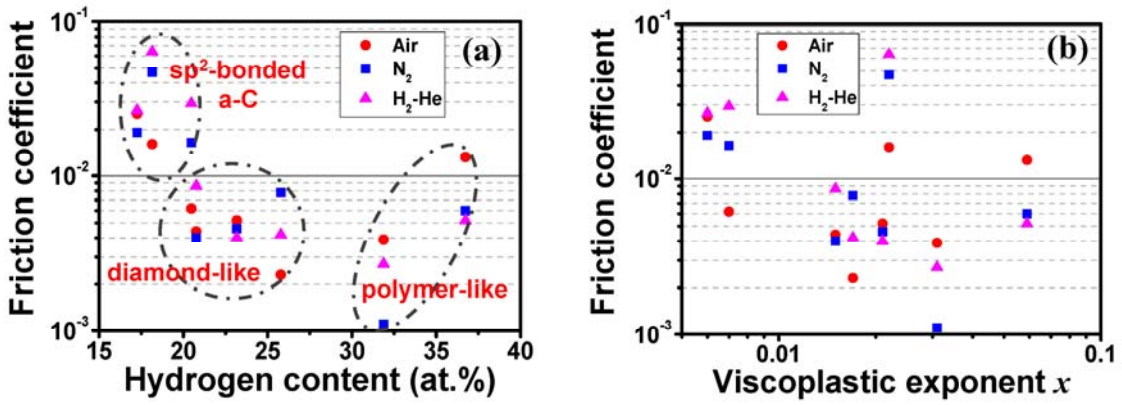

Figure 5.12 Summary of frictional behaviors of a-C:H:Si films in humid air, dry N_2 and diluent H_2: (a) steady-state friction coefficient as a function of hydrogen content, and (b) steady-state friction coefficient as a function of viscoplastic exponent x.

5.4.2 Running-in for Anti-Friction Tribolayer Build-Up

Running-in is a key factor controlling the frictional behaviors in a-C films, especially the build-up of friction-reduction tribolayers at the sliding interface [5.26-28]. MD simulations have revealed that a series of tribochemical reactions occur during this rubbing process, resulting in a remarked restructuring of the film. This restructuring of film involves numerous bond-breaking and bond-forming events occurred within the film (intrafilm) or between the paired films (interfilm) [5.12]. These events mainly include phase transformation of sp^3-to-sp^2, orientation of bonding structure (i.e.,

sp^2-rings rotated parallel to the sliding plane), growth of tribolayer, exposing and re-saturation of dangling bonds and so on [5.29]. When the number of bonds broken and re-formed reaches a steady-state value, the friction will be lower than that of the initial contact [5.30]. As shown in Figures 5.2(a) and 5.4(a), a high initial friction (μ_{in}~0.5-0.7) is always observed for polymer-like a-C:H:Si films before entering the superlow friction state in dry N_2 or diluent H_2. However, this running-in period is quite short (lasting for about 75 cycles) but sufficient for the complete build-up of tribolayers at the sliding interface (Figure 5.9). Moreover, self-mated sliding is more effective in quick development of the friction-reduction tribolayer than sliding against bare SUJ2 ball, as shown in Figure 5.10. Adventitious carbon and iron oxide layers existed on the counterface ball surface slow the growth of tribolayer. Fontaine et al. reported a strong sticking phenomenon occurring before or at the very beginning of sliding [5.20]. It was emphasized that the stronger this phenomenon is the faster is the friction decrease, implying a faster build-up of tribolayer. This is also true in present case when in view of the higher peak friction of self-mating case (μ_{in}~0.65) compared to that (μ_{in}~0.52) of sliding against bare SUJ2 ball (Figure 5.10).

5.5 Summary

The effect of hydrogen on superlubricity in ion vapor deposited a-C:H:Si films has been investigated from a systematic standpoint. A ternary phase diagram of C-Si-H is proposed for synthesizing new a-C:H:Si lubricants. The hydrogen content ranging from 15 to 40 at.% in the films is obtained by changing the applied bias voltage from 0.25 to 3.5 kV, while the Si content is kept constant at around 10 at.%. The results demonstrate that hydrogen-induced diversity in film structure such as polymer-like, diamond-like or sp^2-bonded a-C, and environmental gas characteristic are the two most influential factors controlling the frictional behaviors of a-C:H:Si films. A proper range of H content in the film is required to achieve stable superlow friction in a distinct gaseous atmosphere, i.e., dry N_2, reactive H_2 or humid air. An extremely low friction coefficient

of ~0.001 in dry N_2 can be obtained for the polymer-like a-C:H:Si (31.9 at.% H) film. The rapid build-up of tribolayers on the contact surfaces during running-in period is the key requirement for establishing superlubric state in dry N_2 and diluent H_2. Self-mated sliding is more effective in building up this anti-friction tribolayer than that is slide against bare counterpart.

References

[5.1] C. Casiraghi, A. C. Ferrari, J. Robertson. Raman spectroscopy of hydrogenated amorphous carbons. *Phys. Rev. B* **2005**, 72, 085401.

[5.2] Y. T. Pei, N. G. Chechenin, P. N. Chernykh, A. A. Turkin, D. Vainshtein, J. Th. M. De Hosson. On the quantification of unbound hydrogen in diamond-like carbon-based thin films. *Scripta Mater.* **2009**, 61, 320-323.

[5.3] B. Racine, M. Benlahsen, K. Zellama, M. Zarrabian, J. P. Villain, G. Turban, A. Grosman. Hydrogen stability in diamond-like carbon films during wear tests. *Appl. Phys. Lett.* **1999**, 75, 3479-3481.

[5.4] H. Nakazawa, R. Osozawa, T. Okuzaki, N. Sato, M. Suemitsu, T. Abe. Effects of hydrogen on the properties of Si-incorporated diamond-like carbon films prepared by pulsed laser deposition. *Diamond Relat. Mater.* **2011**, 20, 485-491.

[5.5] A. Erdemir, O. L. Eryilmaz, I. B. Nilufer, G. R. Fenske. Effect of source gas chemistry on tribological performance of diamond-Like carbon films. *Diamond. Relat. Mater.* **2000**, 9, 632-637.

[5.6] A. Erdemir, O. L. Eryilmaz, G. Fenske. Synthesis of diamondlike carbon films with superlow friction and wear properties. *J. Vac. Sci. Technol. A* **2000**, 18, 1987-1992.

[5.7] A. Erdemir, O. L. Eryilmaz, I. B. Nilufer, G. R. Fenske. Synthesis of superlow-friction carbon films from highly hydrogenated methane plasmas. *Surf. Coat. Technol.* **2000**, 133-134, 448-454.

[5.8] C. Donnet, J. Fontaine, A. Grill, T. Le Mogne. The role of hydrogen on the friction mechanism of diamond-like carbon films. *Tribol. Lett.* **2000**, 9, 137-142.

[5.9] F. Rabbani, B. M. Vogelaar. The importance of unbound hydrogen and increased aromatic structure on the friction and wear behaviour of amorphous hydrogenated carbon (a-C:H) coatings. *Diamond Relat. Mater.* **2004**, 13, 170-179.

[5.10] I. Sugimoto, S. Miyake. Oriented hydrocarbons transferred from a high performance lubricative amorphous C:H:Si film during sliding in a vacuum. *J. Appl. Phys.* **1990**, 56, 1868-1870.

[5.11] C. W. Moura e Silva, J. R. T. Branco, A. Cavaleiro. How can H content influence the tribological behaviour of W-containing DLC coatings. *Solid State Sci.* **2009**, 11, 1778-1782.

[5.12] G. T. Gao, P. T. Mikulski, G. M. Chateauneuf, J. A. Harrison. The effects of film structure and surface hydrogen on the properties of amorphous carbon films. *J. Phys. Chem. B* **2003**, 107, 11082-11090.

[5.13] J. Houska, J. E. Klemberg-Sapieha, L. Martinu. Formation and behavior of unbonded hydrogen in a-C:H of various compositions and densities. *Surf. Coat. Technol.* **2009**, 203, 3770-3776.

[5.14] K. Hayashi, K. Tezuka, N. Ozawa, T. Shimazaki, K. Adachi, M. Kubo. Tribochemical reaction dynamics simulation of hydrogen on a diamond-like carbon surface based on tight-binding quantum chemical molecular dynamics. *J. Phys. Chem. C* **2011**, 115, 22981-22986.

[5.15] Z.-D. Sha, V. Sorkin, P. S. Branicio, Q.-X. Pei, Y.-W. Zhang, D. J. Srolovitz. Large-scale molecular dynamics simulations of wear in diamond-like carbon at the nanoscale. *Appl. Phys. Lett.* **2013**, *103*, 073118.

[5.16] I. Sugimoto, S. Miyake. Oriented hydrocarbons transferred from a high performance lubricative amorphous C:H:Si film during sliding in a vacuum. *Appl. Phys. Lett.* **1990**, *56*, 1868.

[5.17] D. B. Asay, M. T. Dugger, J. A. Ohlhausen, S. H. Kim. Macro- to nnoscale wear prevention via molecular adsorption. *Langmuir* **2008**, *24*, 155.

[5.18] Barnette, A. L.; Asay, D. B.; Ohlhausen, J. A.; Dugger, M. T.; Kim, S. H. Tribochemical Polymerization of Adsorbed n-Pentanol on SiO_2 during Rubbing: When Does It Occur and Is It Responsible for Effective Vapor Phase Lubrication? *Langmuir* **2010**, *26*, 16299.

[5.19] P. Wang, M. Hirose, Y. Suzuki, K. Adachi. Carbon tribo-layer for super-low friction of amorphous carbon nitride coatings in inert gas environments. *Surf. Coat. Technol.* **2013**, 221,

163-172.

[5.20] J. Fontaine, T. Le Mogne, J. L. Loubet, M. Belin. Achieving superlow friction with hydrogenated amorphous carbon: some key requirements *Thin Solid Films* **2005**, 482, 99-108.

[5.21] A. Erdemir, J.-M. Martin. *Superlubricity*, Elsevier: Amsterdam, The Netherlands, 2007.

[5.22] V. N. Pokrovskii. The mesoscopic theory of the slow relaxation of linear macromolecules. *Adv. Polym. Sci.* **2001**, 154, 143-219.

[5.23] J. Fontaine, J. L. Loubet, T. Le Mogne, A. Grill. Superlow friction of diamond-like carbon films: a relation to viscoplastic properties. *Tribol. Lett.* **2004**, 17, 709-714.

[5.24] G. Zilibotti, M. C. Righi. Ab initio calculation of the adhesion and ideal shear strength of planar diamond interfaces with different atomic structure and hydrogen coverage. *Langmuir* **2011**, 27, 6862-6867.

[5.25] B. K. Yen. Roles of oxygen in lubrication and wear of graphite in "dusting" and ambient conditions. *J. Mater. Sci. Lett.* **1995**, 14, 1481-1483.

[5.26] M. J. Marino, E. Hsiao, Y. Chen, O. L. Eryilmaz, A. Erdemir, S. H. Kim. Understanding run-in behavior of diamond-like carbon friction and preventing diamond-like carbon wear in humid air. *Langmuir* **2011**, 27, 12702-12708.

[5.27] L. Pastewka, S. Moser, M. Moseler, B. Blug, S. Meier, T. Hollstein, P. Gumbsch. The running-in of amorphous hydrocarbon tribocoatings: a comparison between experiment and molecular dynamics simulations. *Int. J. Mat. Res.* **2008**, 99, 1136-1143.

[5.28] L. Pastewka, S. Moser, M. Moseler. Atomistic insights into the running-in, lubrication, and failure of hydrogenated diamond-like carbon coatings. *Tribol. Lett.* **2010**, 39, 49-61.

[5.29] J. D. Schall, G. T. Gao, J. A. Harrison. Effects of adhesion and transfer film formation on the tribology of self-mated DLC contacts. *J. Phys. Chem. C* **2010**, 114, 5321-5330.

[5.30] G. T. Gao, P. T. Mikulski, J. A. Harrison. Molecular-scale tribology of amorphous carbon coatings: effects of film thickness, adhesion, and long-range interactions. *J. Am. Chem. Soc.* **2002**, 124, 7202-7209.

Chapter 6

Toward Multi-Environment-Adapted and Near-Frictionless Lubrication Interface by Polymer-Like a-C:H:Si Films

This chapter is devoted to comprehensively investigating the local bonding structure of the polymer-like a-C:H:Si films (i.e., H content > 30 at.%) and their anti-friction behaviors in more wide environments since these hydrogen-rich a-C:H:Si films exhibit the most stable and lowest friction coefficient in dry N_2 and H_2, as observed in Chapter 5. Special attention will focus on the role of hydrogen involved in the friction reduction process. The underlying lubrication mechanism will be discussed with respect to the tribochemical interactions between the film interface and the environmental medium.

6.1 Background

As shown in Chapter 5, hydrogen has a paramount role in affecting the tribological properties of a-C:H:Si films. It is impressive to notice that the hydrogen-rich polymer-like a-C:H:Si film (31.9 at.% hydrogenated sampl) exhibit the most superior anti-friction performance in three different gaseous atmospheres, namely dry inert gas N_2, reactive H_2 and humid air. The occurrence of a superlubric state in each environment is always strongly correlated with the formation of tribolayers on the contact surfaces. The chemical bonding states of these tribolayers should have a close relationship with the pristine film structure. However, the exact local structure of this polymer-like a-C:H:Si film, especially the hydrogen bonding state, remains unclear. On

the other hand, it is also highly necessary to further investigate the underlying lubrication mechanism tribochemically induced by the presence of gaseous molecules in more wide service environments, which can provide basic and useful information for designing new solid lubricants in the future.

Until now, two well-known mechanisms have been proposed to disclose the friction-reducing behaviors in these carbon films. One is shear-induced carbon phase transformation such as sp^3-C to sp^2-C rehybridization at sliding interface [6.1-4], where sp^2-C phase is thought to be a softer and low-shear strength phase. For instance, the possible formation of a graphitic tribolayer on the contact surface has been studied by various characterization methods in DLC films during sliding [6.3, 4]. The other prevailing mechanism is surface passivation of dangling bonds at sliding interface by passivating species such as –H, -OH or water molecules [6.5-10]. For example, the extremely low friction coefficient down to 0.001 of highly-hydrogenated a-C:H film is mainly attributed to the surface chemical inertness by H-passivation of carbon dangling σ bonds and the resulting little adhesive force exerting at the sliding interface [6.5, 6, 10]. Similar friction-reduction mechanism has also been found for lubricity of ta-C by glycerol [6.11] and UNCD [6.7-9] or O_2-plasma-treated DNW [6.12, 13] by H_2O molecules. More recently, a shear localization mechanism is postulated to explain the lubricity in a-C [6.14, 15]. Shear localization is characteristic of phase transformation (i.e., sp^3-to-sp^2), bond reorientation and structural ordering preferentially in a localized region, namely tribolayer, resulting in shear weakening. Superlow friction is only feasible under the condition of high phase transformation (i.e., sp^2 fraction more than 80%) and high shear localization (i.e., orientations of most covalent bonds parallel to the sliding direction) in the very thin localized layer around the sliding interface [6.15]. Shear localization is a supplement to the lubrication mechanism of a-C since, on one hand, simple phase transformation cannot guarantee superlow friction, and on the other hand, passivating species are not able to totally shield dangling bonds especially in the sliding cases where dissociation and removal of surface terminations occurs.

In this Chapter, a systematic study is carried out to characterize the polymer-like a-C:H:Si (31.9 at.% H) films in view of their superior anti-frictional performances compared to other structured films. The underlying lubrication mechanism is discussed from the perspective of each contribution of phase transformation, surface passivation and/or shear localization to the friction-reduction behaviors of a-C:H:Si films.

6.2 Experimental Methods

The polymer-like a-C:H:Si film with hydrogen content of ~32 at.% was prepared at the applied bias voltage of 0.5 kV in IVD system. Relevant details on the growth conditions are shown in Chapter 2. The local microstructure of this polymer-like a-C:H:Si film was characterized by HRTEM operating on JEOL JEM-2010HC system at 200 kV. The friction tests were performed on a CSM pin-on-disc tribometer at room temperature. The normal load was set at 2 N. The film-coated Si wafer was fixed on a rotary sample platform using a bare (for test in humid air) or same-film-coated (for test in dry N_2, Ar, H_2 and O_2) SUJ2 ball of 6 mm in diameter as a counterpart. The rotation radius was 3.5 mm, and the linear sliding speed was 15 cm/s (for test in humid air) or 20 cm/s (for test in dry N_2 and H_2). Different gaseous environments including humid air (22 ± 2 % RH), dry inert N_2, Ar, diluent H_2 (40 vol.% H_2 + 60 vol.% He) and O_2 were produced by purging water vapor or distinct gas source into the tribometer chamber until stability before friction test. The outlet pressure of the gas pipeline was 500 Pa. A Nikon optical microscope was used to measure the wear morphology. Raman spectroscopy (Renishaw System, Ar^+ laser, 532 nm) was employed to detect the carbon bonding state change of a-C:H:Si films before and after the friction test. The bonding chemistry of the as-grown and worn surfaces was detected using an imaging 3D time-of-flight secondary ion mass spectrometry (ToF-SIMS, PHI TRIFT III) with a Ga^+ analytical gun as the primary ion source.

6.3 Results

6.3.1 Local Microstructure and the Role of Hydrogen in Lubrication

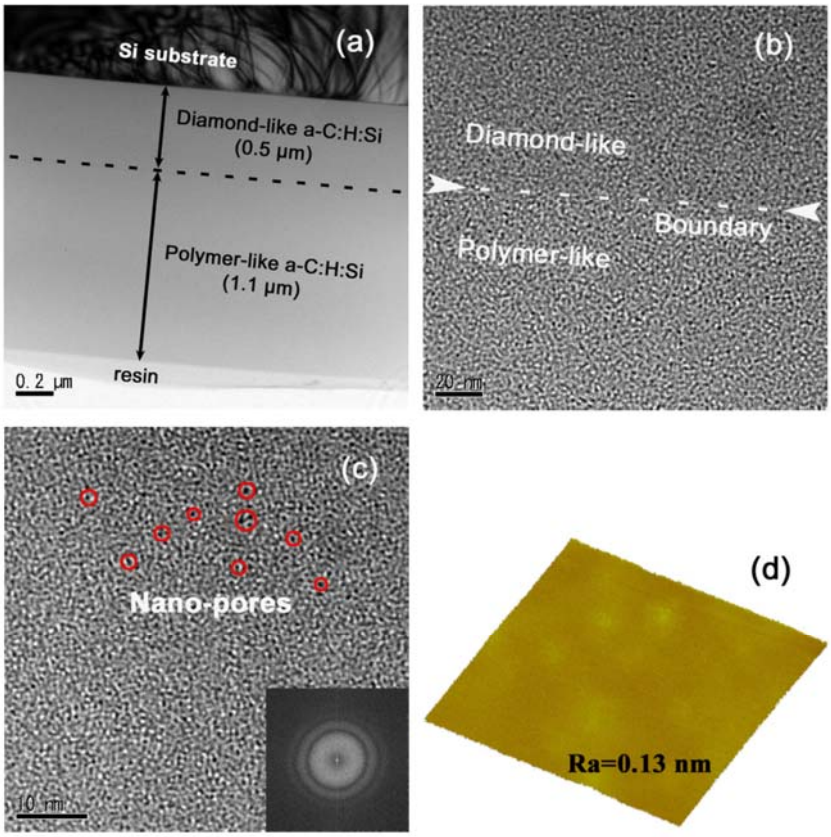

Figure 6.1 Nanostructure of the as-grown a-C:H:Si (31.9 at.% H) film. (a) Cross-sectional HRTEM image showing the bilayer structure: diamond-like a-C:H:Si interlayer and polymer-like a-C:H:Si top layer. (b) HRTEM image indicating the continuous and dense boundary between the diamond-like and polymer-like individual layers. (c) HRTEM image showing the local nanostructure of the polymer-like a-C:H:Si top layer. A large number of nano-scale pores (indicated by red circles) are observed to be evenly distributed in the film. The lower inset shows the corresponding FFT image of the film. (d) 2.5×2.5 μm^2 AFM morphology image showing the ultrasmooth surface with atomic scale roughness Ra=0.13 nm.

The local microstructure of the as-grown polymeric a-C:H:Si (31.9 at.% H) film characterized by HRTEM is shown in Figure 6.1(a). It is seen that the as-deposited a-C:H:Si film was tailored to possess a bilayer structure, in which a 1.1-μm thick

polymer-like a-C:H:Si layer was deposited on top of a 0.5-μm thick diamond-like a-C:H:Si interlayer. This interlayer is effective in improving the bonding strength of the film to the bottom Si substrate as well as in acting as a load support layer for the top polymeric layer due to their relatively high hardness (~23 GPa). The HRTEM image in Figure 6.1(b) shows the continuous and dense boundary interface formed between the diamond-like and the polymer-like individual layers. Note that an obscure phase contrast can also be observed between them, indicating a disparity in composition and bonding structure. The local nanostructure of the top polymer-like layer is further indicated in Figure 6.1(c). It seems that a large number of nanoscale pores with diameter of ~0.5-1.0 nm are evenly distributed in the film. Such a nanoporous structure is thought to be developed under low energy subsurface growth from a hydrogen-rich ion flux produced in the ionization system.

Several early studies have also reported the presence of microvoids in silicon-related materials such as hydrogenated amorphous silicon (a-Si:H) film and hydrogenated amorphous silicon-carbon (a-$Si_{1-x}C_x$:H) alloys [6.16-18]. It is estimated by nuclear magnetic resonance (NMR) [6.17] or small-angle X-ray scattering (SAXS) [6.18] that these microvoids have a volume size of ~1 nm in diameter. These nanopores are expected to act as reservoirs for trapped molecular H_2, which are formed from recombination of abundant hydrogen atom during low-energy ion penetrating. The result in Chapter 2 has confirmed several characteristic infrared vibration bands in the film by Fourier transform infrared spectroscopy (FTIR), including Si-C stretching modes, Si-H_n bending and stretching modes and C-H_n stretching modes, as well as some hydrogen-terminating groups such as Si-CH_2 and Si-CH_3. Such a hydrogen-induced infrared vibration is definitely an indicator for the chain-developed polymeric structure in the a-C:H:Si film. It is previously suggested in a-$Si_{1-x}C_x$:H films that hydrogen is mainly incorporated into the films at positions interrupting bonds of host matrix. Above a certain content of hydrogen, the amorphous network will partly lose its connectiveness so that microvoids are formed. The H-containing species such as molecular H_2, Si-H_n

and C-H_n radicals are then trapped in the microvoids or bonded to the microvoid internal surfaces [6.16]. However, the present HRTEM result still cannot serve as the direct evidence for the existence of molecular H_2 in the film. Other assistant techniques such as NMR and SAXS are necessary to disclose this issue. However, the experimental confirmation of molecular H_2 in the film is quite a difficult task to conduct. Related work is now in progress.

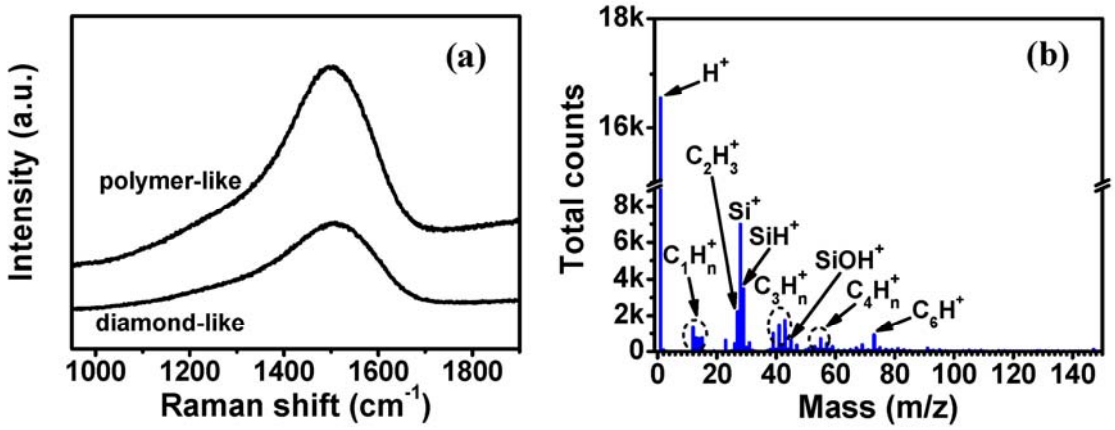

Figure 6.2 (a) Raman spectra of diamond-like a-C:H:Si interlayer and polymer-like a-C:H:Si top layer as shown in Figure 6.1, and (b) ToF-SIMS fragment ion spectrum showing the chemical composition detecting from the as-deposited surface of the polymer-like top layer.

The diffuse rings from the Fast Fourier Transform (FFT) diffraction patterns inset in Figure 6.1(c) clearly indicate the amorphous characteristic of the polymeric a-C:H:Si film. Moreover, it is important to notice an atomically smooth and featureless surface for the as-grown film, as shown in Figure 6.1(d), with a root mean square (RMS) roughness of 0.13 nm. The origin of ultrasmoothness of a-C:H:Si films grown in the present deposition system has been discussed in Chapter 2. Such a surface ultrasmoothness, to the greatest degree, would reduce the mechanical interactions between the contact surfaces during sliding for the lubricating materials [6.19].

The visible Raman spectra in Figure 6.2(a) further indicate that both the diamond-like a-C:H:Si interlayer and the polymer-like a-C:H:Si top layer have an

amorphous carbon bonding characteristic. The shrinking of *D*-peak (deriving from vibration modes of sp^2 atoms in aromatic rings) implies the suppression of ring-like structure by Si incorporation. However, the enhanced photoluminescence (PL) background of the polymer-like top layer compared to the diamond-like interlayer obviously reflects the high hydrogen content and chain-developed structure in this layer [6.20]. The above HRTEM result gives an insight into the possible residing form of hydrogen in the bulk of the polymer-like a-C:H:Si film. In spite of this, we still need to know the accurate bonding state of hydrogen on the film surface since the interfacial property of a film significantly governs the friction and wear behaviors when directly brought into contact sliding. Therefore, the surface chemistry was further detected using an imaging 3D ToF-SIMS, which can provide extra information about the chemical nature of very thin (a few Å to 1-2 nm) surface layers. As shown in Figure 6.2(b), in addition to abundant hydrogen fragments (H), a large number of hydrocarbon fragments (i.e., C_1H_n, C_2H_3, C_3H_n, C_4H_n, C_6H) and Si-containing fragments (i.e., Si, SiH) are also found to exist on the top surface of a-C:H:Si film. This strongly suggests that the original surface of a-C:H:Si film is predominantly passivated by hydrogen atoms, yielding a chemical inertness interface if serving as a sliding counterpart.

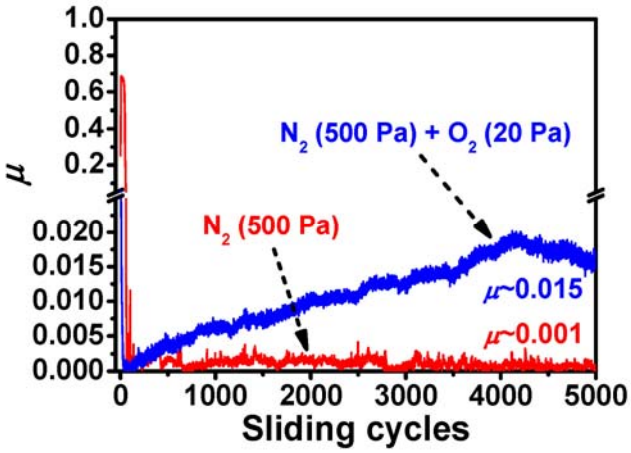

Figure 6.3 Comparison of frictional behaviors of the polymer-like a-C:H:Si (31.9 at.% H) film tribotested in dry N_2 and mixed gas (dry N_2 diluted by a small amount of O_2), respectively, depicting the pivotal role of hydrogen involved in superlubricity.

As well documented, the low friction between two hydrogen-passivated carbon surfaces in dry inert gas is attributed to the electrostatic repulsive forces [6.5, 6, 10] or, recently proposed, the anti-bonding orbital interactions produced between different atoms at the sliding interface [6.21]. In either mechanism, the saturation of carbon dangling bonds by hydrogen atoms is the key point to maintain low friction for carbon surfaces. On the other hand, the presence of reactive gaseous molecules such as H_2O and O_2 in the surroundings is able to change this passivating state or even release hydrogen atoms from the carbon surface [6.22, 23]. For instance, density functional theory (DFT) calculations have demonstrated that oxygen atoms can chemically modify the surface stiff C-H bonds by entering between C and H atoms to form C-O-H radicals and thus may increase the friction [6.22]. Bearing this in mind, we tribotested the polymer-like a-C:H:Si (31.9 at.% H) film in a mixed N_2 + O_2 gas atmosphere by introducing a small amount of O_2 into dry N_2. In addition, a friction test in pure N_2 was also accomplished for comparison. Note that the partial pressure of O_2 flowing around the contact area should be controlled at a level low enough to avoid completely covering the lubrication effect of hydrogen. A pure oxygen or oxygen-rich gaseous atmosphere can dramatically change the frictional behaviors of a-C:H:Si film observed in dry N_2, as will be shown in Figure 6.4. In the present case, the outlet pressure of N_2 from the gas pipeline was 500 Pa, while that of O_2 was set at 20 Pa. The obtained results are shown in Figure 6.3. As already observed above, the friction coefficient of the polymer-like a-C:H:Si in pure dry N_2 film quickly evolves into an extremely stable and low value μ_{ss}~0.001 after a short intensive running period. It is reasonable to assume that the rate of hydrogen loss by thermal heating and/or mechanical action during sliding in dry N_2 is very small. In comparison, the presence of a small amount of O_2 in dry N_2 significantly affects the frictional behavior of a-C:H:Si film. The friction coefficient first falls into a superlow scope of ~0.001, resembling the result in dry N_2. However, it gradually increases with the sliding process going on. At around 2000 cycles, the friction coefficient passes over the threshold value of 0.01 and enters into the ultralow scope.

Finally, it stabilizes at around 0.015 for the rest 4000-5000 sliding cycles. The deterioration of superlubric state and gradual increase in friction are therefore correlated with the change of passivation state on contact surface. The most likely scenario is that free hydrogen exists within the film (i.e., nanopores) serving as a reservoir, and it can replenish or replace those surface hydrogen atoms that may have been released by oxygen. The continuous consumption or even exhaustion of free hydrogen inevitably results in a gradual increase in friction as the available hydrogen can't effectively terminate those newly-produced dangling bonds. However, the present results still cannot serve as the direct evidence for the molecular hydrogen existed in the polymeric structure of a-C:H:Si film. Further work is now in progress to uncover this critical issue.

6.3.2 Ultralow and/or Superlow Friction in Multi-Environments

To further evaluate the frictional behaviors in more wide environments, dry Ar and O_2 have been added as the background atmospheres. The friction tests were carried out using the same parameters as described for the cases of N_2, H_2-He and humid air. Note that the outlet pressure of O_2 is now 500 Pa. For the convenience of comparison, the friction curves are plotted along with the friction results in dry N_2, diluent H_2 and humid air as shown in Chapter 5. The results are indicated in Figure 6.4. The average steady-state friction coefficients in each condition are 0.004 (RH22%-air), 0.001 (dry N_2), 0.012 (dry Ar), 0.003 (40% H_2+60% He) and 0.084 (dry O_2), respectively. The most stable and lowest value (μ_{ss}~0.001) is achieved in dry N_2. In comparison, the friction coefficient obtained in another inert gas (dry Ar) just approaches a quasi-superlubric state (μ_{ss}~0.012). This difference clearly demonstrates that the molecular diversity even for similar kinds of gas can have a profound effect on the frictional behaviors of a-C:H:Si film. Furthermore, the a-C:H:Si film exhibits noticeably increased but still ultralow friction (μ~0.084) even in the corrosive gas O_2. Overall, this polymer-like a-C:H:Si film possesses superior anti-friction properties and can exhibit superlow or ultralow friction in quite wide service environments.

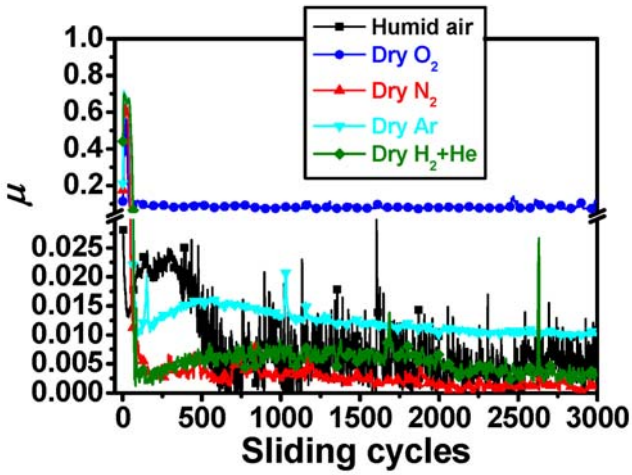

Figure 6.4 Evolution of friction coefficient, versus the number of sliding cycles, of the polymer-like a-C:H:Si film (31.9 at.%) tribotested in multi-environments including humid air (22±2% RH), inert N_2 and Ar gases, reactive gas H_2 (40% H_2 + 60% He) and corrosive gas O_2. Note that the friction results in dry N_2, diluent H_2 and humid air are re-plotted from Chapter 5.

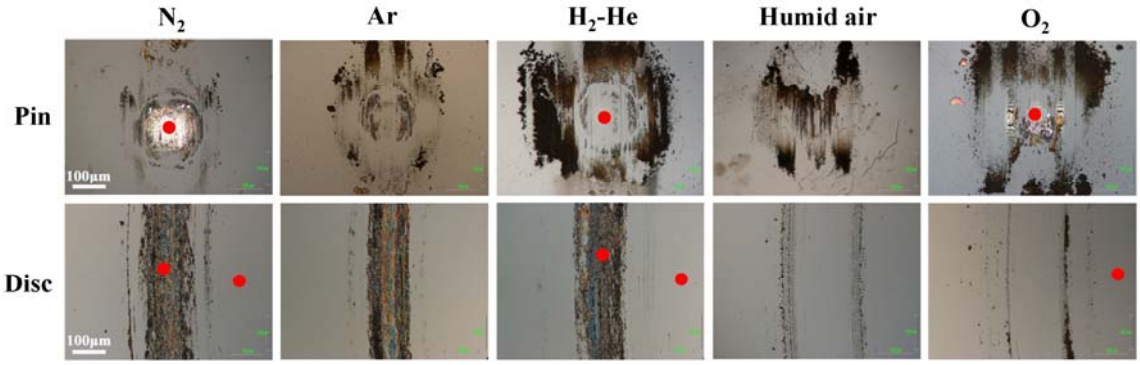

Figure 6.5 Wear morphologies of the sliding pairs after the friction tests in each atmosphere as shown in Figure 6.4. The red dots marked in the contact areas or on the as-grown film surface indicate the positions for Raman analysis in Figure 6.6.

The wear morphologies of the sliding pairs including pin and disc after the friction tests in Figure 6.4 are shown in Figure 6.5. It is obviously seen that black-brown tribolayers are produced and evenly distributed in the wear tracks on the discs, which are transferred from the film materials coated on the SUJ2 balls (as discussed in Chapter 5). Correspondingly, some (in dry N_2) or a large amount of (in Ar and H_2-He mixture)

tribodebris are formed on the ball scar surfaces. On the other hand, no such kind of black-brown tribolayers are found on the film surface in the cases of humid air and dry O_2. However, a noticeable amount of tribolayers can still be found on the ball scar surfaces in these two conditions. The above results clearly demonstrate that the surrounding gaseous atmospheres are deeply involved in the rubbing process, where the chemical characteristics of the gaseous molecules are in relation to the bonding state of the formed tribolayers and the material distributions between the two contact surfaces.

6.3.3 Evolution of Chemical Bonding upon Sliding Contact

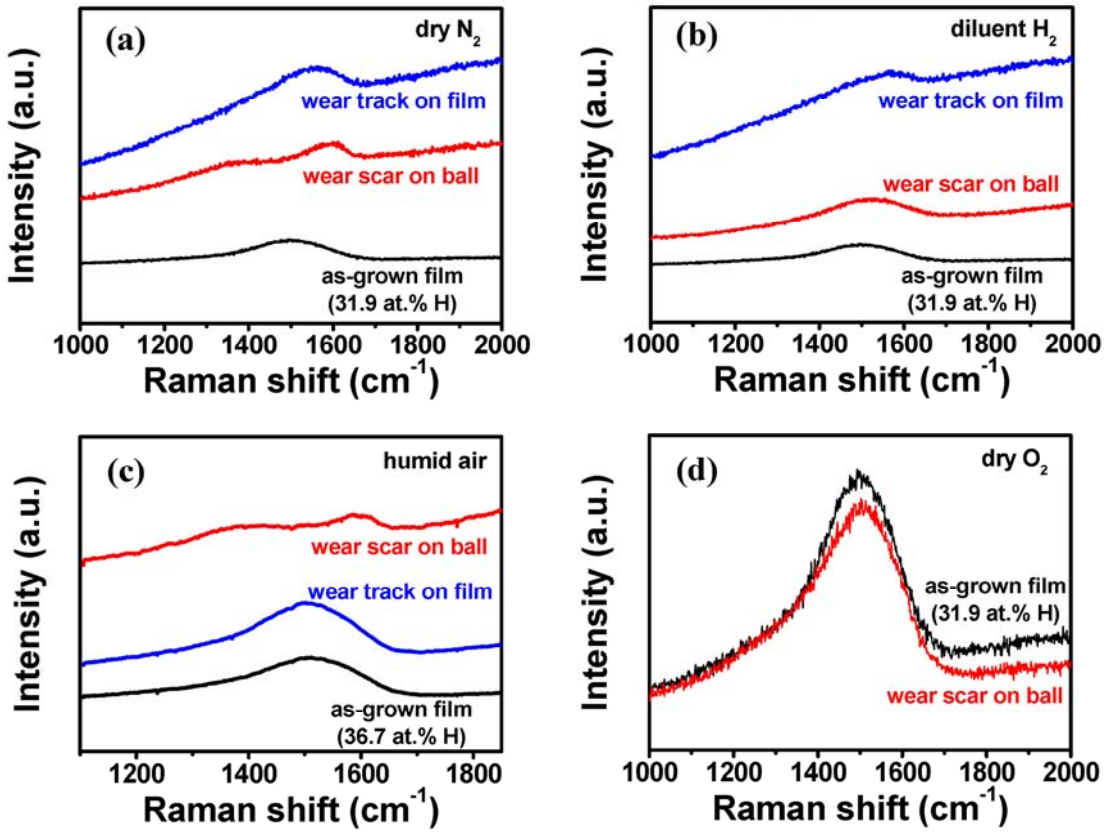

Figure 6.6 Comparison of carbon bonding states characterized by Raman spectra from as-grown film, wear scar on ball and wear track on film-coated Si substrate for the polymer-like a-C:H:Si film after friction test in four representative gaseous environments: (a) dry N_2, (b) diluent H_2, (c) humid air and (d) corrosive O_2. The detecting positions are indicated in Figure 6.5. Note that the obtained Raman spectrum in humid air is from the the a-C:H:Si sample with 36.7 at.% H, as shown in Figure 5.6 and 5.7 in Chapter 5.

To gain deep insight into the bonding state of the contact area, Raman spectroscopy was utilized to detect wear scar on ball, wear track on film and the as-grown film for the polymer-like a-C:H:Si film after friction tests in four representative gaseous environments, as shown in Figure 6.6. In dry N_2 (Figure 6.6(a)), the Raman spectrum taken from the wear scar on ball splits into two obvious *D* and *G* peaks as compared to the as-grown film. The enhancement of *D* peak indicates the increase in ring-like structure of sp^2 carbon bonding [6.20]. Since the film material is almost removed from the Fe surface during sliding (Figures 5.3(a3) and 5.11(a1)), the Raman signal is mainly from the thin tribolayer formed on the wear scar surface and exactly reflects the nature of it. The Raman spectrum taken from the wear track on film is similar to that of wear scar. However, the *D* peak is enveloped in the broad band with *G* peak. This is because the Raman signal also comes from the underlying as-grown film layer in addition to the top tribolayer formed in the wear track. Another noticeable point is the significantly enhanced PL background in both Raman curves. The exact origin is not well understood yet. It could be, most probably, due to the loose and porous structure of the formed tribolayars, which would increase the defect density and therefore activate the photoluminescence [6.24]. In diluent H_2 (Figure 6.6(b)), the major difference in Raman curve shape is the almost absence of *D* peak even for the signal from the wear scar on ball surface. This finding emphasizes the suppressed formation of ring-like bonding structure in the thin shear interface when molecular hydrogen is surrounding the contact surface. Hydrogen is likely to chemically react with the top sliding surface under contact pressure and saturate the sp^2-C bonds existing on the interface. In humid air (Figure 6.6(c)), the tribolayer formed on the bare SUJ2 ball surface is also rich in sp^2-C, especially the increase in aromatic structure. However, Raman spectrum cannot provide detailed information about the hydrophilic passivation state induced by dissociative adsorption of water molecules on Si-OH group, which has already discussed in Chapter 4. Thus, the friction reduction in humid air for polymeric a-C:H:Si film is actually from the joint effects of sp^2 phase shear, hydrogen termination

and water passivation. In comparison, Raman spectrum taken from the wear scar on film-coated ball surface after the friction test in dry O_2 (Figure 6.6(d)) exhibits reduced PL background, implying an H-deficient bonding structure at the sliding interface.

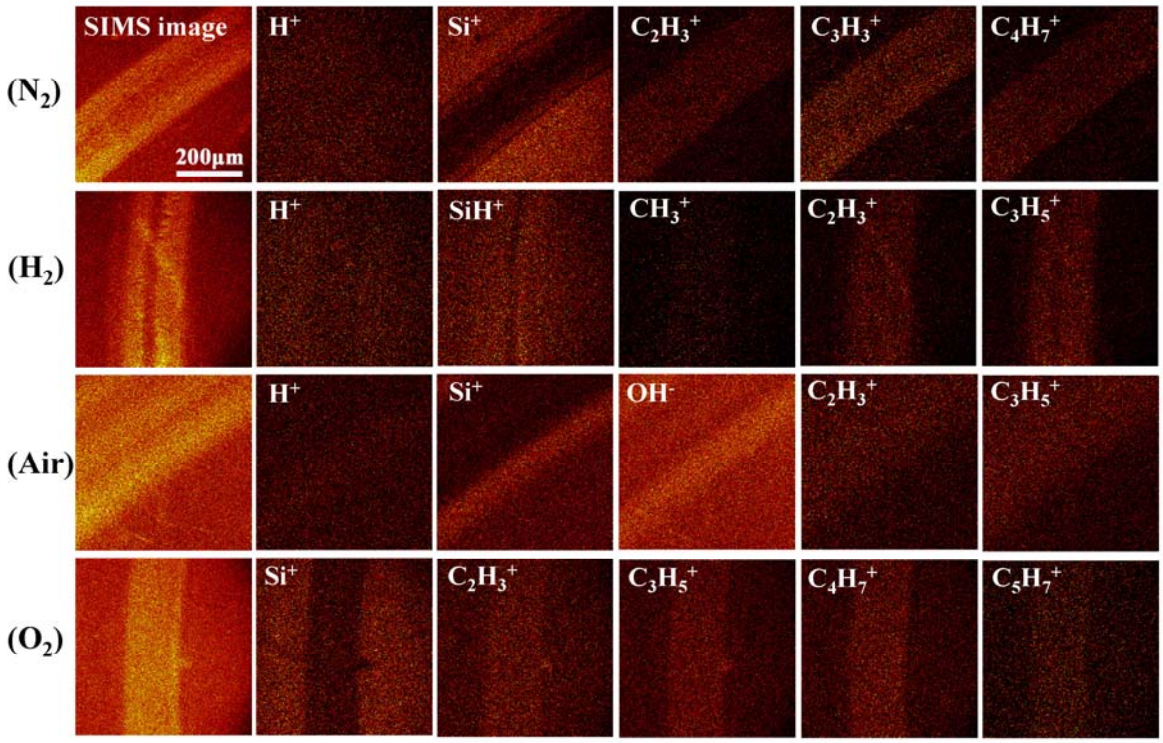

Figure 6.7 2D ToF-SIMS images of main fragment ions indicating the surface chemical bonding state of wear track for the polymer-like a-C:H:Si film (31.9 at.% H) after friction tests (as shown in Figures 6.4 and 6.5) in dry N_2, diluent H_2, humid air and corrosive O_2.

Since Raman spectrum mainly provides carbon bonding information from the bulk, ToF-SIMS was further used to detect the chemical state, for a wide range of species including hydrogen, of the top-most surface of tribolayers formed in the wear track on Si substrate. The results are shown in Figure 6.7. In dry N_2, the wear track surface is uniform in H but lack in Si. This means that the contact surface maintains a high content of hydrogen, along with an aromatic-rich structure (see Figure 6.6(a)) in this very thin shear layer. Thus, the bonding structure in this very thin region of tribolayer is more like a highly hydrogenated graphite-like carbon, referred as GLCHH, as previously proposed

by some researchers [6.20]. The origin of Si-deficiency in this localized layer is still unclear now. In addition, the strengthened signal of some hydrocarbon fractions such as C_2H_3, C_3H_3 and C_4H_7 in the wear track confirms the existence of a hydrogen-rich top surface layer. In diluent H_2, the wear track is totally covered by hydrogen-terminating groups such as Si-H, CH_3, C_2H_3 and C_3H_5. The increased ratio of H/C in these hydrocarbon groups compared to the case in dry N_2 manifests the passivation effect of molecular H_2 on the contact surface. In humid air, the strong signals of Si and OH radicals confirm the presence of a hydrophilic top layer such as Si-OH at the sliding interface. The formation of such a hydrophilic layer along with adsorption of water molecules provides effective boundary lubrication for friction reduction, as already indicated in Chapter 4 for a diamond-like a-C:H:Si film. In the present case of polymer-like a-C:H:Si film, in addition to Si-OH lubrication, hydrogen and some hydrocarbon groups such as C_2H_3 and C_3H_5 are also involved in the rubbing process, indicating a more complex tribochemical process. As for the case in corrosive O_2, oxygen molecules react with Si (more preferentially) and C atoms and simultaneously release part of the surface hydrogen atoms, which results in a more covalent and adhesive top layer containing hydrogen-deficient radials such as C_2H_3, C_3H_5, C_4H_7 and C_5H_7, and thus friction increase during sliding.

6.4 Discussion

It is obviously noticed from the above results that the occurrence of a superlubric state in the polymer-like a-C:H:Si film is strongly correlated with the film structure especially the hydrogen bonding state, the surrounding gaseous atmosphere and the tribointeractions between these components. From a microscopic point of view, this rubbing process involves some key issues such as the phase transformation (i.e., sp^3-to-sp^2 evolution), running-in period, tribolayer formation, pressure-induced bond breaking and formation, hydrogen coverage on the surface, passivation with gaseous species or even shear localization in the very thin top interface.

6.4.1 Tribochemistry Induced by Environmental Gaseous Molecules

Numerous experimental and simulation studies have emphasized the paramount influence of environmental atmosphere on the frictional behaviors of amorphous carbons [6.8, 9, 22, 23, 25-27]. Depending on the chemical characteristics of the gaseous molecules, tribo-interactions at the sliding interface can be divided into non-reactive and reactive, respectively. In the case of dry inert gases (such as N_2 and Ar), there are generally no chemical reactions such as dissociative passivation from the surrounding species occurring on the contact surfaces. Therefore, the coupling carbon films should self-lubricate themselves by their as-grown inherent structures to lower the friction. On the other hand, in reactive atmospheres such as O_2, humid air or H_2, the reactive dissociations of these gaseous molecules would corrode or passivate the sliding surfaces, which cause an increase of adhesive force or a reduction of shear force, respectively. For dry inert gas, superlow friction is more feasible in N_2 than in Ar for the polymeric a-C:H:Si film, as indicated in Figure 6.4. This demonstrates that even a small diversity in molecular characteristic of surrounding gas can have a crucial influence on the frictional behaviors of a-C:H:Si film. The origin of superior anti-friction performance in dry N_2 compared to that in dry Ar is not well understood yet. Some researchers have proposed that the formation of a perpendicularly oriented monolayer adsorbed on the contact interface by physical interactions between π orbital of sp^2-C atoms and lone pair electrons of N_2 is probably the reason for superior friction-reduction behavior in dry N_2 [6.28]. Hydrogen is well known for its lubrication effect by saturation of any covalent dangling bonds exposed to the sliding interface. Friction between such H-passivated surfaces is expected to be low due to the produced electrostatic repulsive forces [6.5, 6, 10] or, recently proposed, the anti-bonding orbital interactions between different atoms at the sliding interface [6.21]. DFT calculations have predicted that a minimum partial pressure of H_2 at room temperature such as P_H=0.38 Pa is required to passivate all the dangling bonds for diamond or diamond-like

surfaces. Ultralow friction can be achieved with a fully H-passivated surface, by either increasing P_H or reducing the surrounding temperature T [6.29]. In spite of this, the present study indicates that not all the hydrogenated carbon films can achieve superlow friction even in a hydrogen-providing atmosphere such as diluent H_2 of 500 Pa, especially for the most hydrogen-deficient sp^2-bonded a-C:H:Si films (see Figure 5.3). This demonstrates that the hydrogen coverage on the pristine film surface is also of critical importance for achieving superlubricity [6.30]. In humid air, the key mechanism for ultralow or superlow friction is surface passivation by gaseous species, especially water molecules. To form boundary lubrication, water molecules have to find some surface sites to reside. For a-C:H:Si films, the formation of a hydrophilic Si-OH layer (Figure 6.7) are expected to adsorb water molecules and thus provide sufficient water coverage on the contact surface. Recent *ab initio* MD simulation has directly observed that load-induced confinement is the driving force for diamond surface passivation by water dissociation. The Pauli repulsion between the fully-saturated bonds, such as C-H and C-OH, can stand the applied load and prevent the facing surfaces from direct contact, which leads to a reduction of friction [6.31]. In corrosive O_2, the occurrence of adhesive bonds at the sliding interface activated by oxygen through releasing of hydrogen and oxidizing the film surface causes a noticeable friction increase. However, the friction in O_2 is still ultralow (μ_{ss}~0.084), which is most likely due to the low shear strength of this oxide layer and partly to the remaining passivation effect from some hydrocarbon radicals (see Figure 6.7).

6.4.2 Synergistic Effect of Phase Transformation, Surface Passivation and Shear Localization

Phase transformation, especially the evolution of sp^3 to sp^2, has been frequently reported in a-C films based on the characterization of tribolayers by Raman, TEM, and NEXAFS [6.1, 3, 4, 14, 32, 33]. Most simulation studies also depict an obvious sp^3-to-sp^2 rehybridization under shear deformation [6.14, 15, 30, 32, 34, 35]. The

formation of a graphitic carbon layer on the contact surface is generally speculated as the origin for friction reduction in a-C materials. However, no direct experimental observation has been provided to confirm this hypothesis. The produced sp^2 phase can exist either in clustered rings or in disordering units. Furthermore, from the steric point of view, it is also difficult to maintain a completely layered graphitic structure for a tribolayer with thickness of several hundred nanometers. Therefore, just simple rehybridization and amorphization cannot guarantee a superlow friction. Recent simulation results by Kunze et al. [6.14] and Ma et al. [6.15] proposes that shear localization is more reasonable to account for the superlow friction in a-C films, due to high phase transformation and gradual ordering occurred in the tribolayer. It is emphasized that amorphous carbon does not undergo homogeneous Newtonian-fluid-like shear deformation throughout the material, but rather exhibit localized deformation in a very thin shear band. This speculation can find some experimental clue from the polymeric a-C:H:Si film when tribotested in dry N_2 (Figures 5.2(a), 5.3(a3) and 6.6(a)). The overall increase in the intensity of the Raman spectrum taken from the wear scar on ball surface indicates a remarkable increase in sp^2-C fraction in the tribolayer. In addition, the enhanced *D* peak implies an abundance of sp^2-bonded rings. Due to the very thin thickness of this tribolayer (Figures 5.3(a3) and 5.11(a1)), the most energetically favored pathway to achieve the recorded extremely low friction (μ_{ss}~0.001) is to be deeply ordered in the very thin localized layer. In Ma's simulation [6.15], this ordering process produced a layer-like shear band. Note that this layer-like sp^2 configuration is not of perfect graphite structure but include some distorted bonds and defects. However, a layered structure was not observed by Kunze [6.14] and his co-workers [6.32]. The morphology of this sp^2-rich tribolayer is still amorphous but orient its bonds mainly parallel to the sliding plane (smoothening effect). Correspondingly, a superlow friction regime (μ<0.01) was recorded by Ma [6.15] while a relatively high friction coefficient (μ~0.12) was observed in the latter case [6.32]. Based on these results, the most likely scenario for the present polymeric a-C:H:Si film

tribotested in dry N_2 is that the topmost sp^2-rich tribolayer possesses some degree of layering and simultaneously orient most of its covalent bonds parallel to the sliding direction. On the other hand, the plentiful hydrogen atoms inherent in the films stabilize the film structure and terminate the dangling bonds around the sliding interface, i.e., forming a GLCHH structure [6.20]. Therefore, the superlow friction for the polymeric a-C:H:Si film in dry N_2 is more likely attributed to the synergistic effect between phase transformation, shear localization and surface passivation. This synergistic effect is further interpreted in another MD simulation that a self-mated H-rich (45 %) a-C:H film undergoes a remarkable sp^3-to-sp^2 transformation in a region of ±1 nm around the sliding interface in the first 5 ns sliding at a pressure of 5 GPa. The film surfaces passivate themselves by hydrogen termination and orientation of sp^2-rings parallel to the sliding direction after about 20 ns, and the friction coefficient then drops to a low value for the rest 20 ns sliding [6.34]. In comparison, the superlubricity for polymeric a-C:H:Si film in diluent H_2 is mainly ascribed to the passivation effect by hydrogen as discussed in Section 6.4.1, since no obvious ring-like structure is detected in the tribolayer (Figure 6.6(b)). The comparison between dry N_2 and H_2 implies that the degree of clustering of aromatic rings is favored with the increase of the chemical inertness of the surrounding gas. However, further work such as TEM observation is still needed to disclose the exact bonding structure of the produced tribolayers. In addition, how to avoid vast film material loss from the polymeric-film-coated ball in the running-in period when tribotested in dry N_2 or H_2 (i.e., Figures 5.3(a3), 5.5(a3) and 5.9) is also necessary, for providing more durable lubrication.

6.5 Summary

In this Chapter, a polymer-like a-C:H:Si film, which has a nanoporous microstructure, high hydrogen content (~32 at.%), atomically smooth surface (Ra~0.1 nm) and chain-developed sp^3-rich bonding network, is proposed for serving as a new multi-environment-adapted anti-friction lubricant. This polymeric sample can exhibit

superlow friction (μ~0.001-0.01) in various gaseous environments including humid air, inert gases (N_2 and Ar) and reactive gas (H_2), and can even maintain ultralow friction (μ~0.08) in a corrosive gas (O_2). Hydrogen is highlighted for its decisive role in obtaining superlow friction. The occurrence of superlubricity in a-C:H:Si films is sometimes attributed to a synergistic effect of phase transformation, surface passivation and shear localization, for example, the acquisition of an extremely low friction coefficient of ~0.001 in dry N_2. The contribution of each mechanism to the friction reduction depends on the specific tribotesting condition. The present realization of superlubricity by one material such as the polymer-like a-C:H:Si film in multi-environments may open up a new pathway for designing more efficient lubricating materials in the near future.

References

[6.1] A. P. Merkle, A. Erdemir, O. L. Eryilmaz, J. A. Johnson, L. D. Marks. In situ TEM studies of tribo-induced bonding modifications in near-frictionless carbon films. *Carbon* **2010**, 48, 587-591.

[6.2] L. Pastewka, S. Moser, P. Gumbsch, M. Moseler. Anisotropic mechanical amorphization drives wear in diamond. *Nat. Mater.* **2011**, 10, 34-38.

[6.3] Y. Liu, A. Erdemir, E. I. Meletis. An investigation of the relationship between graphitization and frictional behavior of DLC coatings. *Surf. Coat. Technol.* **1996**, 86-87, 564-568.

[6.4] J. C. Sánchez-López, A. Erdemir, C. Donnet, T. C. Rojas. Friction-induced structural transformations of diamondlike carbon coatings under various atmospheres. *Surf. Coat. Technol.* **2003**, 163-164, 444-450.

[6.5] C. Donnet, J. Fontaine, A. Grill, T. Le Mogne. The role of hydrogen on the friction mechanism of diamond-Like carbon films. *Tribol. Lett.* **2000**, 9, 137-142.

[6.6] A. Erdemir, O. L. Eryilmaz, I. B. Nilufer, G. R. Fenske. Effect of source gas chemistry on tribological performance of diamond-like carbon films. *Diamond. Relat. Mater.* **2000**, 9, 632-637.

[6.7] A. R. Konicek, D. S. Grierson, P. U. P. A. Gilbert, W. G. Sawyer, A. V. Sumant, R. W. Carpick. Origin of ultralow friction and wear in ultrananocrystalline diamond. *Phys. Rev. Lett.* **2008**, 100, 235502.

[6.8] A. R. Konicek, D. S. Grierson, A. V. Sumant, T. A. Friedmann, J. P. Sullivan, P. U. P. A. Gilbert, W. G. Sawyer, R. W. Carpick. Influence of surface passivation on the friction and wear behavior of ultrananocrystalline diamond and tetrahedral amorphous carbon thin films. *Phys. Rev. B* **2012**, 85, 155448.

[6.9] N. Kumar, R. Ramadoss, A. T. Kozakov, K. J. Sankaran, S. Dash, A. K. Tyagi, N. H. Tai, I.-N. Lin. Humidity-dependent friction mechanism in an ultrananocrystalline diamond film. *J. Phys. D Appl. Phys.* **2013**, 46, 275501.

[6.10] A. Erdemir. The role of hydrogen in tribological properties of diamond-like carbon films. *Surf. Coat. Technol.* **2001**, 146-147, 292-297.

[6.11] J.-M. Martin, M.-I. De Barros Bouchet, C. Matta, Q. Zhang, W. A. Goddard III, S. Okuda, T. Sagawa. Gas-phase lubrication of ta-C by glycerol and hydrogen peroxide. Experimental and computer modeling. *J. Phys. Chem. C* **2010**, 114, 5003-5011.

[6.12] K. J. Sankaran, N. Kumar, H.-C. Chen, C.-L. Dong, A. Bahuguna, S. Dash, A. K. Tyagi, C.-Y. Lee, N.-H. Tai, I.-N. Lin. Near frictionless behavior of hydrogen plasma treated diamond nanowire films. *Sci. Adv. Mater.* **2013**, 5, 687-698.

[6.13] R. Radhika, N. Kumar, K. J. Sankaran, R. Dumpala, S. Dash, M. S. R. Rao, D. Arivuoli, A. K. Tyagi, N. H. Tai, I.-N. Lin. Extremely high wear resistance and ultra-low friction behaviour of oxygen-plasma-treated nanocrystalline diamond films. *J. Phys. D Appl. Phys.* **2013**, 46, 425304.

[6.14] T. Kunze, M. Posselt, S. Gemming, G. Seifert, A. R. Konicek, R. W. Carpick, L. Pastewka, M. Moseler. Wear, plasticity, and rehybridization in tetrahedral amorphous carbon. *Tribol. Lett.* **2014**, 53, 119-126.

[6.15] T.-B. Ma, L.-F. Wang, Y.-Z. Hu, X. Li, H. Wang. A shear localization mechanism for lubricity of amorphous carbon materials. *Sci. Rep.* **2014**, 4, 3662.

[6.16] W. Beyer. Structural and electrical properties of silicon-based amorphous alloys. *J. Non-Cryst. Solids* **1987**, 97-98, 1027-1034.

[6.17] Y. J. Chabal, C. K. N. Patel. Molecular hydrogen in a-Si:H. *Rev. Mod. Phys.* **1987**, 59, 835-844.

[6.18] D. L. Williamson, A. H. Mahan, B. P. Nelson, R. S. Crandall. Microvoids in amorphous $Si_{1-x}C_x$:H alloys studied by small-angle X-ray scattering. *Appl. Phys. Lett.* **1989**, 55, 783-785.

[6.19] F. Berndt, H.-J. Kleebe, G. Ziegler. Evidence for structural changes of amorphous carbon coatings on silicon carbide during tribological tests. *J. Am. Ceram. Soc.* **1999**, 82, 3161-3166.

[6.20] C. Casiraghi, A. C. Ferrari, J. Robertson. Raman spectroscopy of hydrogenated amorphous carbons. *Phys. Rev. B* **2005**, 72, 085401.

[6.21] S. Bai, T. Onodera, R. Nagumo, R. Miura, A. Suzuki, H. Tsuboi, N. Hatakeyama, H. Takaba, M. Kubo, A. Miyamoto. Friction reduction mechanism of hydrogen- and fluorine-terminated diamond-like carbon films investigated by molecular dynamics and quantum chemical calculation. *J. Phys. Chem. C* **2012**, 116, 12559-12565.

[6.22] S. Dag, S. Ciraci. Atomic scale study of superlow friction between hydrogenated diamond surfaces. *Phys. Rev. B* **2004**, 70, 241401.

[6.23] G. Zilibotti, M. C. Righi, M. Ferrario. Ab initio study on the surface chemistry and nanotribological properties of passivated diamond surfaces. *Phys. Rev. B* **2009**, 79, 075420.

[6.24] J. Robertson. Recombination and photoluminescence mechanism in hydrogenated amorphous carbon. *Phys. Rev. B* **1996**, 53, 16302-16305.

[6.25] K. Kato, N. Umehara, K. Adachi. Friction, wear and N_2-lubrication of carbon nitride coatings: a review. *Wear* **2003**, 254, 1062-1069.

[6.26] J. Andersson, R. A. Erck, A. Erdemir. Friction of diamond-like carbon films in different atmospheres. *Wear* **2003**, 254, 1070-1075.

[6.27] Y. Qi, E. Konca, A. T. Alpas. Atmospheric effects on the adhesion and friction between non-hydrogenated diamond-like carbon (DLC) coating and aluminum – a first principles investigation. *Surf. Sci.* **2006**, 600, 2955-2965.

[6.28] L. Ji, H. Li, F. Zhao, W. Quan, J. Chen, H. Zhou. Effects of environmental molecular characteristics and gas–surface interaction on friction behaviour of diamond-like carbon films. *J. Phys. D Appl. Phys.* **2009**, 42, 135301.

[6.29] H. Guo, Y. Qi, X. Li. Predicting the hydrogen pressure to achieve ultralow friction at diamond and diamondlike carbon surfaces from first principles. *Appl. Phys. Lett.* **2008**, 92, 241921.

[6.30] G. T. Gao, P. T. Mikulski, G. M. Chateauneuf, J. A. Harrison. The effects of film structure and surface hydrogen on the properties of amorphous carbon films. *J. Phys. Chem. B* **2003**, 107, 11082-11090.

[6.31] G. Zilibotti, S. Corni, M. C. Righi. Load-induced confinement activates diamond lubrication by water. *Phys. Rev. Lett.* **2013**, 111, 146101.

[6.32] L. Pastewka, S. Moser, M. Moseler, B. Blug, S. Meier, T. Hollstein, P. Gumbsch. The running-in of amorphous hydrocarbon tribocoatings: a comparison between experiment and molecular dynamics simulations. *Int. J. Mat. Res.* **2008**, 99, 1136-1143.

[6.33] T. W. Scharf, I. L. Singer. Quantification of the thickness of carbon transfer films using Raman tribometry. *Tribol. Lett.* **2003**, 14, 137-145.

[6.34] L. Pastewka, S. Moser, M. Moseler. Atomistic insights into the running-in, lubrication, and failure of hydrogenated diamond-like carbon coatings. *Tribol. Lett.* **2010**, 39, 49-61.

[6.35] G. T. Gao, P. T. Mikulski, J. A. Harrison. Molecular-scale tribology of amorphous carbon coatings: effects of film thickness, adhesion, and long-range interactions. *J. Am. Chem. Soc.* **2002**, 124, 7202-7209.

Chapter 7

Conclusions and Future Prospects

In this ending chapter, conclusions concerning the major findings on superlubricity are drawn from the previous several chapters. In addition, a brief vision of future respect on the research of superlubricity is presented.

7.1 Conclusions

The work in this thesis has shed some light on the basic features of superlubricity in ion vapor deposited amorphous carbon films including pure a-C:H film and Si-incorporated a-C:H:Si films. Overall, the theme of this thesis mainly focuses on two aspects, which have paramount effets on superlubricity of a-C material, namely the film structure and the tribotesting condition. The major conclusions concerning this work are drawn as follows:

■ **Nanostructure-tailored and ultrasmooth (Ra~0.1 nm) a-C:H and a-C:H:Si films have been successfully synthesized by ion vapor deposition system.** The underlying growth mechanisms based on energetic ion subplatation have been revealed. The ion-impact induced subsurface "polishing" process such as surface diffusion and relaxazatioin is the driving force for smoothening of the film surface, which is accompanied by an extremely small growth exponent β~0. Depending on the incident ion energy, the bonding structure of a-C:H:Si films evolves from hydrogen-rich chain-developed polymer-like, to hard cross-linked diamond-like, and finally to hydrogen-deficient sp^2-bonded a-C.

■ **The key factors controlling the superlubric behaviors of pure hydrogen-rich a-C:H film have been systematically investigated.** The film structure, counterpart

material (self-mated or bare steel ball), atmospheric environment, contact pressure (non-Amontonian behavior) and sliding velocity are playing paramount roles in determining the friction behavior of a-C:H film. An extremely low friction coefficient of ~0.001 can be obtained at normal load of 10 N in dry N_2. Such a near-frictionless rubbing hardly results in any wear and loss of material.

■ **Superlow friction is realized in humid air through suppression of moisture sensitivity by Si incorporation into a-C:H films.** A Si content of about 10 at.% is more appropriate to achieve ultralow or even superlow friction in humid air. The tribochemical interaction of water molecules with the carbonaceous film suface has been elucidated. It is found that the surface density of tribo-formed silicon hydroxyl group (Si-OH), humidity level and contact pressure determine the frictional performance of a-C:H:Si films. The dissociative formation of OH-terminated surface and the orientation of molecular structure of adsorbed water is the origin of ultralow and/or superlow friction in humid air. At an appropriate humidity level, the formation of a low shear-strength layer-like H_2O film can provide effective boundary lubrication torward the sliding interface.

■ **A lubrication material system based on C-Si-H ternary phases has been proposed for synthesized new anti-friction a-C:H:Si films.** The H content ranging from ~15 to ~40 at.% in the films is obtained by changing the applied bias voltage from 0.25 to 3.5 kV, while the Si content is kept constant at around 10 at.%. The hydrogen-induced diversity in film structure such as polymer-like, diamond-like or sp^2-bonded a-C, and the environmental gas characteristic are the two most influential factors controlling the frictional behaviors of a-C:H:Si films. A proper range of H content is required to achieve stable superlow friction in a distinct atmosphere, i.e., dry N_2, reactive H_2 or humid air.

■ **A polymer-like a-C:H:Si film has been developed to exhibit ultralow and/or superlpw friction in multi-environments.** This polymeric sample can exhibit superlow friction (μ~0.001-0.01) in humid air, inert gases (N_2 and Ar) and reactive gas (H_2), and

can maintain an ultralow friction (μ~0.08) in O_2. Hydrogen is highlighted for its decisive role in obtaining superlow friction. The underlying lubrication mechanisms based on the intra- and inter-film interactions along with the tribointeractions with the atmospheric gases have been reveald. The occurrence of superlubricity in a-C:H:Si films is sometimes attributed to a synergistic effect of phase transformation, surface passivation and shear localization, for example, the acquisition of an extremely low friction coefficient of ~0.001 in dry N_2.

7.2 Future Prospects

7.2.1 Urgent Issues to be Solved

Even though great advancements have been achieved in the past two decades, some critical issues still exist that need to be solved in the future, as put forward below:

■ For the lubrication mechanism of a-C films, most research work at present focuses on characterizing the tribo-produced materials (i.e., tribolayers) after the friction tests. Therefore, it is an ex-suit analysis result, which can't reflect the actural phenomenons occurred at the sliding interface. From this perspective, it is highly necessary to develop some unique experimental methods to in suit observe and detect the tribochemical interactions taking place between the contact surfaces.

■ For the theoretical studies such as molecular dynamics (MD) simulations of frictional behaviors, most of the reported work has been carried out in a relatively ideal condition (i.e., without considering the effect of environmental medium) due to the limitation of computer technology. However, with the development of computational power and algorithm, it is required to increase the time and length scales available to simulations. The gap between experiments and simulations should be narrowed.

■ For the application of a-C as a superlubric material in industry, we still lack basic background concerning this possibility. Most studies on superlubricity of a-C are still at the stage of theoretical and laboratory research, which is quite different from the case of

industry, for instance, the lubrication system in carbon engine. Therefore, it is highly necessary to make the future research activities approach as close as possible to the actural conditions of industrial service environments.

7.2.2 Prospective Applications

Superlubricity of amorphous carbon films is drawing growing and extensive attention in scientific community due to the high significance it carries for the potential applications in industrial activities. The following table lists some prospective applications in industry for amorphous carbon films.

Table 7.1 Prospective applications of superlubric amorphous carbon films.

Applications	Environ.	Temp. (°C)	Pressure	Film type	μ
Bearings, bushings, seals, gears, magnetic disk, caron engines (i.e., fuel injectors, camshafts, valve tappets and piston pins/rings), razor blades, hip implants	**Humid air, oil, body fulid**	**-200 - 400**	**High**	**Diamond-like a-C:H:Si**	**0.005 – 0.1**
Aerospace components (bushings, reaction wheels, shafts, gyroscopes, solor arrays, antenna drives, gears, latches, pumps, etc.)	**Vacuum/H_2**	**Up to ~600**	**Moderate - high**	**Polymeric a-C:H:Si or a-C:H**	**0.001 – 0.05**
Bearings, seals, pumps, valves, motor brushers, piston skirts	**Humid air, oil**	**-200 - 400**	**Low - moderate**	**Mainly sp^2-bonded a-C:H:Si**	**0.01 – 0.1**
Mechanical valve parts, camshafts, seals, piston pins	**Humid air, oil**	**-200 - 400**	**High**	**ta-C**	**0.02 – 0.1**
Bearings (rollers, inner/outer races, etc.)	**Humid air, oil**	**RT - 300**	**High**	**MeC/a-C:H (Me=Ti, W, Cr)**	**~0.05-0.1**

Publications and Proceedings

Journal papers:

[1] **X. Chen**, T. Kato. Superlubricity of hydrogenated amorphous carbon films: an updated review, in preparation for submission.
[2] **X. Chen,** T. Kato, M. Nosaka. Origin of superlubricity in a-C:H:Si films: a relation to film bonding structure and environmental molecular characteristic, ***ACS Applied Materials & Interfaces***, in press.
[3] **X. Chen,** T. Kato. Growth mechanism and composition of ultrasmooth a-C:H:Si films grown from energetic ions for superlubricity, ***Journal of Applied Physics***, 2014, 115(4): 044908.
[4] **X. Chen**, T. Kato, M. Kawaguchi, M. Nosaka, J. Choi. Structural and environmental dependence of superlow friction in ion vapour-deposited a-C : H : Si films for solid lubrication application, ***Journal of Physics D: Applied Physics***, 2013, 46(25): 255304.

Conference proceedings and posters:

[1] **X. Chen**, M. Kawaguchi, J. Choi, N. Matsumoto, M. Nosaka, T. Kato. Low friction characteristics of a-C:H:Si films prepared by ion vapor deposition. Oral presentation, JAST, 2012, Hokkaido, Japan.
[2] **X. Chen**, M. Kawaguchi, J. Choi, M. Nosaka, T. Kato. Lubrication effect of hydrogen on superlubricity in ion vapor deposited a-C:H:Si films. Oral presentation, JAST, 2013, Tokyo, Japan.
[3] **X. Chen**, M. Kawaguchi, J. Choi, M. Nosaka, T. Kato. Gas-surface interfacial tribochemistry and superlubric mechanism of a-C:H:Si films in different gaseous atmospheres. Oral presentation, JAST, 2013, Fukuoka, Japan.
[4] **X. Chen**, M. Kawaguchi, J. Choi, M. Nosaka, T. Kato. A novel polymer-like a-C:H:Si film grow from energetic ions for superlubricity. Poster, The 5th Advanced Forum on Tribology, 2014, Fuji, Japan.
[5] **X. Chen**, M. Kawaguchi, J. Choi, M. Nosaka, T. Kato. Hydrogen dependence and tribochemical mechanism of superlubricity in ion vapor deposited a-C:H:Si films. Oral presentation, 7th China International Symposium on Tribology, 2014, Xuzhou, China.
[6] **X. Chen**, M. Kawaguchi, J. Choi, M. Nosaka, T. Kato. Growth mechanism and dynamic smoothening behavior of a-C:H:Si films for superlubricity. Oral presentation, JAST, 2014, Tokyo, Japan.

Appendix

Home-made code for HCF calculation in MATLAB:

```
% clear all; close all; clc;
% tst = [1:1:512]'*[1:1:512];
% tst is the orignal data

clear all;
load ori_data.mat

N = 512;

m = 200;

for k = 1:m

rst2(k) = 0;

  for i = 1:N

       rst1(k)=0;

            for j = 1:N-k

                 rst1(k)=rst1(k)+(tst(i,j+k)-tst(i,j)).^2;

            end

       rst2(k)=rst2(k)+rst1(k);

  end

  rst(k) = rst2(k)'/N/(N-k); % rst is the final data, vector

end
```